

**Epi/Genomic characterization and molecular
mechanisms of immunotherapy resistance in
Hgf-Cdk4^{R24C} preclinical model of human melanoma**

Doctoral thesis
to obtain a doctorate (Ph.D.)
from the Faculty of Medicine
of the University of Bonn

Atie Kashef

from Shiraz, Iran

2022

Written with authorization of

The Faculty of Medicine of the University of Bonn

First reviewer: Prof. Dr. med. Jennifer Landsberg

Second reviewer: Prof. Dr. Benedikt Brors

Day of oral examination: 13. September 2022

For the Clinic and Policlinic of Dermatology and Allergology

Director: Prof. Dr. med. Dr. ès sci. Prof. h. c. Thomas Bieber

Table of Contents

List of Abbreviations	7
1 Introduction	10
1.1 Skin melanoma and its molecular subtypes	10
1.2 The next generation of targeted therapies and immunotherapies revolutionized melanoma therapies using genomic and epigenomic melanoma profiles	11
1.3 Phenotype plasticity and melanoma cell dedifferentiation as non-genetic candidate mechanisms to combat therapy resistance	12
1.4 MITF gene in melanocytic differentiation and microenvironment-induced melanoma phenotype plasticity	15
1.5 DNA methylation as the first-line epigenetic regulator to screen for tissue-specific and adaptive differentiation	16
1.6 Preclinical models and comparative analysis for molecular characterization and precision therapy in melanoma	17
1.6.1 Genetically engineered murine (GEM) models of human melanoma	18
1.7 Mechanisms of resistance to melanoma therapies	21
1.7.1 Inflammation-induced melanoma cell dedifferentiation as a mechanism of acquired resistance to ACT-therapy	22
1.8 Research gap and objectives of this study	23
1.8.1 Mutational characterization and comparative analysis of preclinical model Hgf-Cdk4 ^{R24C} and HCmel cells	24
1.8.2 Molecular dynamics of resistant phenotype in melanoma cells of preclinical model Hgf-Cdk4 ^{R24C} , using exome data, expression profiles, and DNA methylation profiles	24

1.9	Genome-wide experimental and analytical methods; advantages and limitations	26
1.9.1	Genome-wide DNA methylation profiling	26
1.9.2	Genome-wide expression profiling	27
2	Materials and Methods	31
2.1	Murine melanoma cell lines	31
2.1.1	Origin and characteristics of the cell lines	31
2.1.2	Cell lines culture and authentication	34
2.2	DNA and RNA isolation	35
2.3	Mutational profiling using whole-exome sequencing (WES) technology	36
2.3.1	Sequencing technology and library preparation for WES experiment	36
2.3.2	Exome data processing	37
2.3.3	Somatic variant calling and variants annotation	38
2.3.4	Mutational analysis; somatic mutations heatmap, signatures, and intersections	39
2.4	Expression profiling using bulk RNA sequencing (RNAseq) technology	40
2.4.1	RNAseq library preparation and method	40
2.4.2	RNAseq data processing	41
2.4.3	Differential expression analysis to identify significant differentially expressed genes between primary and ACT-resistant cell lines	42
2.4.4	Biological function enrichment analysis	42
2.5	DNA-methylation profiling using MeDIP-seq	43
2.5.1	MeDIP sequencing library preparation and sequencing technology	43
2.5.2	MeDIP-seq data processing and quality control	43
2.5.3	Quantitative CpG enrichment and differential DNA-methylation analysis	44
2.5.4	Functional enrichment analysis of DMRs	45
3	Results	46
3.1	Genomic characterization of the preclinical mice driven cell lines recapitulate diverse molecular subtypes of human melanoma	46
3.1.1	Exome sequencing, somatic variant calling, and evaluation of the results	46

3.1.2	Mutational loads and driver mutations in HCmel and BCmel primary melanoma cell lines (compared to other murine melanoma cell lines)	47
3.1.3	Mutational characterization of ACT-resistant HCmel cell lines compared to their corresponding primary cell lines	48
3.1.4	Acquired mutations in ACT-resistant cell lines: Random genomic aberrations/mutations can cause dedifferentiation in melanoma cells leading to ACT-resistance in the Hgf-Cdk4 mouse model	48
		50
3.2	Expression profiling revealed differentiation signature in HCmel melanoma cell lines	57
3.2.1	Bulk mRNA enrichment, quantification of transcript counts, and evaluation of the results	57
3.2.2	Principal component analysis on expression profiles indicates two distinct groups of primary and resistant cell lines	57
3.2.3	Differentially expressed genes in primary and ACT-resistant cell lines indicated downregulation of melanocytic differentiation genes in resistant phenotypes	58
3.3	MeDIP-seq experiment and DNA-methylation profiling of the cell lines revealed the source of difference by DNA-methylation between primary and resistant cell lines	66
3.3.1	MeDIP-seq data quality and post alignment coverage report	66
3.3.2	ACT-Resistant melanoma cells showed a distinct DNA-methylation landscape from primary melanoma cells	66
3.3.3	CpG Islands indicate the source of difference by DNA-Methylation between primary and resistant cell lines	67
3.3.4	Differentially methylated genes contribute to melanoma cell differentiation signature and reflect the proinflammatory microenvironment	67
3.3.5	Mutational load increased but could not fully explain the mechanism of reversible and de-differentiation mediated resistance	68
4	Discussion	75
4.1	Key findings of this study	75

4.1.1	Hgf-Cdk4 ^{R24C} melanoma cell lines harbor additional driver mutations similar to the “Triple-WT” molecular subtype of human melanoma	75
4.1.2	Epigenetic alterations act beyond the somatic mutations in inflammation-induced reversible melanocytic dedifferentiation and ACT-therapy resistance	76
4.2	Clinical relevance and applications	79
4.2.1	MITF pathway offers a potential target to improve immunotherapy using DNA-methylation targeted drugs	79
4.2.2	AXL is a potential target to overcome resistance to immunotherapy and targeted therapy in melanoma	79
4.2.3	Targeting melanocytic dedifferentiation drivers as a mechanism of resistance to improve immunotherapy outcomes	80
4.3	Future perspectives and research suggestions	80
4.3.1	Functional validation	80
4.3.2	Bioinformatic validation; detection of immunogenic signatures which correlate with methylation alterations of MITF pathway in relevant clinical cohorts	81
4.3.3	Histone modifications and methylation assays	82
5	Abstract	85
6	List of Figures	87
7	List of Tables	89
8	References	90
9	Acknowledgment	106
10	Curriculum Vitae	107

List of Abbreviations

ACT	Adoptive Cell Transfer
AXL	AXL Receptor Tyrosine Kinase
Aza	Azacitidine
BAM	The binary file format of aligned sequencing reads
BCL2	B Cell Lymphoma 2
BRAF	B-Raf proto-oncogene
bp	Base pair
BS	Bisulfite
cDNA	Complementary
CGI	CpG Island
c-Jun	Jun proto-oncogene
CDK4	Cyclin-Dependent Kinase 4
CDK2	Cyclin-Dependent Kinase 2
c-Met	Met receptor tyrosine kinase
CNV	Copy number variant
COSMIC	Catalog of Somatic Mutations in Cancer
CpG	5'Cytosine–phosphate–3'Guanine dinucleotide
CTLA-4	Cytotoxic T Lymphocyte Associated protein 4
DAVID	Database for Annotation Visualization and Integrated Discovery
DNA	Deoxyribo-Nucleic Acid
DMBA	7,12-Dimethylbenzo(a)Anthracene
DMR	Differentially Methylated Region
DP	Quality parameter for depth of sequencing

ECM	Extra Cellular Matrix
ERK	ERK mitogen-activated protein kinase
FASTQ	Text-based format of raw sequencing reads
FDA	Food and Drug Administration
FBS	Fetal Bovine Serum
FPKM	Fragments per Kilobase per Million
GATK	Genome Analysis Toolkit
GEM	Genetically Engineered Mouse model
GLM	Generalized Linear Model
Gna11	G Protein Subunit Alpha 11
GO	Gene Ontology
GPNMB	Glycoprotein Nmb
GRCm38	Genome Reference Consortium Mouse Build 38
HGF	Hepatocyte Growth Factor
ICB	Immune Checkpoint Blockade
IRF4	Interferon Regulatory Factor 4
JUN	Jun proto-oncogene encoding gene
kb	kilobase
KRAS	KRAS proto-oncogene
MAPKi	MAPK signaling pathway inhibitor
MEK	MEK mitogen-activated protein kinase
MITF	Melanocyte Inducing Transcription Factor Microphthalmia-associated Transcription Factor
MLANA	Melan A
MPS	Melanocytic Plasticity Signature
mtrDNA	Mitochondrial DNA
NGS	Next-Generation Sequencing
NRAS	NRAS proto-oncogene
NF1	Neurofibromin 1
OCA2	OCA2 melanocyte-specific transporter protein
PCA	Principle Component Analysis
PCR	Polymerase Chain Reaction

PD1	Programmed cell death protein 1
PD-L1	Programmed Death Ligand 1
PMEL	Premelanosome protein
QSEA	Quantitative Sequencing Enrichment Analysis
QC	Quality Control
qPCR	Quantitative Polymerase Chain Reaction
QUAL	Variant calling quality parameter
Rac1	RAC Family Small GTPase 1 (murine gene)
RAS	Rat Sarcoma proto-oncogene
RAB27A	RAB27A, Member RAS Oncogene Family
RNA	Ribonucleic acid
RPMI	Roswell Park Memorial Institute growth medium
SLC45A2	Solute Carrier Family 45 Member 2
SNV	Single nucleotide variant
SOX10	SRY-Box Transcription Factor 10
TCGA	The Cancer Genome Atlas
TFAP2A	Transcription Factor AP-2 Alpha
TGF-β	Transforming Growth Factor beta
TNF	Tumor Necrosis Factor
Trp53	Transformation-related protein 53 Tumor suppressor P53
TRPM1	Transient Receptor Potential Cation Channel Subfamily M Member 1
TYR	Tyrosinase gene
UV	Ultra Violet radiation
VCF	Variant Call Format
XRCC6	X-Ray Repair Cross Complementing 6
ZFP536	Zinc Finger Protein 536

1 Introduction

1.1 Skin melanoma and its molecular subtypes

Melanoma is the deadliest type of skin cancer which begins by aberrant genetic and epigenetic control in melanocytes(Sarkar et al., 2015)(Dahl and Guldborg, 2007). Melanoma tumors bear a higher mutational load in comparison to other tumors and are known as highly heterogenous by somatic mutations as well as tumor phenotypes(PCAWG Mutational Signatures Working Group et al., 2020). Genetic heterogeneity, microenvironment-dependent epigenetic reprogramming, and tumor immunity make melanomas very challenging and interesting targets of research in both aspects of etiology and precision medicine (Merlino et al., 2016).

Genome-wide studies using high-throughput sequencing technologies rapidly advanced our understanding of molecular subtypes and mechanisms of melanoma genesis, metastasis, and response to the therapies. Using large scale melanoma exome sequencing, a landscape of driver mutations in melanomas has been described with the major mutational signatures and driver genes/pathways; This analyses of mutational and copy number data revealed that BRAF, NRAS, and NF1 are the most frequently mutated genes in melanomas and cytosine to thymidine (C>T) transitions account for 46% of mutational signatures which are known for UV-induced mutagenesis(Hodis et al., 2012). Using whole-genome, exome, and transcriptome sequencing followed by protein-based analysis further studies classified cutaneous melanomas by genomic mutations and immune signatures. According to this genomic classification, four major molecular subtypes of cutaneous melanomas were identified either as mutated in BRAF, RAS, NF1, or Triple-wild-type. In addition, each subtype was independently identified with signatures of tumor immunogenic microenvironment which contribute to the evaluation of immunotherapeutic strategies and patients' survival(Akbani et al., 2015).

Other researchers expanded on the insight of genomic drivers in major subtypes of melanoma using whole-genome data; it was shown that cutaneous, acral, and mucosal melanomas exhibit different mutational profiles which should be considered to improve targeted therapies in each subtype(Hayward et al., 2017).

1.2 The next generation of targeted therapies and immunotherapies revolutionized melanoma therapies using genomic and epigenomic melanoma profiles

Like the other types of cancer, melanoma is a genetic disorder that could be precisely characterized and controlled by molecular mechanisms. Targeted therapy using molecular drugs and monoclonal antibodies first became possible by understanding the driver genes and proteins in cancer. The most advanced FDA-approved therapies for melanoma include single-targeted or combination of targeted drugs to inhibit BRAF, MEK, RAS signaling as well as immunotherapies using antibody-mediated blockade of immune checkpoints CTLA-4 and PD-1 (Merlino et al., 2016).

Epigenetic markers and alterations also became a trending focus of research in melanoma genesis and precision therapies since they are known for reversible regulation and microenvironmental interplay with tumor genetics.

Hugo et al published robust shreds of evidence that DNA methylation alterations contribute to resistance mechanisms in mitogen-activated protein kinase inhibitor (MAPKi) therapies. Using patient-matched melanoma exomes, transcriptomes and methylomes they indicated that interplay of CpG-methylation changes with tumor microenvironment and immunity in MAPKi-resistant melanomas are modulated beyond the genetic changes (Hugo et al., 2015).

Epigenetic regulation in cancer works via different mechanisms including DNA methylation, histone acetylation, histone methylation, and Non-coding RNA (Cheng et al., 2019). Growing evidence by epi/genetic research during recent years developed the idea of targeting epigenetic markers using “epidrugs” –including inhibitors of DNA methyltransferases and histone deacetylases– to improve cancer treatments. Despite genetic mutations, epigenetic alterations (epimutations) are reversible and reprogrammable. An increasing number of epidrugs are receiving FDA approval or passing through preclinical and clinical trials which aim to reprogram resistance mechanisms and to increase the efficacy of targeted therapies against cancer (Dahl and Guldborg, 2007)(Miranda Furtado et al., 2019). In the following paragraphs, I focus on cellular and molecular mechanisms which raised questions about epi/genetic dynamics of melanomas in therapy context and their contribution to epidrugs discovery.

1.3 Phenotype plasticity and melanoma cell dedifferentiation as non-genetic candidate mechanisms to combat therapy resistance

Therapeutic approaches for melanoma have benefited from multifaceted research and growing experimental data from melanoma cells behavior. Epi/genetic studies demonstrated molecular knowledge about melanoma cells differentiation, cell cycle and proliferation, metabolism, and other non-genetic mechanisms which affect melanomas phenotype, dynamics, and their responses to the therapies. These mechanisms have been studied for contribution to tumor metastasis and resistance to therapies that also led to epidrugs research and development(Miranda Furtado et al., 2019).

Melanoma phenotype plasticity has been introduced as a mechanism of resistance to targeted therapies and immunotherapies. This phenomenon indicates phenotype switching between different states of differentiation, proliferation, or invasion in melanomas through the epithelial-mesenchymal transition of melanoma cells (Rambow et al., 2019)(Hoek et al., 2008). Phenotype plasticity is controlled under numerous secreted factors in the tumor microenvironment (secretome). Transforming growth factor (TGF β), extracellular matrix (ECM) proteins, cytokines, proinflammatory factors like tumor necrosis factor (TNF), and immune cells are of the most influential secreted factors which drive loss of melanocytic differentiation (Arozarena and Wellbrock, 2019) (Figure 1.1). Melanocytic plasticity signature (MPS) in melanomas was recently identified using comparative genomic and transcriptomic analysis on multiple preclinical models and clinical cohorts. MPS was applied for predicting patients' survival and response to immunotherapy (ICB)(Pérez-Guijarro et al., 2020)(Tsoi et al., 2018).

Experimental and molecular data have provided evidence indicating that phenotype plasticity happens via epi/genetic reprogramming in melanoma cells in interaction with the tumor microenvironment, stress factors, and immune cells. Melanoma cells dedifferentiation under proinflammatory tumor microenvironment has been explained as a mechanism of resistance to adoptive T-cell transfer immunotherapy in melanomas (Landsberg et al., 2012). Tumor microenvironment and immunity are known as influencers of melanoma cell plasticity which leads to loss of responsiveness to immunotherapies (Hölzel et al., 2013)(Riesenberg et al., 2015). On the other hand, in human melanoma cells epigenetic downregulation of developmental and differentiation genes like SOX10

and MITF (melanocyte inducing transcription factor also known as the microphthalmia-associated transcription factor) leads to aberrant signaling and dedifferentiation and consequently acquired therapy resistance (Shaffer et al., 2017). Analyses of expression and DNA methylation data in TCGA melanoma cohorts confirmed that downregulation of MITF –a known key gene of melanocytic differentiation– correlates with hypermethylation of CpG islands in this gene. Interestingly further experiments in human melanoma cell lines also showed that MITF expression could be restored using a hypomethylation agent (Lauss et al., 2015). Altogether, dedifferentiation-mediated resistance in melanoma therapy appeared as a convincing and highly interdisciplinary target of research to improve the efficacy of targeted therapies and immunotherapies.

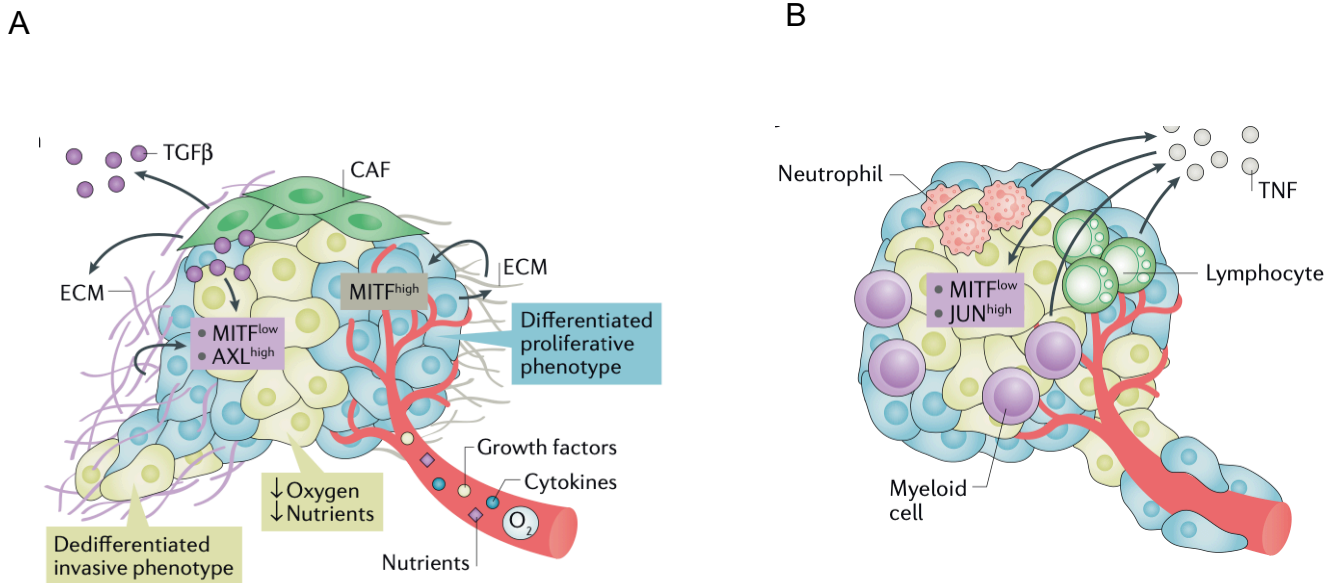


Figure 1.1 Adaptive phenotype plasticity in melanoma.

A) The secretome in tumor microenvironment controls phenotype switch between differentiated ($MITF^{high}$) proliferative melanoma and dedifferentiated ($MITF^{low}$) invasive melanoma. Phenotype plasticity is controlled under numerous secreted factors in tumor microenvironment (secretome) including transforming growth factor ($TGF\beta$) and extracellular matrix (ECM) proteins secreted by cancer associated fibroblasts (CAFs). In addition, metabolic factors like hypoxia and restriction of nutrients (glucose and glutamine) are known for contribution to loss of melanocytic differentiation signature $MITF^{low}$, AXL^{high} .

B) Proinflammatory factors like tumor necrosis factor (TNF), cytokines, and immune cells are of other complex secretome in melanoma microenvironment which drive phenotype switch and contribute to loss of melanocytic differentiation signature $MITF^{low}$, JUN^{high} . (Arozarena and Wellbrock, 2019)

1.4 MITF gene in melanocytic differentiation and microenvironment-induced melanoma phenotype plasticity

MITF gene is known as the key transcription factor of melanocytic differentiation (Hemesath et al., 1994). MITF expression is crucial in normal melanocytic differentiation as well as melanoma cell proliferation and melanoma progression. In addition to melanocytic differentiation, MITF controls cell cycle, metabolism, and cell survival. The most important target genes of MITF in melanocytic differentiation include TYR, TYRP1, DCT, PMEL, and MLANA. Other important target genes of MITF in melanocytes and melanoma cells include CDK2 in cell cycle control, BCL2 and BCL2A1 in survival, and PPARGC1A in metabolism (Kawakami and Fisher, 2017).

Downregulation of MITF and dedifferentiated phenotype have been observed in targeted therapy and immunotherapy resistant melanomas (Konieczkowski et al., 2014)(Müller et al., 2014). Transcriptional and mutational analysis in a big cohort of matched samples from melanoma patients under ICB immunotherapy recently revealed dedifferentiation and downregulation of MITF accompanying with downregulation of MHC1(major histocompatibility complex I) in anti-PD1 resistant melanomas. (Lee et al., 2020). Previously, experimental data demonstrated that downregulation of MITF which leads to epithelial-mesenchymal transitioning and dedifferentiation in a pro-inflammatory microenvironment, correlate with escaping the immune recognition by adoptive T-cell transfer (ACT) therapy (Landsberg et al., 2012).

Multiple in-vivo and in-vitro studies have suggested that melanoma progression and dedifferentiation-mediated resistance develop through phenotype plasticity or “phenotype-switch model” indicating the interplay of MITF signaling with melanoma microenvironment(Arozarena and Wellbrock, 2019).

Phenotype-switch model has been first described based on in-vitro observations of melanoma cell lines with two distinct MITF expression profiles and corresponding tumor behavior: “proliferative” with positive expression of MITF, and “invasive” with negative expression of MITF(Hoek et al., 2006). However, this concept was further supported by in-vivo observations and could explain the central role of MITF in microenvironment-induced or adaptive reprogramming of melanoma cells differentiation (Hoek et al., 2008).

Upregulation of MITF has been assigned to the melanocytic stage in a progressive four-stage melanocytic differentiation signature which was established based on expression data of melanomas. This signature was demonstrated on observations of reversible dedifferentiation and melanoma phenotype switching in response to ACT immunotherapy as well as MAPKi targeted therapy (Tsoi et al., 2018)(Mica et al., 2013).

In conclusion, dysregulated expression of MITF in melanoma (MITF^{low} melanomas) is bounded with adaptive melanocytic dedifferentiation, proliferation, and higher immunogenic response with proinflammatory and increased immune cells infiltration(Huergo-Zapico et al., 2018)(Landsberg et al., 2012)(Riesenberg et al., 2015).

1.5 DNA methylation as the first-line epigenetic regulator to screen for tissue-specific and adaptive differentiation

DNA methylation is known as the most stable and inheritable epigenetic mark in mammalian cell development and differentiation. DNA methylation changes reflect the history of cancer cells in response to the tumor microenvironment and the tissue of origin even after long-term culture (Schellenberg et al., 2011). DNA methylation is mediated by DNA methyltransferases on cytosine(C) of CpG dinucleotides and represents the only covalent modification of DNA in mammals. CpG dinucleotides tend to locate in promoter regions of genes which are called “CpG Islands”. Hypermethylation of CpG islands often contributes to the downregulation of gene expression while hypomethylation of methylated promoters contributes to upregulation or ectopic expression of the corresponding gene(Bernstein et al., 2007). Global hypomethylation and site-specific hypermethylation of tumor suppressors or other gene promoters are well-known epigenetic modifications associated with cancer phenotype(Feinberg et al., 2006). Experimental data have shown that DNA methylation alterations can also reflect chromatin changes and align with histone modifications. Therefore, DNA methylation is known as the first useful and cost-effective epigenetic marker to screen(Kim and Costello, 2017)(Shipony et al., 2014).

Adaptive phenotype-switch model and dedifferentiation-mediated resistance to melanoma therapies appeared to be controlled beyond mutational load and genetic changes rather by epigenetic modifications(Hugo et al., 2015). DNA methylation changes have been found aligned with chromatin remodeling in MITF-mediated phenotype switching in

melanoma cells: open chromatin correlated with a decreased level of methylation and repressed chromatin correlated with an increased level of methylation(Verfaillie et al., 2015). In another genome-wide analysis of methylation profiles from invasive melanomas, hypermethylation of MITF promoter and its target genes in melanocytic differentiation pathway –MLANA, TYR, and RAB27A– have been observed(Lauss et al., 2015).

1.6 Preclinical models and comparative analysis for molecular characterization and precision therapy in melanoma

Preclinical models of human melanoma have tremendously contributed to current insight on mechanisms of melanoma progression, tumor characteristics, and developing novel therapeutic strategies. Comparative or cross-species analyses implement data from human tumors, animal tumors, and preclinical models of human tumors to identify conserved epi/genetic alterations and mechanisms in tumor genesis and progression. Such alterations and mechanisms have been promising targets of research and development for cancer therapies and specifically melanoma therapies.

There are multiple approaches including different species to model human melanoma in other animals or organoids but here I focus on murine models of human melanoma and specifically the genetically engineered mouse (GEM) models which have been implemented for this study.

To date, murine melanoma models have been generated based on four main strategies:

- 1) Human melanoma cell xenografts were implanted into immunocompromised mice.
- 2) Murine melanoma cells –driven by genetic engineering or autochthonous melanomas– were implanted into syngeneic wild-type mice with no immune manipulation.
- 3) Melanoma is driven by genetic engineering with or without carcinogen induction in mice.
- 4) Melanoma cells –driven by genetic engineering or autochthonous melanomas– were implanted into a genetically engineered model with the manipulated tumor microenvironment.

Each model comes with different advantages and disadvantages (Pérez-Guijarro et al., 2017)(Zaidi et al., 2008). Melanoma cell xenografts recapitulate the complex genetic

heterogeneity of human melanomas and have been used to predict the tumor response to drugs; however, predicting the clinical outcomes remains challenging. Syngeneic models provide more feasible transplantation with a functional immune system. Genetically engineered murine (GEM) models provide a precise platform to reproduce specific genetic mutation and molecular signaling of melanoma genesis and therefore recapitulate human melanomas of that specific molecular profile. GEM models of melanoma are popular for studying molecular mechanisms of melanoma progression and therapy resistance. They evade the heterogeneity and complex genetic aberrations of human melanomas and keep the focus of study on particular molecular mechanisms (van der Weyden et al., 2016)(Saleh, 2018).

1.6.1 Genetically engineered murine (GEM) models of human melanoma

Genetically engineered mouse models of cutaneous melanoma have been established for decades and provided a vital platform for modeling precise genetic alterations of human patients and their consequences. They carry a variety of engineered mutations or modifications which lead to activation of oncogenes, inactivation of tumor suppressors, and melanocyte-specific expression of key genes in melanoma genesis HRAS, NRAS, BRAF (Figure 1.2 A). GEM melanoma models could be developed without carcinogens induction or they are induced with carcinogens like UV (ultraviolet) radiation and DMBA (7,12-dimethylbenz(a)anthracene)(Pérez-Guijarro et al., 2017)(van der Weyden et al., 2016). UV-induced GEM models have been anticipated to become the best tools for molecular studies of melanoma progression, target validation, and therapy resistance.

1.6.1.1 A Hgf-Cdk4^{R24C} preclinical model of melanoma for precision ACT-therapy

Hgf-Cdk4^{R24C} has been initially established for studying the impact and molecular mechanisms of UV carcinogen in melanoma genesis as well as developing ACT immunotherapy against invasive melanoma. This GEM model has been engineered with overexpression of HGF (hepatocyte growth factor) in addition to an oncogenic mutation in Cdk4 (cyclin-dependent kinase 4) (Gaffal et al., 2011)(Tormo et al., 2006)(Bald et al., 2014) (Figure 1.2 B).

Hgf-Cdk4^{R24C} appeared as a successful model of invasive human melanoma with a similar phenotype of clinical patients and immunotolerant in transplantation. Further in-vivo and in-vitro studies using Hgf-Cdk4^{R24C} melanoma indicated adaptive phenotype-switch and dedifferentiation as a mechanism of resistance to immunotherapy (Landsberg et al., 2012).

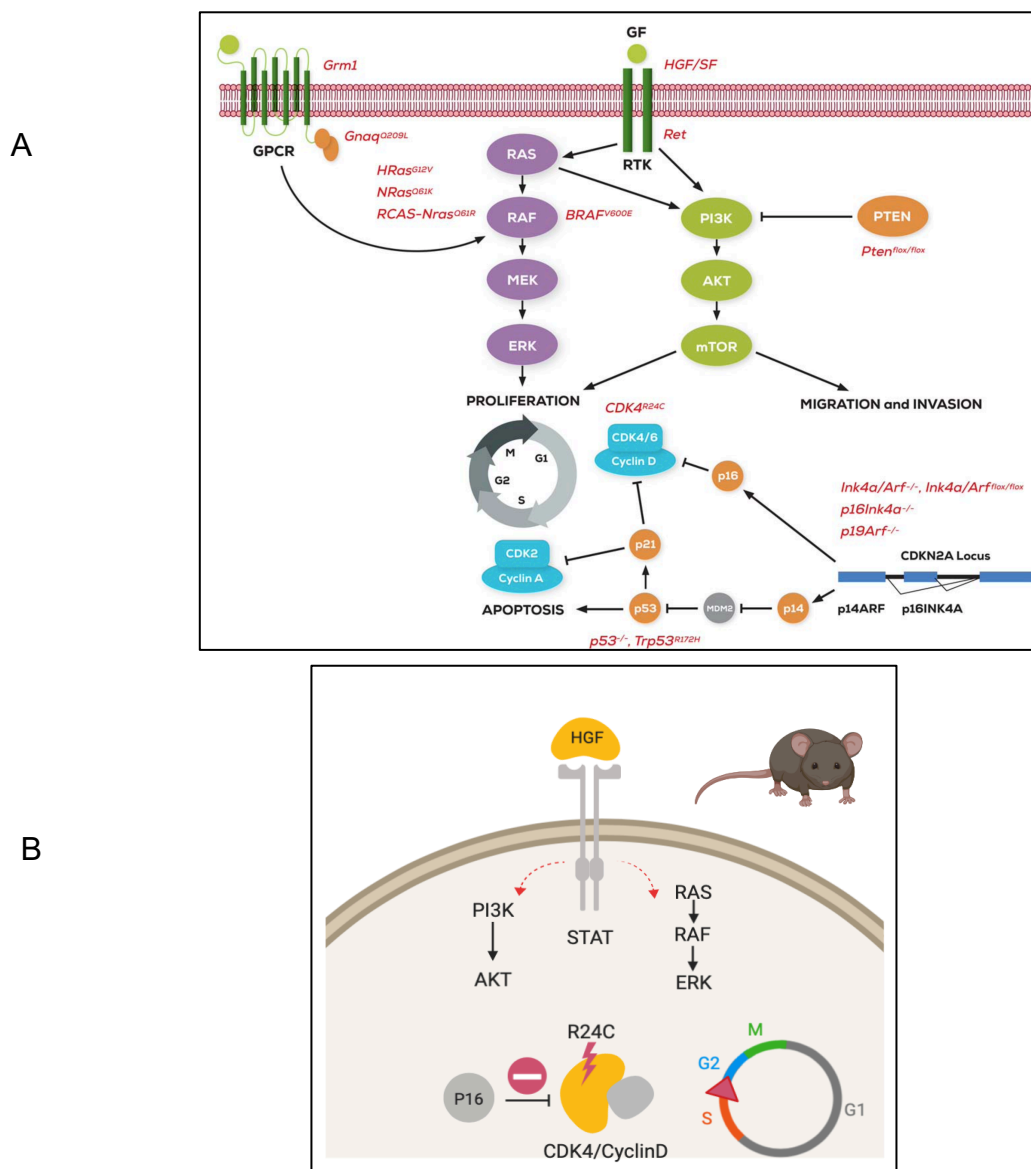


Figure 1.2 Targeted genes and pathways in genetically engineered murine (GEM) models of cutaneous melanoma.

A) Activated rat sarcoma protein (RAS)/raf proto-oncogene serine threonine protein kinase (RAF)/mitogen-activated protein kinase kinase (MEK)/extracellular signal-regulated kinase (ERK) (RAS/RAF/MEK/ERK) and phosphoinositide-3 kinase (PI3K) pathways recapitulate the most frequently altered pathways of proliferation in human melanomas. Specific allelic modifications available in current preclinical murine models of melanoma are highlighted in red (Pérez-Guijarro et al., 2017). **B)** Hgf-Cdk4^{R24C} murine model of melanoma includes oncogenic activation of cyclin-dependent kinase 4 (CDK4) and stimulation of tyrosine kinases in proliferation signaling by overexpression of growth factor (HGF). This model has been developed for studying the mechanisms of resistance to Adoptive T cell transfer immunotherapy (ACT) by Landsberg and colleagues. Figure is generated using Biorender.com.

1.7 Mechanisms of resistance to melanoma therapies

Targeted therapy and immunotherapy have shown unprecedented advances in clinical response and tumor regression. However, successful tumor remission is not durable and the majority of melanomas either exhibit intrinsic resistance or they acquire resistance to the therapeutic regimes. Mechanisms of resistance are very complex and include genetic mutations as well as non-genetic alterations in melanoma cells and also induced by the tumor microenvironment (Figure 1.3). Addressing these mechanisms contribute to the improvement of quality response, patient survival, and precision medicine in cancer (Winder and Virós, 2018).

Intrinsic resistance to immunotherapeutic regimes in melanoma cells can be associated with genetic or non-genetic events that arise natural resistance in tumor entities. For example, upregulation of genes involved in epithelial-mesenchymal transition (AXL, ROR2, WNT5A, LOXL2, TWIST2, TAGLIN, FAP), as well as genes in angiogenesis and wound healing, have been shown to be associated with intrinsic resistance to anti-PD1 immunotherapy (Hugo et al., 2016). This expression signature significantly overlaps with the expression signature which was previously observed in acquired MAPKi-resistant melanomas with evidence of non-genomic programming through DNA-methylation alterations (Hugo et al., 2015). Loss of PTEN is another melanoma cell-intrinsic mutation that leads to upregulation of immunosuppressive cytokines and consequently decreased T-cell mediated immunotherapy (Peng et al., 2016).

Immunotherapy resistance in melanomas can be acquired through immunity-related events which affect T-cell recognition and tumor cell killing: for example, mutations in genes of interferon-receptor signaling and mutations which affect antigen presentation. Another example is $\text{INF}\gamma$ (Interferon- γ) stimulus which plays a dual function in anti-tumor immune response as well as immune escape. Continuous exposure to $\text{INF}\gamma$ leads to constitutive upregulation of PD-L1 –the ligand for PD1 receptor– by T_{reg} (regulatory) cells and consequently suppression of T cell-mediated response (Spranger et al., 2013) (Tumeh et al., 2014). T_{reg} cells exhibit regulatory immunosuppressive function by repressing the proliferation and activation of effector T cells. Infiltration of c-Met⁺ (Met receptor tyrosine kinase) neutrophils in the tumor microenvironment are associated with adaptive

suppression of T cell-mediated immune response and effector functions by expression of inhibitory ligand PD-L1 (Glodde et al., 2017).

Another mechanism of adaptive resistance to immunotherapy and impaired recognition of tumor-specific T cells was explained by melanoma phenotype switching in the pro-inflammatory tumor microenvironment. I will focus on this mechanism in the following paragraphs.

1.7.1 Inflammation-induced melanoma cell dedifferentiation as a mechanism of acquired resistance to ACT-therapy

Natural selection of tumor cells/clones with less immunogenic or antigen-deficient phenotypes has been explained under the term “cancer immunoediting” as a mechanism in acquired resistance to T cell-mediated immunotherapy. This simply implies that immunoselection of antigen-deficient melanoma cells leads to T cell tolerance and outgrowth of such tumor cells (Khong and Restifo, 2002) (Winder and Virós, 2018) (Matsushita et al., 2012).

Landsberg and colleagues established a preclinical model for ACT immunotherapy in a genetically engineered mouse model that successfully recapitulated the clinical behavior of therapy-resistant melanoma. This model was aimed to study the mechanisms of T cell-mediated immunotherapy resistance and brought experimental evidence of immunoevasion by dedifferentiation phenotype switching and loss of melanoma cell-specific antigens. Interestingly this dedifferentiated resistant phenotype was reversible and mirrored non-genetic and tumor-microenvironmental events. Landsberg and colleagues showed that in the Hgf-Cdk4^{R24C} model under adoptive T cell transfer (ACT) therapy, melanoma evolve a dedifferentiated phenotype with a proinflammatory tumor microenvironment and significant secretion of TNF α (tumor necrosis factor α). Their data addressed the loss of melanocytic antigens aligned with adaptive dedifferentiation as a mechanism of immunotherapy resistance and loss of melanoma-specific T cell recognition (Landsberg et al., 2012). Moreover, they confirmed that melanoma cell differentiation is lost through downregulation of the MITF pathway and melanocytic genes expression.

Further molecular experiments using expression profiles of murine and human melanoma cells revealed that pro-inflammatory immune response with the signature of TNF α and

other pro-inflammatory cytokines –which were produced by T cells in the tumor microenvironment during ACT therapy– is interconnected with upregulation of transcription factor c-Jun (Jun proto-oncogene) and downregulation of MITF signaling. The MITF^{low}/c-JUN^{high} signature was demonstrated in melanomas with the significant secretion of proinflammatory cytokine TNF α as well as myeloid cells infiltration into the tumor microenvironment (Riesenberg et al., 2015). They observed that the expression of c-Jun is antagonistic to the expression of MITF and downregulates the melanocytic differentiation genes expression.

Proinflammatory-induced and reversible melanocytic dedifferentiation was later identified as a mechanism of acquired resistance to ACT therapy in a clinical melanoma patient. Interestingly it was also confirmed in corresponding human melanoma cells that dedifferentiated phenotype is reversible in response to the withdrawal of pro-inflammatory stimuli (Mehta et al., 2018).

Taken together, proinflammatory induced phenotype switching from differentiated MITF^{high} melanoma to dedifferentiated MITF^{low} melanoma explained how melanomas switch their behavior from proliferative to invasive and acquire ACT therapy resistance through immunoselection of antigen-deficient phenotype.

1.8 Research gap and objectives of this study

Landsberg and colleagues showed the interconnection of dedifferentiated melanoma phenotype and melanoma cell plasticity with proinflammatory tumor microenvironment and T cell-mediated therapy resistance. However, the molecular modulators of this interconnection remained unknown. I am specifically interested in epi/genetic mechanisms that could explain the evolution of reversible melanocytic dedifferentiation in ACT therapy-resistant melanoma phenotype. According to previous experimental data, there was a clear need for integrative analysis of genomic, transcriptomic, and particularly epigenetic alterations to gain a deeper mechanistic understanding of dedifferentiation-mediated therapy resistance. I hypothesized that proinflammatory induced reversible dedifferentiation in melanoma is programmed by epigenetic alterations –specifically changing DNA methylation marks– beyond somatic mutations. To test this hypothesis, I

took advantage of the established primary melanoma and therapy-resistant melanoma cell lines from the Hgf-Cdk4^{R24C} preclinical model at Prof. Landsberg's lab.

1.8.1 Mutational characterization and comparative analysis of preclinical model Hgf-Cdk4^{R24C} and HCmel cells

I aimed to genetically characterize melanoma cells of our preclinical model Hgf-Cdk4^{R24C} in order to identify the somatic mutational load and possible driver mutations as well as their relevance to therapy resistance mechanisms. This identification contributed to genetic classification and molecular subtyping of our preclinical model compared to other available cell lines of murine models of human melanoma BCmel4, Mel114433, B9013HCB, B2905, and B16-F10.

1.8.2 Molecular dynamics of resistant phenotype in melanoma cells of preclinical model Hgf-Cdk4^{R24C}, using exome data, expression profiles, and DNA methylation profiles

I proposed a dynamic or reversible molecular mechanism for reversible dedifferentiation-mediated therapy resistance which could interconnect the proinflammatory tumor microenvironment with dedifferentiated phenotype and loss of T cell-specific antigens in resistant melanoma cells. Therefore, I aimed to analyze molecular profiles of genomic mutations, gene expressions, and DNA methylation in primary and resistant melanoma cells of the Hgf-Cdk4^{R24C} preclinical model. I conducted differential analysis and integrative analysis to identify the source of molecular differences between primary and resistant melanoma cells which indicated programming mechanisms of these phenotypes.

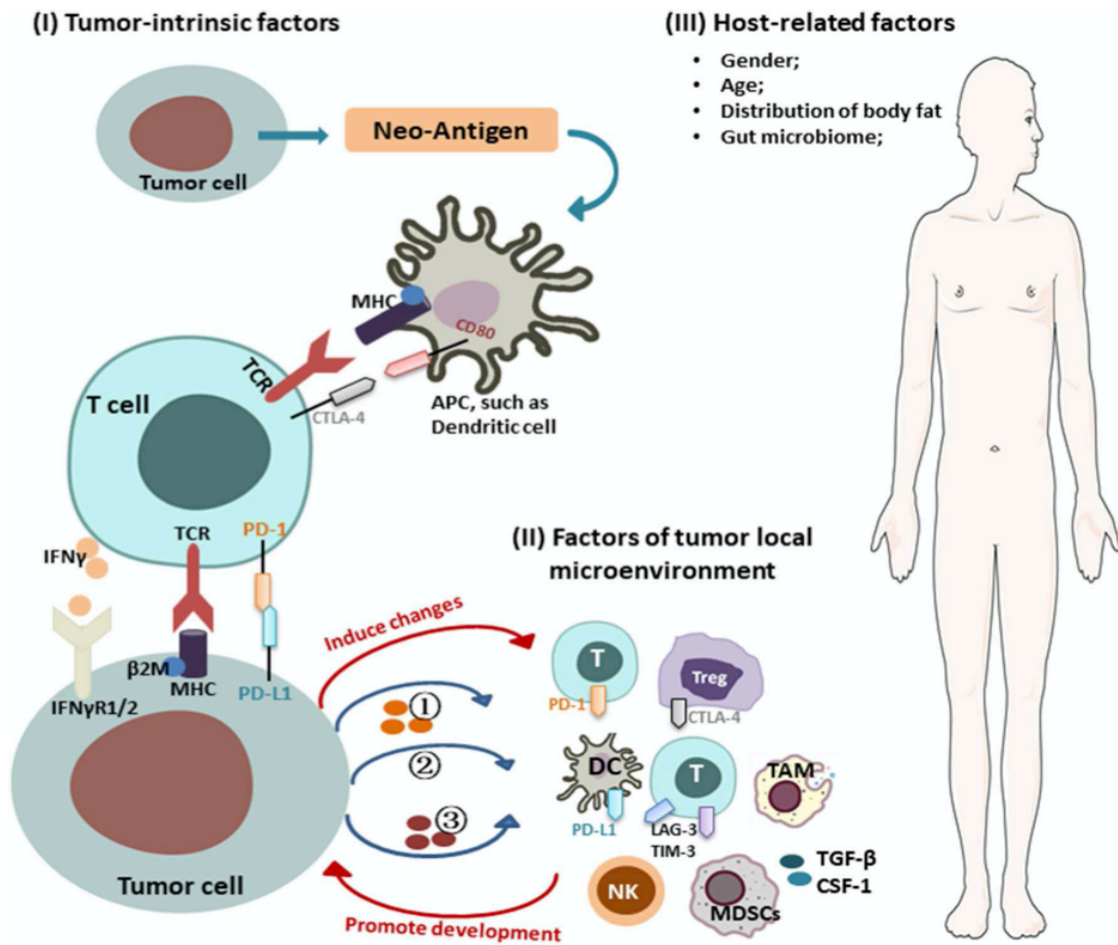


Figure 1.3 Mechanisms of resistance to cancer immunotherapy.

Key mechanisms of resistance to immunotherapy are summarized in three categories: tumor intrinsic factors, host-related factors, and tumor microenvironmental factors (Bai et al., 2020).

1.9 Genome-wide experimental and analytical methods; advantages and limitations

High-throughput sequencing technologies have equipped biomedical researchers to conduct genomic and epigenomic profiling and analyses. The more layers of molecular data we add, the more complete picture we get from underlying biomechanisms. Nevertheless, the variety of choices for experimental technologies and analytical methods may impose some complexities on researchers. Particularly when it comes to comparative genomics and non-human species the availability and compatibility of the methods must be considered. In the following paragraphs, I briefly review the commonly used methods for genome-wide profiling of DNA methylation, gene expression, and somatic mutations, and elaborate on our method of choice for experimental advantages as well as limitations.

1.9.1 Genome-wide DNA methylation profiling

Commonly used methods for DNA methylation profiling mainly differ from the target population of the cells (pooled cells or single cell), the tools of genomic DNA fragmentation (restriction enzymes or sonication), the method of methylated DNA enrichment (affinity enrichment or bisulfite conversion), and the method of reading DNA fragments (sequencing or microarray)(Figure 1.4) (Yong et al., 2016). Genome-wide DNA methylation profiling methods which apply microarray technology are limited to their defined target region and not suitable for exploratory analyses outside the targeted genomic subset and for different species. Bisulfite (BS) conversion-based DNA sequencing is known as the gold standard method for DNA methylation profiling that includes conversion of unmethylated cytosine to uracil using sodium bisulfite followed by sequencing. This method yields single-base resolution of methylated DNA, however, it limits many researchers by the costs of deep sequencing for genome-wide approaches (Yong et al., 2016) (Frommer et al., 1992)(Meissner, 2005).

In this study, I took advantage of genome-wide coverage and lower costs of the MeDIP sequencing experiment for global profiling of methylated DNA as well as its availability for mouse genome. Methylated DNA Immunoprecipitation followed by next-generation sequencing (MeDIP-seq) offers a cost-effective alternative to genome-wide bisulfite sequencing with reasonable resolution (100-300 bp) and accurate enrichment of

methyated DNA based on specific antibody affinity. MeDIP-seq outperforms other genome-wide DNA methylation assays RRBS(reduced representation bisulfite sequencing) and Infinium (BS conversion-based DNA methylation array) for genomic coverage (Bock et al., 2010). However, MeDIP-seq data require statistical correction for CpG bias and transformation to absolute methylation measures. For this, I adopted a specific bioinformatic framework for quantitative sequence enrichment analysis which has been validated by BS-based measurements and experimental data (Grimm et al., 2013)(Lienhard et al., 2017). Nevertheless, MeDIP-seq has limited statistical power to detect differential methylation in poor CpG regions and does not provide single-base resolution. Therefore, I recommend MeDIP-seq as the first experimental choice for global DNA methylation profiling and further validation using BS-conversion-based methods followed by sequencing for deeper methylated DNA readouts.

1.9.2 Genome-wide expression profiling

Commonly used technologies for genome-wide expression analysis include microarrays and transcriptome sequencing (RNA-seq). Both methods provide accurate high-throughput readouts of transcripts, but transcriptome sequencing outperforms microarrays for genomic coverage and it became more favorable as the costs of sequencing are decreasing. RNA sequencing is currently known as the most robust measurement for genome-wide expression and transcriptional activity(Corchete et al., 2020)(Geraci et al., 2020).

The most challenging part of high-throughput expression profiling is the statistical analyses of several thousand transcripts; This represents a very complex type of multiple testing which could produce an unexpectedly high number of false-positive associations. Several statistical methods have been developed to deal with this problem with a specific focus for normalization. Here I briefly introduce some of the most popular normalization methods for RNA-seq analysis including our method of choice –DESeq:

- Transcript length normalization includes depth normalized reads divided by the length of the corresponding transcript in kilobases. This computation yield reads per kilobase per million reads (RPKM) values which used to be the most common measurement for RNA-seq data analysis (Mortazavi et al., 2008). This method may not perform well for bulk RNA-seq and differential analysis because it is not

maintained across samples and could cause biases (Li et al., 2015) (Robinson and Oshlack, 2010).

- The trimmed mean of M-values (TMM) method takes the observations with closest average expression to mean of all samples as a reference and compares all other samples as tests to it. This normalization method provided one of the most simple yet robust ways to estimate the ratio of RNA production and was implemented in popular statistical frameworks like edgeR (Robinson and Oshlack, 2010).
- DESeq method performs an internal normalization on transcript counts where the geometric mean of all transcript counts is calculated and compared to the median of the ratio for each gene (transcript). DESeq method performs similarly to the TMM method in terms of qualitative characteristics of normalized data, the results of differential analysis, and maintaining a false-positive rate. In addition, the DESeq method is specifically developed for differential expression analysis in experiments with smaller sample sizes and overdispersion (Anders et al., 2015)(Anders and Huber, 2010).

Yet, there is no single best pipeline that could be used for all RNA-seq experiments and research applications. Every experiment could adopt a combination of established analytical methods as well as specific modifications upon the aim of the study (Figure 1.5)(Conesa et al., 2016).

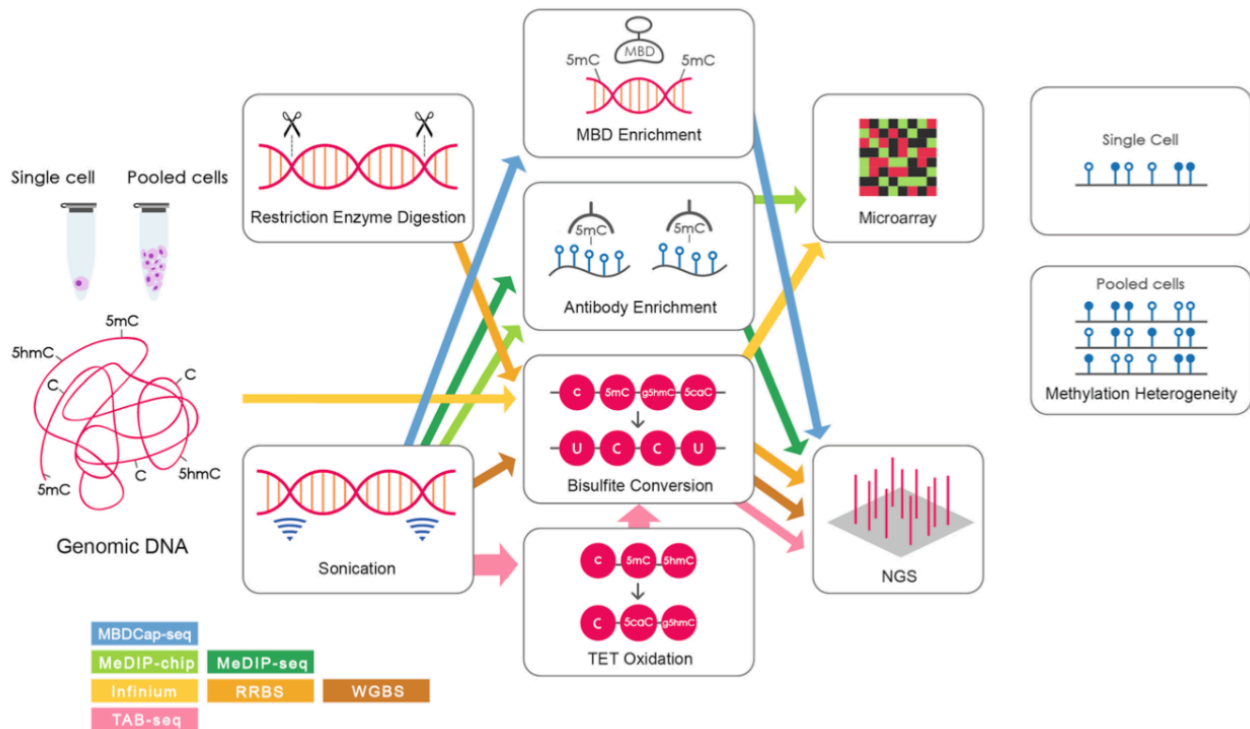


Figure 1.4 A summary of commonly used methods for genome-wide DNA methylation profiling

(Yong et al., 2016). Major differences between the methods are demonstrated by approaching the cell populations or single cell profiling, fragmentation of DNA by random sonication or defined cleavage, enrichment of methylated DNA by bisulfite conversion or enrichment proteins, and reading the methylated DNA by sequencing or microarray.

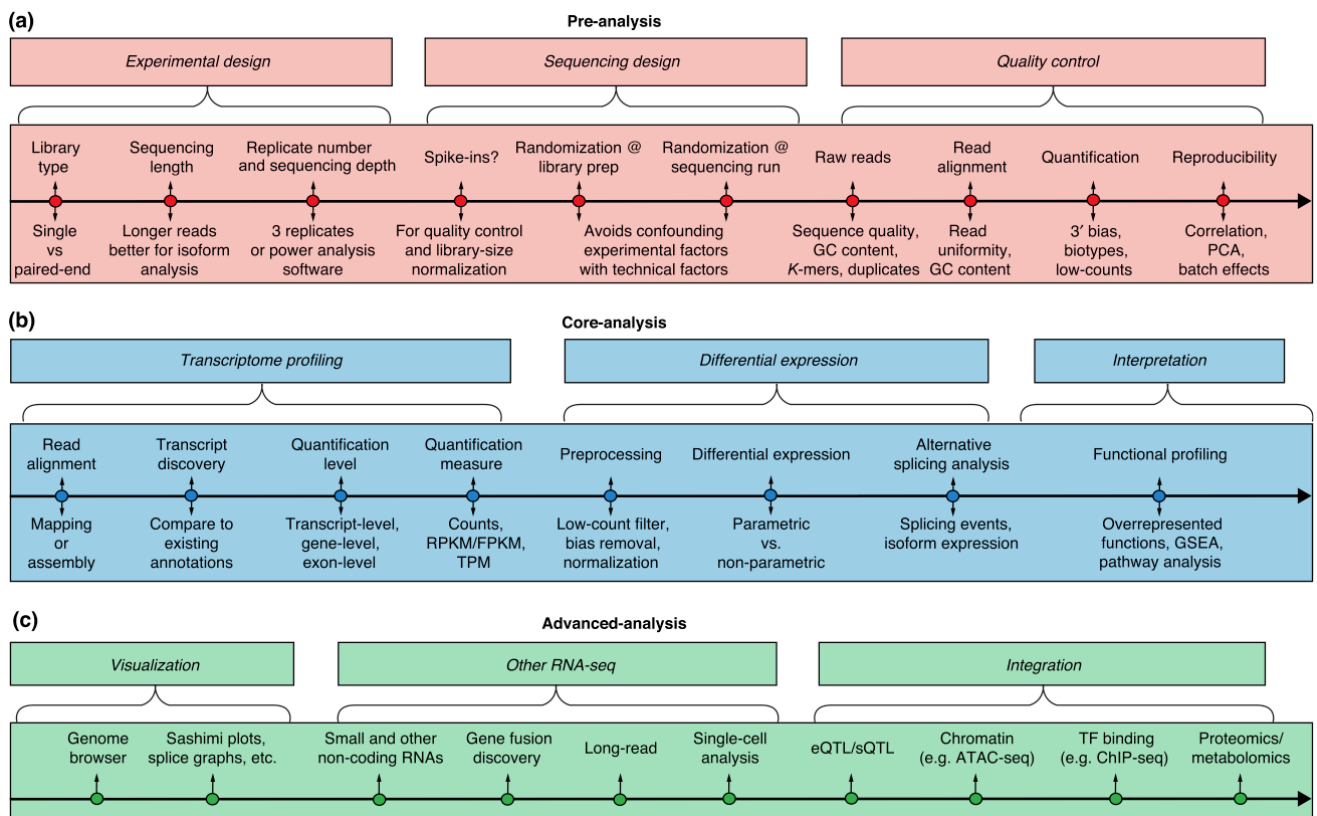


Figure 1.5 Main steps of RNA sequencing experiment and analytical approaches

A) Pre-analysis include design of experiment and sequencing method as well as quality control of the sequencing data.

B) Core-analysis include main analytical approaches for gene expression profiling and analysis: differential expression and biological interpretation.

C) Advanced analysis includes variety of visualizations upon aim of experiment, non-coding RNA and alternative transcripts profiling, single cell RNA sequencing, and variety of omics data integration.

2 Materials and Methods

2.1 Murine melanoma cell lines

2.1.1 Origin and characteristics of the cell lines

HCmel3, HCmel12, HCmel17, HCmel31 melanoma cell lines were generated from DMBA-induced Hgf^{tg}Cdk4^{R24C} primary melanomas with pigmented phenotype as previously described (Landsberg et al., 2012)(Bald et al., 2014)(Ho et al., n.d.). BCmel4 melanoma cell line was driven from a Tyr::Cre^{ERT2} Braf^{L-SL-V600E} Cdk4^{R24C} mouse with the amelanotic phenotype(Ho et al., n.d.). All melanoma cell lines were generated from mice on the C57BL/6 strain background purchased from Charles River and according to the institutional and national guidelines for the care and use of laboratory animals with approval by the local government authorities (LANUV, NRW, Germany).

Splenocyte cell line HCBT was generated from the spleen tissue of a Hgf^{tg}Cdk4^{R24C} mouse as matched normal tissue for all melanoma cell lines in this study.

ACT-resistant cell lines in this study include HCmel3-R1, HCmel3-R2, HCmel3-R2-2, and HCmel17-R cell lines which were generated from a Hgf^{tg}Cdk4^{R24C} relapsed melanoma under Adoptive Cell Transfer (ACT) therapy.

Tumor tissues were collected, dissociated mechanically, incubated with 1 mg ml⁻¹ of collagenase D (Roche) for 30 min at 37 °C, and filtered through 70-µm cell strainers (BD Biosciences). One-million cells were seeded into collagen-coated 6-well plates and cultured in complete RPMI 1640 medium supplemented with 10% FCS (Biochrome), 2 mM L-glutamine (Gibco), 10 mM non-essential amino acids (Gibco), 1 mM HEPES (Gibco), 20 µM 2-mercaptoethanol, 100 IU ml⁻¹ penicillin and 100 µg ml⁻¹ streptomycin (Invitrogen).

To perform Adoptive T-cell transfer (ACT) protocol mice were preconditioned by intraperitoneal injection of 2 mg cyclophosphamide 1 day before intravenous delivery of 2 × 10⁶ naive gp100-specific CTLs isolated from spleens of TCR-transgenic Pmel-1 mice that were activated in vivo by one intraperitoneal injection of 5 × 10⁸ plaque-forming units of the recombinant adenoviral vector Ad-gp100. Fifty micrograms of CpG 1826 (MWG Biotech) and 50 µg of poly(I: C) (Invivogen) in 100 µl PBS were injected peritumorally after

3, 7, and 10 days. Ad-gp100 was propagated on HEK 293 cells, purified by cesium chloride density-gradient centrifugation and subsequent dialysis according to standard protocols as previously described (Landsberg et al., 2012).

CL1 cell line of M1 tumor was generated from a UV induced $Braf^{CA/+}; Pten^{flox/+}; Cdkn2a^{flox/+}, Tyr-Cre^{ERT-tg}$ melanoma, CL2 cell line of M2 tumor from a UV-induced $Braf^{CA/+}; Cdkn2a^{flox/+}, Tyr-Cre^{ERT-tg} Hgf^{tg}$ melanoma, and CL4 cell line of M4 tumor from a UV-induced Hgf^{tg} melanoma as previously described (Pérez-Guijarro et al., 2020).

The B16-F10 cell line was generated as the 10th serial passage subclone of the spontaneous B16 tumor line in C57BL/6 mice and purchased from the American Type Culture Collection (ATCC) (Del Castillo Velasco-Herrera et al., 2018).

Table 2.1 Origin and characteristics of the cell lines

Cell line	Murine background	Genetic modification	Carcinogen	Tumor Phenotype	Therapeutic protocol
HCmel3	C57BL/6	Hgf ^{f9} Cdk4 ^{R24C}	DMBA	Primary	
HCmel3-R1 (HCmel1515)	C57BL/6	Hgf ^{f9} Cdk4 ^{R24C}	DMBA	Resistant	ACT
HCmel3-R2 (HCmel2514)	C57BL/6	Hgf ^{f9} Cdk4 ^{R24C}	DMBA	Resistant	ACT
HCmel3-R2-2 (HCmel3037)	C57BL/6	Hgf ^{f9} Cdk4 ^{R24C}	DMBA	Resistant	ACT
HCmel17	C57BL/6	Hgf ^{f9} Cdk4 ^{R24C}	DMBA	Primary	
HCmel17-R (HCmel3814)	C57BL/6	Hgf ^{f9} Cdk4 ^{R24C}	DMBA	Resistant	ACT
HCmel12	C57BL/6	Hgf ^{f9} Cdk4 ^{R24C}	DMBA	Primary	
HCmel31	C57BL/6	Hgf ^{f9} Cdk4 ^{R24C}	DMBA	Primary	
BCmel4	C57BL/6	Tyr-Cre ^{ERT2} Braf ^{LSL-} V600E Cdk4 ^{R24C}	DMBA	Primary	
HCBmel (splenocyte)	C57BL/6	Hgf ^{f9} Cdk4 ^{R24C}	DMBA	Normal	
CL1 (Mel114433)	C57BL/6	Braf ^{CA/+} Pten ^{flox/+} Cdkn2a ^{flox/+} Tyr-Cre ^{ERT-tg}	UV	Primary	
CL2 (B9013HCB)	C57BL/6	Braf ^{CA/+} Cdkn2a ^{flox/+} Tyr-Cre ^{ERT-tg} Hgf ^{f9}	UV	Primary	
CL4 (B2905)	C57BL/6	Hgf ^{f9}	UV	Primary	
B16-F10	C57BL/6	None	None	Primary	

2.1.2 Cell lines culture and authentication

All the HCmel and BCmel cell lines were cultured in RPMI medium supplemented with 10% FBS and 1% L-glutamine at 37°C in 5% CO₂.

Table 2.2 Medium components for cell culture

Cell culture medium components	Provider
RMPI 1640	Invitrogen
FBS Superior S0615	Biochrom
Penicillin-Streptomycin	Gibco™ 15140122
Sodium Pyruvate MEM 100 mM	Gibco/Invitrogen; 11360-039
MEM Non-Essential Amino Acids Solution 10 mM	Gibco/Invitrogen ; 11140-035
HEPES Buffer Solution 1M	Gibco, 15630-056
Trypsin-EDTA	Gibco, 25300-054
PBS Dulbeccos	Life Technologies 14190094

Cell lines were confirmed as Mycoplasma negative using Mycoplasma-specific PCR. CL1 (Mel114433), and CL4 (B2905) were cultured in RPMI medium supplemented with 10% FBS and 1% L-glutamine. CL2 cell line (B9013HCB) was cultured in Tu2% medium. Authentication of CL1, CL2, and CL4 cell lines was performed by WES, genotyping the alleles in corresponding mouse models and SKY analysis, and was confirmed as Mycoplasma negative using a Mycoplasma detection kit (Lonza, LT07-418)

B16-F10 cells were screened for the presence of mycoplasma and other mouse pathogens (Charles River Laboratories, Wilmington, MA, USA). Cells were cultured at 37°C in 5% CO₂ in high glucose Dulbecco's modified Eagle's medium (DMEM)

supplemented with 10% fetal bovine serum, 29.2 mg·mL⁻¹ L-glutamine, 10 000 units·mL⁻¹ penicillin and 10 000 µg·mL⁻¹ streptomycin.

2.2 DNA and RNA isolation

For HCmel and BCmel cell pellets were collected for each cell to simultaneously extract DNA and RNA using the AllPrep DNA/RNA Mini kit (Cat No. 80204, Qiagen) according to the manufacturer's instructions. Mouse genomic DNA concentration was measured using Nanodrop.

Cell line	DNA ng/µl
HCmel3	62,99
HCmel3R-2	35,08
HCmel3R-1	61,30
HCmel3R-2-2	30,33
HCmel17	35,75
HCmel17-R	59,98
HCmel12	45,59
HCmel31	27,01
BCmel4	39,38
HCBmelMilz	56,66

For B16-F10 cells DNA was extracted from cell pellets using the QIAGEN Puregene Core Kit A.

2.3 Mutational profiling using whole-exome sequencing (WES) technology

2.3.1 Sequencing technology and library preparation for WES experiment

For HCmel, BCmel, and HCBT cell lines DNA quality was measured using Bioanalyzer DNA high sensitivity kit (Agilent Technologies). Exome capture preparation was performed using SureSelectXT Kit for Illumina platform (ILM) of Agilent Technologies. Library preparation for PairedEnd 100-bp sequencing was performed using HiSeq SBS Kit V4 (250 cycle kit) reagents for accurately determining the DNA sequence of each cluster on a flow cell using sequencing by synthesis (SBS) technology on the HiSeq system. Next-Generation Sequencing experiments were performed at the Sequencing Core Facility of the Max-Planck Institute for Molecular Genetics in Berlin.

For CL1, CL2, and CL4 cell lines Mouse genomic DNA concentration was measured using the picogreen assay. A total of 200 ng of DNA was sheared by Covaris Instrument (E210) to ~150–200 bp fragments. Shearing was performed in a Covaris snap cap tube (microTUBE Covaris p/n 520045) with the following parameters: duty cycle, 10%; intensity, 5; cycle burst, 200; time, 360 s at 4 °C. Samples quality assessment was validated by Bioanalyzer DNA high sensitivity kit of Agilent Technologies.

Agilent SureSelectXT library prep ILM Kit (Agilent Technologies, G9611A) was used to prepare the library for each sheared mouse DNA sample. DNA fragment ends were repaired, followed by adenylation of the 3' end and then ligation of the paired-end adaptor. Adaptor-ligated libraries were then amplified (pre-capture PCR amplification: 98 °C 2 min, ten cycles; 98 °C 30 s; 65 °C 30 s; 72 °C 1 min; then 72 °C 10 min, 4 °C hold) by Herculase II fusion enzyme (Agilent Technologies, 600679). After each step, DNA was purified by Ampure XP beads (Beckmann Coulter Genomics, A63882). DNA Lo Bind Tubes, 1.5 ml

of PCR clean (Eppendorf, 022431021), or 96-well plates were used to process the samples.

Samples were analyzed by bioanalyzer using a DNA-1000 kit (Agilent, 5067-1504). The concentration of each library was determined by integrating under the peak of approximately 225–275 bp. Then each genomic DNA library (~750–1,000 ng) was hybridized with biotinylated mouse-specific capture RNA baits (SureSelectXT Mouse All Exon, 5190-4641, 16 reactions) in the presence of blocking oligonucleotides. Hybridization was performed at 65 °C for 16 h using SureSelectXT kit reagents. Bait-target hybrids were captured by streptavidin-coated magnetic beads (Dynabeads MyOne Streptavidin T1, Life Technologies, 6560) for 30 min at room temperature. Then after a series of washes to remove the nonspecifically bound DNA, the captured library was eluted in nuclease-free water and half volume was amplified with individual index (post-capture PCR amplification: 98 °C 2 min; ten cycles, 98 °C 30 s; 57 °C 30 s; 72 °C 1 min; then 72 °C 10 min, 4 °C holds). A Bioanalyzer high sensitivity kit was used to validate the size of the libraries before sequencing.

For the B16-F10 cell line, Paired-end 75-bp libraries were prepared and sequenced using the Illumina HiSeq platform for whole-genome sequencing.

2.3.2 Exome data processing

For HcMel, BcMel, and HcBmel cell lines raw sequence reads (FASTQ files) were evaluated for base quality (Phred-scaled score) per position and per read, read length, GC%, and sequencing depth/coverage using Pre-alignment-QAQC toolkit of Partek Flow (v 8.0).

Sequencing reads were aligned against the Genome Reference Consortium Mouse Build 38 (GRCm38 or mm10) using BWA-mem algorithm (Li, 2013) (BWA v 0.7.15) on Partek Flow with the following input parameters: mismatch penalty 4, gap open penalty 6, min seed length 19, bandwidth 100, extension drop-off 100, reseeding factor 1.5, MEM occurrence limit 10000, matching score 1, gap extension penalty 1, clipping penalty 5, unpaired penalty 9, alignment score cutoff 30. Alignments were sorted, indexed, and converted to BAM files using SamTools and custom command lines of Partek Flow.

Alignment coverage report and target enrichment map were obtained using Post-alignment-QC custom command lines of Partek Flow with the following parameters: coverage level 1,20,50,100, Auto-detect strand specificity, and Annotation model of Ensembl Transcripts release 95.

Aligned reads were filtered for duplicates (reads with same start positions), low mapping score (Min mapping quality 20), mismatch sections (Max mismatched bases 2), singletons, and unaligned reads using custom command lines of Partek Flow.

For CL1, CL2, CL4 cell lines I used processed whole-exome sequencing data (VCF files) deposited on NCBI Gene Expression Omnibus (GEO) under GSE144946. FASTQ sequence reads were mapped to the mouse reference genome mm10 with BWA or Bowtie. All analyses were carried out on NIH's biowulf2 high-performance computing environment. Statistical analysis was carried out in the R environment.

For the B16-F10 cell line, I used published whole-genome sequencing data deposited in the European Nucleotide Archive (ERP001691) (Del Castillo Velasco-Herrera et al., 2018, p. 16). Raw reads were mapped to the mouse reference genome (GRCm38p1) using BWA-mem v 0.7.5 and PCR duplicates marked using Picard tools MarkDuplicates v 1.72.

2.3.3 Somatic variant calling and variants annotation

Somatic variant calling, filtering, and genomic annotations were performed at the Lab of Computational Onco-Immunology –Division Applied Bioinformatics, DKFZ Heidelberg– by Dr. Charles Imbusch under the supervision of Prof. Benedikt Brors. GATK MuTect (Cibulskis et al., 2013) algorithm (v 1.7.0) was used to call single nucleotide variants (SNVs) and short indels in HCBmel and BCMel cells. Normal splenocyte-driven cell line HCBmel was used for matched Normal/Tumor somatic variant calling to filter germline variants in melanoma cell lines. An in-house black list was implemented to filter for murine background variants and low-quality calls. Filtered variants were annotated for functional consequences using the ANNOVAR software tool (Wang et al., 2010) according to the mm10 reference genome. The somatic mutational load was computed as the count of nonsynonymous somatic mutations detected by WES data analyses for every cell line.

For the B16-F10 cell line, single nucleotide variants (SNVs) and short indels were called using Samtools mpileup (v 0.1.19-58-g3d123 cd) and the resulting variants were filtered using VCFTools (Danecek et al., n.d.). Variants with low variant quality (QUAL < 20), or the number of reads supporting the variant less than 5 (DP < 5) or SNPGAP less than 10, were discarded. All the variants reported by the Mouse Genomes Project(Keane et al., 2011) were filtered for the genetic backgrounds of each cell line group. Variants located within ± 50 bp of structural variants reported by the mouse genomes project were discarded. Variants were annotated for functional consequences using Ensemble's Variant Effect Predictor v74(McLaren et al., 2016).

The resulting variants were filtered for duplicates, mismatches, singletons, unaligned reads, poor-quality reads (DP<5), and poor-quality calls (QUAL<20) using VCFtools (Danecek et al., n.d.).

For CL1, CL2, CL4 Single-nucleotide variants were identified using SAMtools-mpileup or GATK HaplotypeCaller. Mouse germline single-nucleotide polymorphisms were filtered out using the Sanger Mouse Genomes Project database for variants identified from whole-genome sequencing of 36 mouse strains. Variants with a Phred-scaled quality score of less than 30 and variants in normal spleen samples of the in-house collection were filtered. Variants were annotated using ANNOVAR software to identify nonsynonymous mutations.

2.3.4 Mutational analysis; somatic mutations heatmap, signatures, and intersections

For HCmel and BCmel cell lines I interpreted key functional genes in melanoma progression and Immunotherapy resistance using the insights of “Genomic Classification of Cutaneous Melanoma”(Akbari et al., 2015), the “Landscape of Driver Mutations in Melanoma”(Hodis et al., 2012)(Hayward et al., 2017), and Cancer Mutation Census (CMC) (GRCh37.COSMIC v92)(Tate et al., 2019).

I implemented the somatic variants data (VCF files) to extract somatic mutational signatures for each cell line according to Wellcome Trust Sanger Institute (WTSI) Mutational Signature Framework in human cancer (COSMIC signatures) (Australian

Pancreatic Cancer Genome Initiative et al., 2013) using deconstructSigs method (v 1.8.0)(Rosenthal et al., 2016) in R (v 4.0.0).

I used UpsetR(Lex and Gehlenborg, 2014) (v 1.4.0) on R (v 4.0.0) to extract the exclusive intersections of mutated genes between HcMel primary and ACT-resistant cell lines and visualize the acquired mutations which candidates for therapy resistance mechanism. I used Integrative Genomic Viewer (IGV) v 2.4.14 (Thorvaldsdottir et al., 2013) to confirm the presence of germline mutations and acquired somatic mutations in ACT-resistant cell lines within their corresponding BAM files.

For CL1, CL2, CL4 cell lines mutation signature analysis, 5' and 3' nucleotide sequences flanking the mutations were retrieved from the mm10 reference genome using Bedtools Getfasta. The frequency of 96 trinucleotides (six substitutions multiplied by 16 combinations of 5' and 3' nucleotides) was computed for each sample with an in-house R script. Cosmic Signatures were identified using the R package deconstructSigs.

For the B16-F10 cell line, somatic mutational signatures were identified using the filtered somatic single nucleotide variants and the non-negative matrix factorization method from the SomaticSignatures R package (v 2.6.1).

2.4 Expression profiling using bulk RNA sequencing (RNAseq) technology

2.4.1 RNAseq library preparation and method

For HcMel cell lines total RNA was implemented to enrich mRNA components using Illumina TruSeq Stranded mRNA LT Sample Prep kit. Sequencing library preparation was performed using the HiSeq SBS Kit V4 250 cycle reagents kit to run paired-end 51-bp sequencing on the HiSeq2500 system. Next-Generation Sequencing experiments were performed at the Sequencing Core Facility of the Max-Planck Institute for Molecular Genetics in Berlin.

For CL1, CL2, CL4 cell lines between 100 ng to 1 µg of total RNA were used to capture mRNA with oligonucleotide-dT coated magnetic beads. The mRNA was fragmented, and then a random-primed cDNA synthesis was performed. The RNA was fragmented into

small pieces and cleaved RNA fragments were copied into first-strand cDNA using RT and random primers, followed by second-strand cDNA synthesis using DNA polymerase I and RNase H. The resulting double-strand cDNA was used as input to a standard Illumina library prep with end repair, adaptor ligation, and PCR amplification being performed to obtain a sequencing-ready library. The final purified product was then quantitated by qPCR before cluster generation and sequencing.

For the B16-F10 cell line, 1 µg of total RNA per sample was submitted for sequencing. Unstranded 75-bp paired-end barcoded libraries were prepared with the standard Illumina library preparation kit. RNA libraries were sequenced on the Illumina HiSeq platform and the data was deposited in public databases (European Nucleotide Archive (ERP001690) and ArrayExpress (E-ERAD-94)).

2.4.2 RNAseq data processing

For HcMel cell lines I used Partek Flow platform (v 8.0) for feasible application of Next Generation Sequencing (NGS) analysis tools and following data processing:

Pre-alignment QA/QC was performed to evaluate read length, read quality, GC%, and read counts. Filtering contaminant reads were done using Bowtie2 (Langmead and Salzberg, 2012) (v 2.2.5) with the following parameters; seed length 22, seed mismatches 0, seed extension attempts 2, the interval between seeds S-1.0-1.25, align to both strands, ambiguous character functions L-0.0-0.15, gaps per read 15, gap end buffer 4, ambiguous character penalties 1, alignment score cutoff L,-0.6,-0.6, mismatch penalty range 6-2, read gap penalties 5-3, reference gap penalties 5-3, max fragment length 500, min fragment length 0, mate orientations forward-reverse. I removed rDNA, mtrDNA, and mismatches before submitting them for alignment. I trimmed 3' adaptors (AGATCGGAAGAGCACACGTCTGAACTCCAGTCA, AGATCGGAAGAGCGTCGTGTAGGGAAAGAGTGT) using CutAdapt tool (v 1.2.1) with following parameters; max error rate 0.1, match times 1, min overlap length 3, min read length 25, quality cutoff 0, zero-cap true.

Filtered reads were subsequently aligned using STAR aligner (Dobin et al., n.d.) (v 2.6.1d) against Genome Reference Consortium Mouse Build 38 (mm10). Aligned reads (BAM files) were directly quantified for gene/transcript counts using the HTSeq program (Anders

et al., 2015) (v 0.11.0) with the following parameters; strand specificity true, min QUAL 10, union overlap mode. HTSeq provides a framework to compute the counts of aligned reads for each gene that overlaps with identical positions of a single gene exon. The output of HTSeq is a count table of gene-transcripts per sample which I obtained for further analyses using the DESeq2 method.

Principal Component Analyses (PCA) was performed using DESeq2 statistical framework in R to explore the variance-covariance of gene expression values within the cell lines for experimental quality control and unsupervised clustering analyses.

2.4.3 Differential expression analysis to identify significant differentially expressed genes between primary and ACT-resistant cell lines

Differential expression analysis was performed between HcMel primary cell lines and their ACT-resistant/escaper cell lines using expression profiles based on DESeq2 (v 3.5) method on R for moderated estimation of Fold Change(FC) and dispersion(Love et al., 2014). DESeq2 applies the Wald test to compare the two groups and to compute the probability of differential expression for each gene between two samples (p-value). I considered a significant cut-off for differentially expressed genes with log-FC of 2 or greater for upregulation and -2 or smaller for downregulation when the adjusted p-value ((Benjamini-Hochberg correction for multiple testing) is smaller than 0.01. Further exploratory analyses and data visualization (volcano plot) was performed to define stricter cut-off of significance based on log-FC and biological functions.

2.4.4 Biological function enrichment analysis

To perform biological functions enrichment for differentially expressed genes, corresponding Gene Ontology terms were implemented by REVIGO(Supek and Bosnjak, 2011) to extract significant biological functions. I confirmed the results using the DAVID algorithm for biological functions and classification (v6.8)(Huang et al., 2007).

I used clusterProfiler (v 3.16.0) (Yu, 2018) in R to compare biological themes amongst gene clusters. I selected significant differentially expressed gene clusters with the three highest functional enrichment scores to show the biological significance of differentially expressed genes between primary and ACT-resistant cell lines.

2.5 DNA-methylation profiling using MeDIP-seq

2.5.1 MeDIP sequencing library preparation and sequencing technology

For all HCmel, BCmel, and HBCmel cell lines Magnetic Methylated DNA Immunoprecipitation kit (MagMEDIP Kit Cat.No. C02010020 mc-magme-A10) by Diagnode was used for capturing methylated DNA. DNA was sheared by sonication to fragments between 100-600 bp. 1 µg or more of sonicated DNA was immunoprecipitated (IP) with a 5-methylcytosine antibody. IP-methylated-DNA was washed and purified using magnetic wash buffer and magnetic rack according to the manufacturer's instructions. IP-methylated-DNA was subsequently purified using IPure kit (Cat.No.AL-100-0100) and validated by qPCR using methylated and unmethylated specific primers for the mouse. Library preparation for next-generation sequencing was performed using NEB Next Ultra Ligation kit reagents. A sequencing experiment was performed using HiSeq SBS Kit, V4 250 cycle kit to run 51-bp paired-end sequencing on the HiSeq2500 machine. Preparation of the libraries and Next Generation Sequencing experiments were performed at the Sequencing Core Facility of the Max-Planck Institute for Molecular Genetics in Berlin.

2.5.2 MeDIP-seq data processing and quality control

raw sequence reads (FASTQ files) were evaluated for base quality (Phred-scaled score) per position and per read, read length, GC%, and sequencing depth/coverage using the Pre-alignment-QAQC toolkit of Partek Flow (v 8.0).

Sequencing reads were aligned against the Genome Reference Consortium Mouse Build 38 (GRCm38 or mm10) using BWA-mem algorithm (Li, 2013) (BWA v 0.7.15) on Partek Flow with the following input parameters: mismatch penalty 4, gap open penalty 6, min seed length 19, bandwidth 100, extension drop-off 100, reseeding factor 1.5, MEM occurrence limit 10000, matching score 1, gap extension penalty 1, clipping penalty 5,

unpaired penalty 9, alignment score cutoff 30. Alignments were sorted, indexed, and converted to bam files using SamTools and custom command lines of Partek Flow.

Alignment coverage report and target enrichment map were obtained using Post-alignment-QC custom command lines of Partek Flow with the following parameters: coverage level 1,20,50,100, Auto-detect strand specificity, and Annotation model of Ensembl Transcripts release 95.

Aligned reads were filtered for duplicates (reads with same start positions), low mapping score (Min mapping quality 20), mismatch sections (Max mismatched bases 2), singletons, and unaligned reads using custom command lines of Partek Flow.

2.5.3 Quantitative CpG enrichment and differential DNA-methylation analysis

I performed quantitative sequence enrichment analysis using QSEA (Lienhard et al., 2017) for enriched CpG sites. This includes normalization, transformation to absolute methylation level, and differential methylation analysis.

I used QSEA for statistical modeling and transformation of MeDIP-seq enrichment data to absolute methylation levels similar to BS-sequencing read-outs. The transformation works based on a Bayesian model that explicitly takes background reads and CpG density-dependent enrichment profiles of the experiments into account. Data normalization accounts for the effect of CNVs on the read counts. For differential methylation analysis, QSEA implements generalized linear model (GLM) and a likelihood ratio test, similar to tests I performed to detect differentially expressed genes in DEseq2. Using this method, read counts were modeled with a negative binomial distribution with mean and dispersion parameters. For each window, it fits a GLM with a logarithmic link function. Significance testing is performed by fitting a reduced model, then the likelihood ratio (LR) of the models was compared to a Chi-squared distribution.

Read pairs greater than 1000bp were filtered to reduce non-specific enrichment background reads. Beta values were computed as an estimation of methylation level using the ratio of intensities between methylated and unmethylated CpG sites. Genomic regions (bins) with greater than 2 CpG sites were included to compute Beta values with a confidence interval of 20%.

CpG density was mapped using CpG Islands (CGIs) reference of UCSC for mouse genome (mm10) and CGI shores were considered 2kb upstream and downstream of each CGI. Transcription Start Site (TSS) bins were mapped according to Ensemble Transcripts reference for mouse genome (GrCm38.5 Biomart). Gene promoter regions were considered in 2kb upstream and downstream of TSS (TSS shores).

PCA was performed to explore and visualize the variance-covariance of bins with confident Beta values within DNA-methylation profiles. Clustering analysis was performed within the regions with 1% highest CpG density for primary and ACT-resistant (HCmel) cell lines. Splenocyte and BCmel cell lines were implemented as controls for different epigenetic backgrounds and identical DNA-methylation profiles.

Differentially methylated regions (DMRs) were computed using the QSEA method comparing primary and ACT-resistant cell lines of the Hgf-Cdk4 model. Clustering analysis was performed as quality control of experimental design for DMRs with a p-value smaller than 0.01 and a q-value smaller than 0.05 to evaluate the significance of clustering between primary and resistant cell lines.

DMRs were annotated using Ensemble Transcripts reference (GrCm38.5_biomart) and Cancer Gene Census was used to extract functional implications in melanoma.

Database for Annotation, Visualization, and Integrated Discovery (DAVID)(Huang et al., 2007) was used to classify biological functions of significant differentially methylated genes.

2.5.4 Functional enrichment analysis of DMRs

I used clusterProfiler(Yu, 2018) (v 3.16.0) in R version 4.0.0 to compare Bioprocesses and Gene Ontology (GO) among gene clusters. I selected significant differentially methylated genes with the highest functional enrichment scores (top 3 levels) to show their biological significance in primary and ACT-resistant cell lines.

3 Results

3.1 Genomic characterization of the preclinical mice driven cell lines recapitulate diverse molecular subtypes of human melanoma

Preclinical mice models of human melanoma have been broadly used to improve precision immunotherapy and targeted therapy in melanoma, but they have not been well characterized for mutational landscapes. To characterize somatic mutational profiles and processes I selected two transgenic models and corresponding cell lines which were previously established and developed for ACT therapy in the lab of Experimental Dermatology, University Hospital of Bonn: Hgf-Cdk4 and Braf-Cdk4 (Landsberg et al., 2012)(Bald et al., 2014)(Ho et al., n.d.). I conducted whole-exome sequencing (WES) analysis for four primary melanoma cell lines driven from Hgf-Cdk4; HCmel3, HCmel17, HCmel12, HCmel31, and one cell line driven from Braf-Cdk4 model; BCmel4. Normal spleen tissue of an Hgf-Cdk4 mouse was been used as germline mutational background for all melanoma cell lines in this study.

In addition, I used publicly available genomic data -whole exome and whole genome- of murine models $Braf^{CA/+}$; $Pten^{flox/+}$; $Cdkn2a^{flox/+}$, $Tyr-Cre^{ERT-tg}$, $Braf^{CA/+}$; $Cdkn2a^{flox/+}$, $Tyr-Cre^{ERT-tg}$ Hgf^{tg} , Hgf^{tg} (successively CL1, CL2, CL4 cell lines), and B16 (B16-F10 cell line) to recapitulate different molecular subtypes of human skin melanoma for comparative mutational analysis.

3.1.1 Exome sequencing, somatic variant calling, and evaluation of the results

To analyze somatic mutational landscapes of HCmel and BCmel melanoma cell lines we performed somatic variant calling using exome data for each cell line. Evaluation of exome sequencing data showed high base call accuracy with an average Phred score of 35, and a low duplication rate which supports greater than 92% unique reads. Evaluation of exome capture efficiency reported 60-70% coverage of targeted regions with 20-fold sequencing depth for 90% of replicates that show successful target enrichment to perform variant calling for each cell line (Figure 3.1 and Figure s1 in supplements).

To evaluate the correlation of the cell lines based on their exome mutational profiles hierarchal clustering was performed on their somatic single nucleotide variants (SNVs);

results show consistency with the origin of the cell lines and our experimental design. (Figure 3.2)

3.1.2 Mutational loads and driver mutations in HCmel and BCmel primary melanoma cell lines (compared to other murine melanoma cell lines)

Comparison of nonsynonymous single nucleotide somatic mutations count between all HCmel and BCmel cell lines showed that BCmel4 harbors the lowest mutational load with 48 and HCmel12 the highest mutational load with 521 mutations. Hcmel3 and HCmel17 show very similar mutational load successively with 438 and 443 while HCmel31 stands in the middle with 203 nonsynonymous somatic mutations. Somatic signatures analysis showed a predominance of A>T base transversions which is consistent with 7,12-dimethylbenz(a)anthracene (DMBA) exposure during tumorigenesis of HCmel and BCmel melanomas.

I compared these results with the somatic mutation profiles of CL1, CL2, CL4 cell lines which were driven from UV-induced melanomas, and B16-F10 which was driven from spontaneous melanoma; CL1 harbors germline modifications in Braf, Cdkn2a, and PTEN genes and appeared to harbor higher somatic mutational load than all HCmel and BCmel cell lines. CL2 harbors germline mutations in Braf, Hgf, and Cdkn2a and showed a lower mutational load than HCmel12, HCmel3, and HCmel17 but similar to HCmel31. CL4 stands in the middle bearing germline modification of Hgf, and mutational load in between CL1 and CL2 (Figure 3.3 B). Somatic mutational signatures of CL1, CL2, and CL4 showed prevailed C>T base transitions which mirror UV-induced melanoma genesis in corresponding tumors (Figure 3.3 A). To compare mutational characteristics of the cell lines with human melanoma key driver genes I adopted “Genomic Classification of Cutaneous Melanoma”, the “Landscape of Driver Mutations in Melanoma”, and the Cancer Mutation Census (CMC). A matrix of mutated genes in preclinical models depicts diverse genetic subtypes of human melanoma and highlights that Hgf-Cdk4 and Hgf-Braf models together recapitulate the melanomas classified under BRAF-RAS-NF1-wild-type and BRAF-mutated (Figure 3.3 C).

3.1.3 Mutational characterization of ACT-resistant HCmel cell lines compared to their corresponding primary cell lines

Landsberg and her colleagues at the lab of Experimental Dermatology, University Hospital of Bonn, previously showed that dedifferentiated melanomas resist ACT immunotherapy in a pro-inflammatory tumor microenvironment. I was interested to dissect the genetic drivers of this dedifferentiated resistant phenotype versus epigenetic selection. To meet this aim, I first analyzed somatic mutational loads and somatic mutational signatures using corresponding exome sequencing data and with the same methods previously described for primary melanoma cell lines of Hgf-Cdk4 melanoma. I used four ACT-resistant escapers of HCmel3 and Hcmel17 for this analysis: HCmel3-R, HCmel3-R1, HCmel3-R2, HCmel3-R2-2, and HCmel17 (Figure 3.4). Mutational loads show increased in all ACT-resistant escapers compared to their primary cell lines while somatic signatures do not show any difference (Figure 3.5).

3.1.4 Acquired mutations in ACT-resistant cell lines: Random genomic aberrations/mutations can cause dedifferentiation in melanoma cells leading to ACT-resistance in the Hgf-Cdk4 mouse model

To identify acquired mutations that could drive melanocytic dedifferentiation leading to ACT-resistance in the Hgf-Cdk4 model I detected nonsynonymous somatic variations which were exclusively shared between Hgf-Cdk4 driven cell lines with ACT-resistant phenotype (HCmel-R cell lines). 132 mutated genes were exclusively shared between HCmel3-R1, HCmel3-R2, HCmel3-R2-2, and HCmel17-R and were not mutated in HCmel3 and HCmel17. I focused on genes with known functional implications in melanoma genesis, differentiation, and immunotherapy resistance which were mutated in all ACT-resistant cell lines. 116 of these genes were identified as functionally known using DAVID functional annotation and Gene Ontology enrichment analysis, and 7 genes were tiered by COSMIC Cancer Mutation Census (CMC v92) namely CASP8, DCAF12I2, EXT2, GNAQ, LZTR, MUC4, SMC1A.

I identified AXL as a solely mutated gene which was also differentially downregulated in all ACT-resistant melanoma cell lines compared to primary melanoma cell lines. This exonic mutation in AXL is a T>A genomic base transition which translates to W317R in the amino acid sequence of AXL receptor tyrosine kinase.

Finally, I curated a list of 37 mutated genes in all ACT-resistant melanoma cell lines using databases mentioned before, experimental data, and scientific literature; These mutated genes may suggest potential candidates for contribution to ACT-resistance mechanisms in melanoma cells solely or in contribution to epigenetic drivers and regulators (Table 3.1).

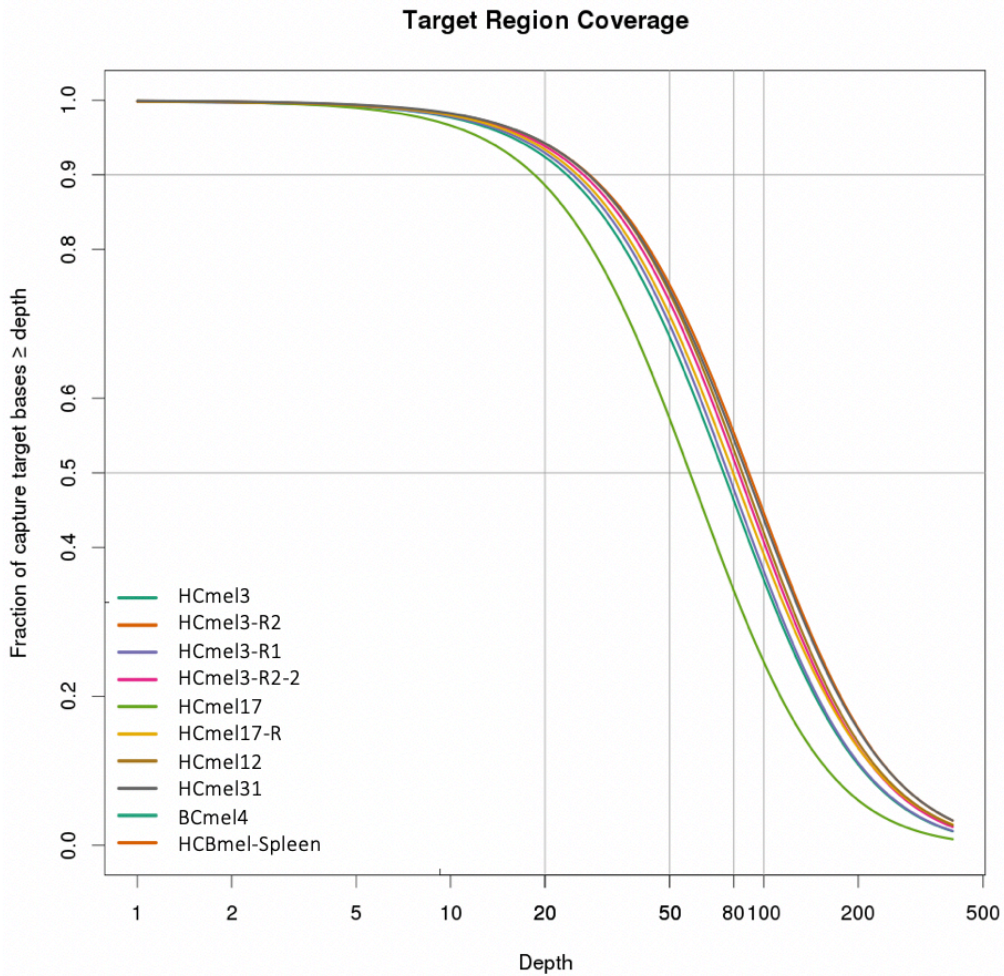
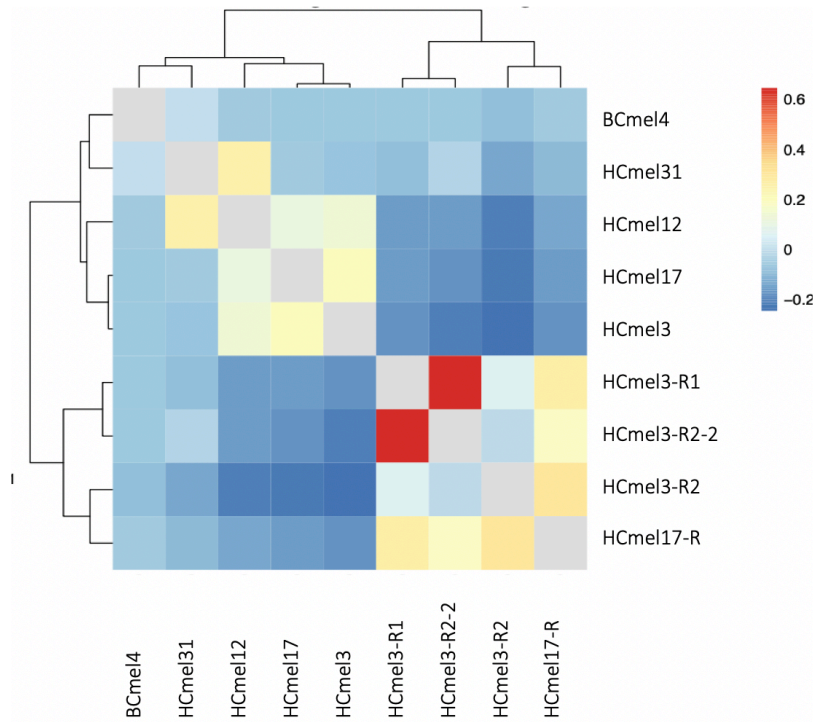


Figure 3.1 Exome data quality and sequencing coverage for HCmel and BCmel cell lines.

Evaluation of sequencing coverage of targeted exomes shows that our experiment provides 20 unique reads for targeted regions in 90% of replicates. This plot was generated by Dr. Stefan Börno at the sequencing core facility of the Max Planck Institute in Berlin, where we performed the NGS experiments of this study.

A



B

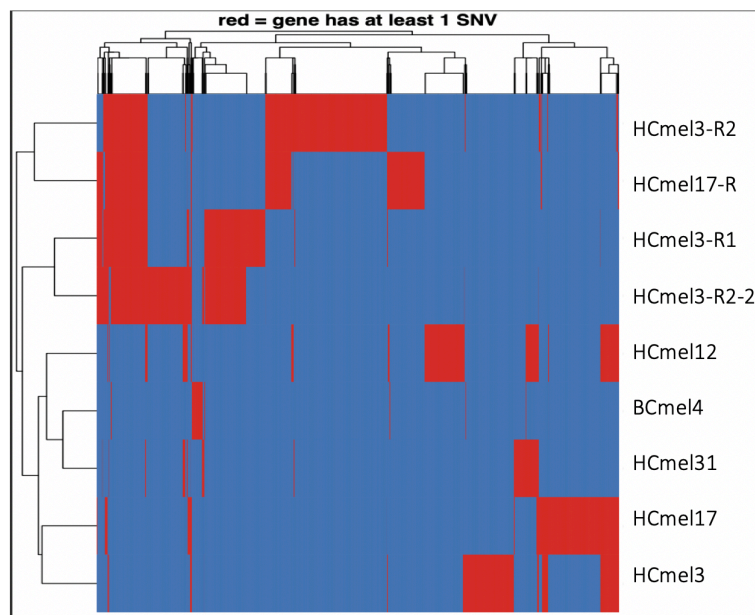


Figure 3.2 Evaluation of somatic variant calling in BCmel and HCmel exome profiles.

A) Pearson correlation of single nucleotide variants (SNVs) was performed as a quality control of somatic variant calling to discard self-correlation between samples. B) Hierarchical clustering of the cell lines using SNVs in Exome profiles consists with the origin of the cell lines and our experimental design. These plots were generated by Dr. Charles Imbusch as he contributed to somatic variants calling which was comprehensively explained in methods.

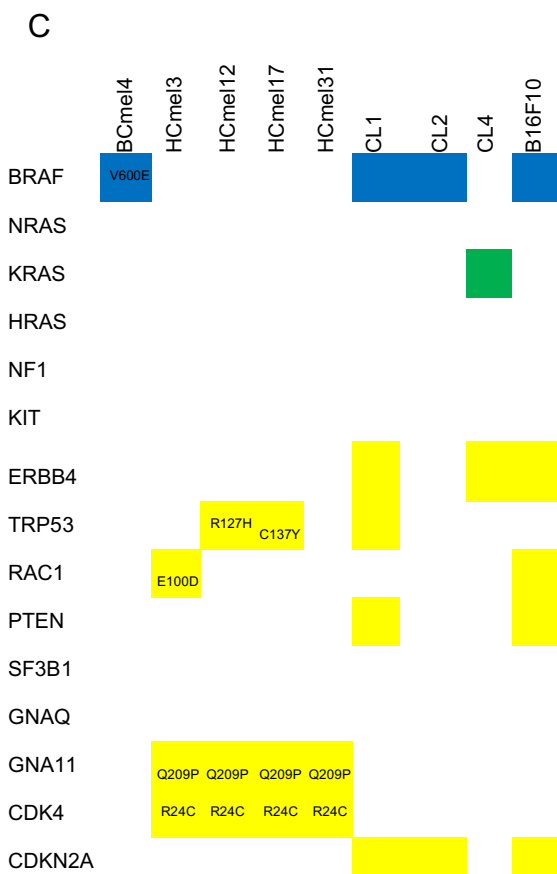
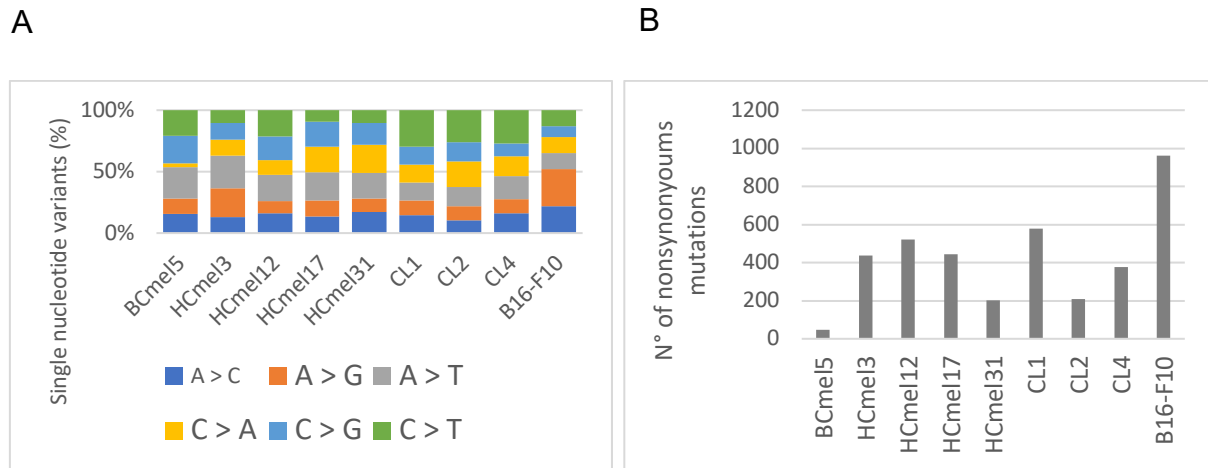


Figure 3.3 Comparison of mutational landscapes between primary melanoma cell lines of different GEM models and spontaneous melanoma (B16)

A) Somatic mutational signatures in HCmel and BCmel cell lines compared to CL1, CL2, CL4, and B16-F10 cell lines recapitulate diversity of major base alterations and melanoma genesis in preclinical models. **B)** Mutational loads show the number of single nucleotide nonsynonymous somatic mutations in every cell line with diverse genetic backgrounds. **C)** Matrix of mutations in key driver genes of human melanoma mirrors the genetic characteristics of preclinical models in our study. Color codes were adopted from “Genomic classification of Cutaneous Melanoma” (Akbari et al.); blue for BRAF-mutated, green for RAS-mutated, and yellow for BRAF-RAS-NF1-wilde-typemelanomas.

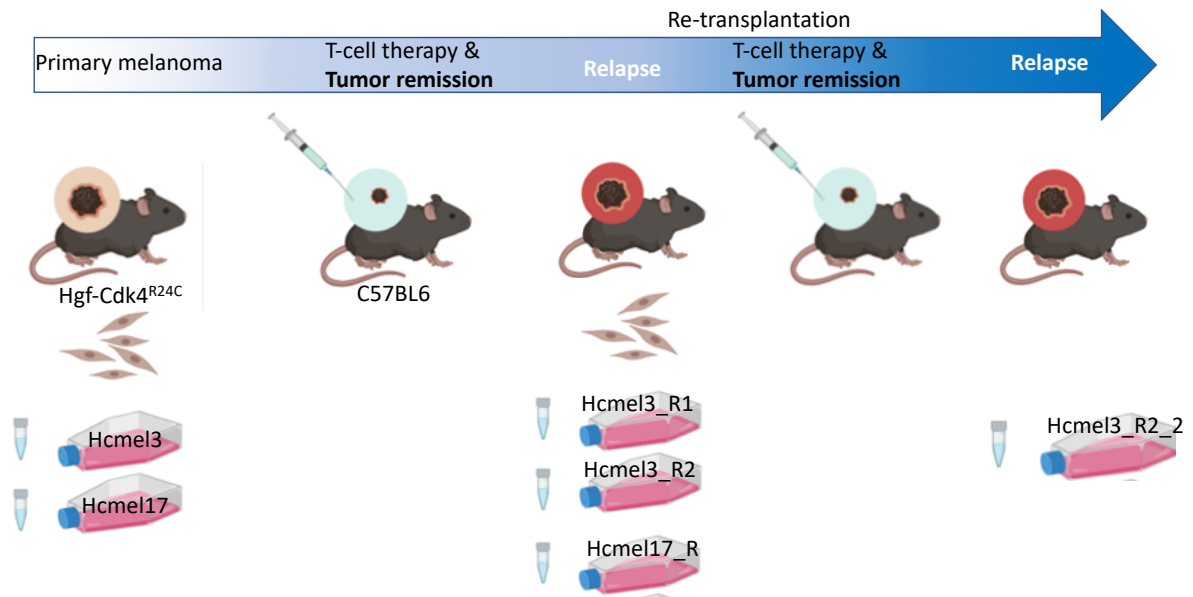


Figure 3.4 Hgf-Cdk4R24C murine preclinical model of melanoma for studying resistance mechanism to adoptive T cell transfer (ACT) immunotherapy

Graphical summary of experimental design to generate HCmel primary melanoma cell lines and their ACT-resistant (HCmel-R) escapers for molecular studies on pro-inflammatory induced dedifferentiation and ACT-resistance (Created with BioRender.com).

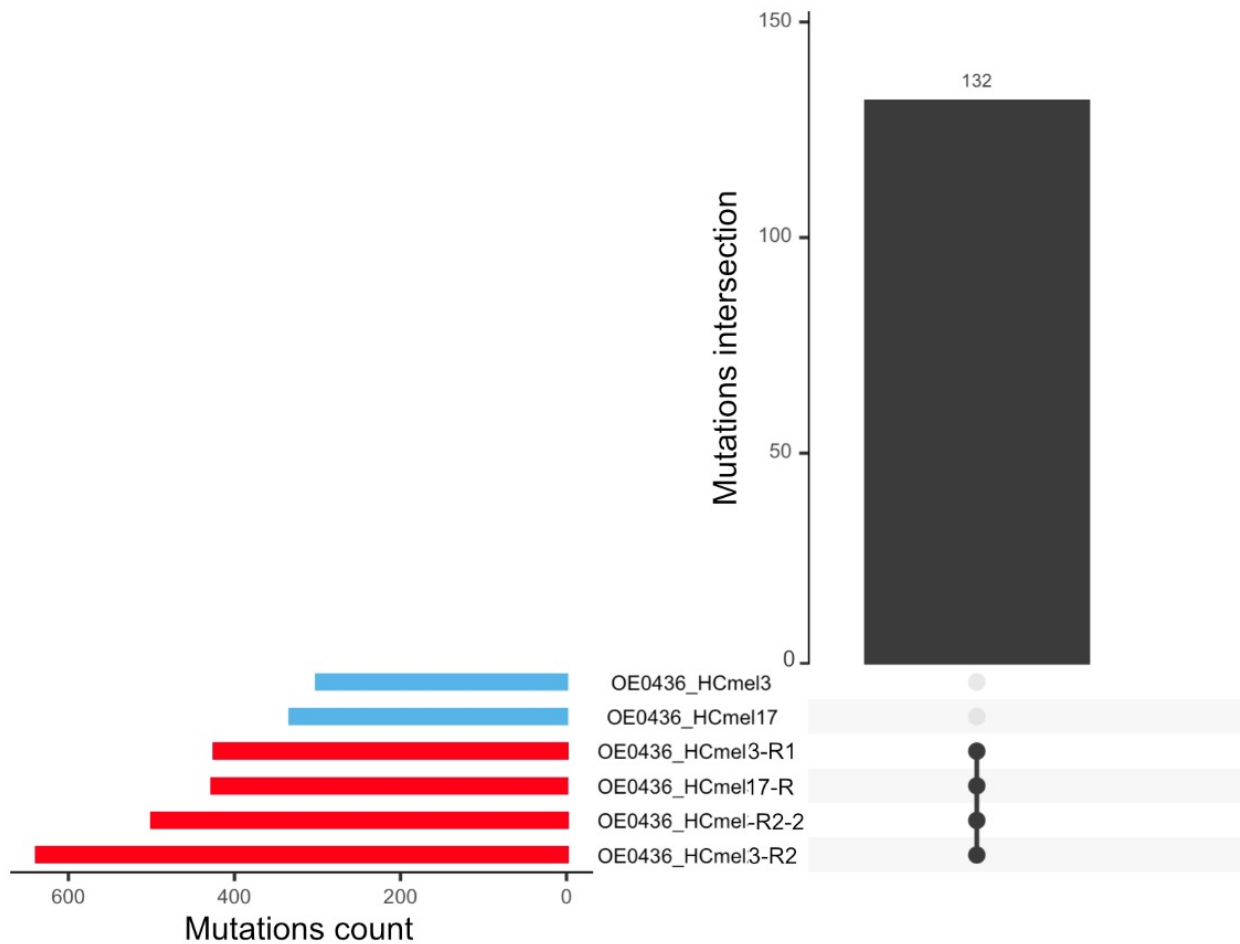


Figure 3.5 Somatic nonsynonymous mutations were acquired in ACT therapy-resistant HcMel-R melanoma cell lines compared to primary HcMel cell lines.

Left: bar plot shows mutational loads (set size) increased in resistant cell lines compared to primary cell lines (HcMel3 and HcMel17). Right: upset plot shows intersect (intersection size) of exclusively shared mutated genes within one upset. 132 mutated genes are exclusively shared between resistant cell lines HcMel3-R1, HcMel3-R2, HcMel3-R2-2, and HcMel17-R.

Table 3.1 Exclusively shared mutated genes between all ACT-resistant (HCmel-R) melanoma cell lines candidate for contribution to resistance mechanisms

37 genes (out of 132) were selected for known biological functions and potential relevance to melanoma cell proliferation, differentiation, and immunogenic response. Cancer Mutation Census (CMC) tier 1 is colored in red meaning strong relevance to cancer and oncogenic transformation, tier 2 is colored in orange meaning a strong indication of a role in cancer with less experimental evidence. Genes involved in immunity are colored in purple and genes with a known role in epigenetic control and differentiation are colored in green.

Gene ID	Mutations	CMC tier	Biological functions on GO, DAVID, and Protein Atlas (THPA)
AHR	c.T835G: p.F279V	NA	Development and differentiation, cell cycle regulation
ARHGAP21	c.G4186C: p.D1396H c.G4216C: p.D1406H	NA	GTPase-activating protein, Cell adhesion
ATR	c.A2864T: p.Q955L	1; Tumor suppressor	Suppression of growth, genome instability, escaping programmed cell death, change of cellular energetics
AXL	c.T949A: p.W317R	NA	Cell proliferation, differentiation, survival, motility, immunologic response
BCR	c.A448T: p.S150C	1; Fusion	Cell survival, differentiation, and function of B cells
CASP8	c.G1312A:p.G438R	1; Tumor suppressor	Proliferative signaling, tumor-promoting inflammation, invasion and metastasis, angiogenesis, escaping programmed cell death
CD9	c.T442G: p.L148V	NA	Cell adhesion and motility, tumor metastasis, immunologic response
CLGN	c.A149T: p.K50M	NA	Differentiation factor
DCAF12L2	c.G982A:p.A328T	2; NA	Cell cycle, apoptosis
EXT2	c.A314C: p.K105T	1; Tumor suppressor	Prognostic marker in renal cancer
EYA3	c.A160G: p.M54V c.A112G: p.M38V	NA	Transcription regulator, DNA repair, developmental protein
FBXL4	c.A1755T: p.K585N	NA	Cell cycle control
GDF6	c.A428T: p.H143L	NA	Growth, differentiation factor, apoptosis, cytokine
GNAQ	c.A626T: p.Q209L	1; Oncogene	Proliferative signaling
GSTA4	c.T647A: p.V216D	NA	Cellular defense

HIVEP2	c.A922T: p.R308X	NA	DNA-binding transcription regulator, enhanced in keratinocytes
IGSF9B	c.G318T: p.E106D c.G318T: p.E106D	NA	Immunoglobulin superfamily member, Cell adhesion, enhanced in keratinocytes
IHH	c.T643G: p.W215G	NA	Developmental protein-enhanced in undifferentiated cells, prognostic marker in endometrial cancer
ITPR3	c.A2439T: p.K813N	NA	Metabolism and growth
KRT13	c.A833T: p.E278V	NA	Cell structure, prognostic marker in renal cancer
LZTR1	c.T427G: p.L143V	2; Tumor suppressor	Negative regulator of RAS-MAPK signaling
MMP8	c.A329T: p.H110L	NA	Matrix metalloproteinase
MTF1	c.A1163T: p.Q388L	NA	DNA-binding transcription regulator
MUC4	c.G29A: p.W10X	2; Oncogene	Tumor progression and growth, apoptosis repressor
PAX4	c.T409G: p.L137V	NA	DNA-binding transcription regulator, Differentiation
PAXIP1	c.A2932C: p.M978L	NA	DNA repair and transcription regulation
PLCG2	c.A812C: p.K271T	NA	Transmembrane signaling, prognostic marker in renal cancer, mutated in autoinflammation
POLR2H	c.T154G: p.L52V	NA	DNA-binding subunit of RNA-polymerase II, prognostic marker in renal cancer
PRMT5	c.A1159T: p.R387W	NA	Methyltransferase , transcription and chromatin regulator, methylates multiple target genes in cell proliferation, migration, and differentiation
SMC1A	c.C1756T: p.R586W	2; Tumor suppressor	Cell cycle regulation, DNA repair
TIPARP	c.A1637G: p.N546S	NA	Transferase, transcription regulator for AHR, prognostic marker in breast cancer
TNFSF4	c.A34T: p.N12Y	NA	Cytokine of TNF family, antigen presentation (APC), and stimulating T-cell proliferation
TRIML1	c.G1174A: p.D392N	NA	Transferase and developmental protein in Ubl pathway
UBL7	c.T137G: p.L46R	NA	Ubl conjugation pathway
WNT10A	c.T746A: p.V249E	NA	Developmental protein in WNT signaling pathway, oncogenesis
ZFC3H1	c.A3093T: p.E1031D	NA	Subunit of PAXT complex, prognostic marker in renal cancer
ZW10	c.T1326A: p.D442E	NA	Cell cycle regulation and cell division

3.2 Expression profiling revealed differentiation signature in HCmel melanoma cell lines

To expand on molecular characterization of Hgf-Cdk4 preclinical model-driven cell lines I conducted expression profiling using RNA sequencing data for primary melanoma cell lines (HCmel3, HCmel17, HCmel12, HCmel31) and their escapers on ACT therapy (HCmel17-R, HCmel3-R1, HCmel3-R2, HCmel3-R2-2). I was particularly interested in expression signatures related to resistance mechanisms in these cell lines.

3.2.1 Bulk mRNA enrichment, quantification of transcript counts, and evaluation of the results

Evaluation of mRNA sequencing data showed high base call accuracy with an average Phred score of 37 which means greater than 99.9% accurate identification of nucleobases. Target enrichment efficiency assay reported greater than 80% on-target coverage with ~40-fold sequencing depth. These values showed successful target enrichment and sufficient data quality to perform gene expression profiling for each cell line (Figure 3.6 and Figure s2 in supplements).

3.2.2 Principal component analysis on expression profiles indicates two distinct groups of primary and resistant cell lines

To explore the relationships and co-variances between the cell lines I first conducted an unsupervised clustering principal component analysis (PCA) based on log-transformed normalized transcripts counts for all samples. PCA results showed that expression profiles distinctly differ between primary and ACT-resistant cell lines. The clustering pattern of the samples on the PCA plot showed consistency with our experimental design and origin of the cell lines (Figure 3.7).

3.2.3 Differentially expressed genes in primary and ACT-resistant cell lines indicated downregulation of melanocytic differentiation genes in resistant phenotypes

According to previous experimental data published by Landsberg et al., dedifferentiation and phenotypic plasticity suggest a resistance mechanism in preclinical melanomas against T-cell therapy. To study molecular elements of this resistant phenotype in the Hgf-Cdk4 preclinical model, I differentially analyzed the expression profiles of ACT-resistant HCmel cell lines (HCmel3-R1, HCmel3-R2, HCmel3-R2-2, and HCmel17-R) compared to primary HCmel cell lines (HCmel3, HCmel17, HCmel12, HCmel31). Differential expression analyses confirmed downregulation of melanocytic differentiation key genes in ACT-resistant melanoma cells highlighting *Mitf*, *Pmel*, *Tyr*, *Sox10*, and *Mlana*. On the other hand, upregulated genes underlined proliferative and metastatic functions in resistant cell lines namely *Fosl1*, *Cdk6*, *Col8a1*, *Col12a1*, and *Hdgf*. Furthermore, functional interactions in most variable differentially expressed genes of resistant profiles built up three major clusters of “cell cycle”, “differentiation regulators” and “melanocytic differentiation” (Figure 3.8 A-D).

A



B

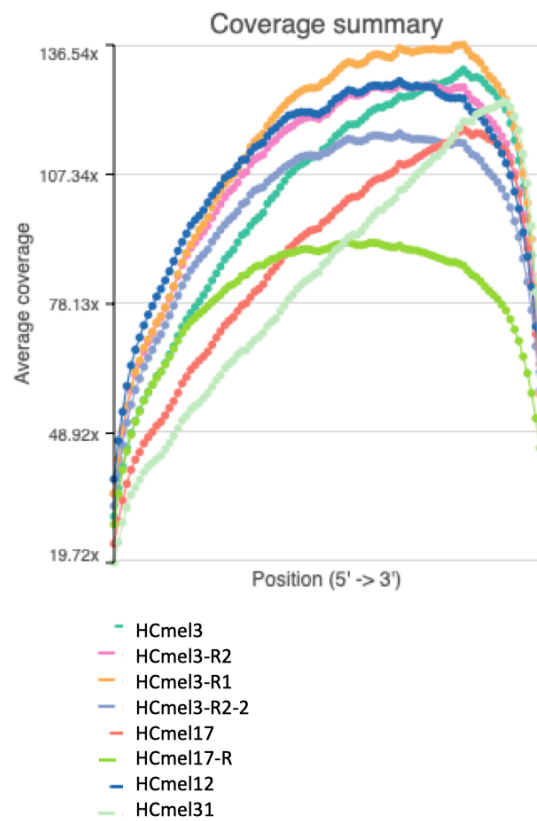


Figure 3.6 RNA sequencing experiment, data quality, and coverage report for HCmel cell lines.

A) Graphical summary of the RNAseq experiment workflow (Created with BioRender.com).

B) RNA sequencing coverage summary describes at least 40x of reads per position that aligned to known reference sequence (Created using PartekFlow alignment tools).

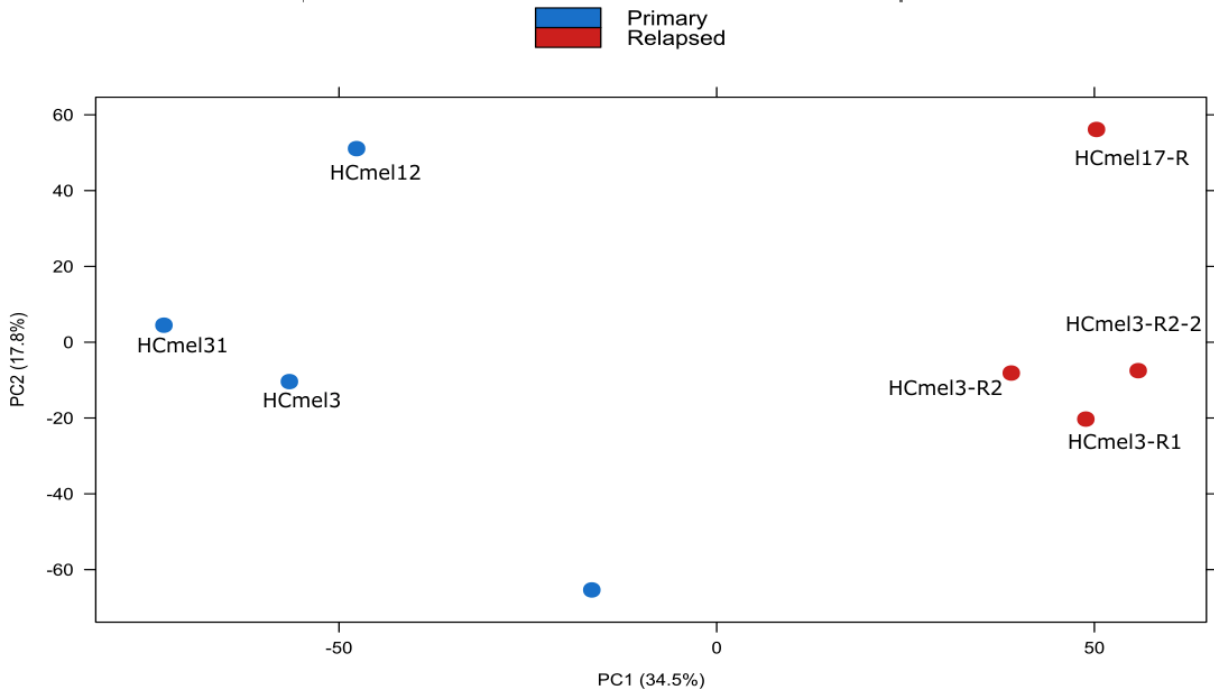


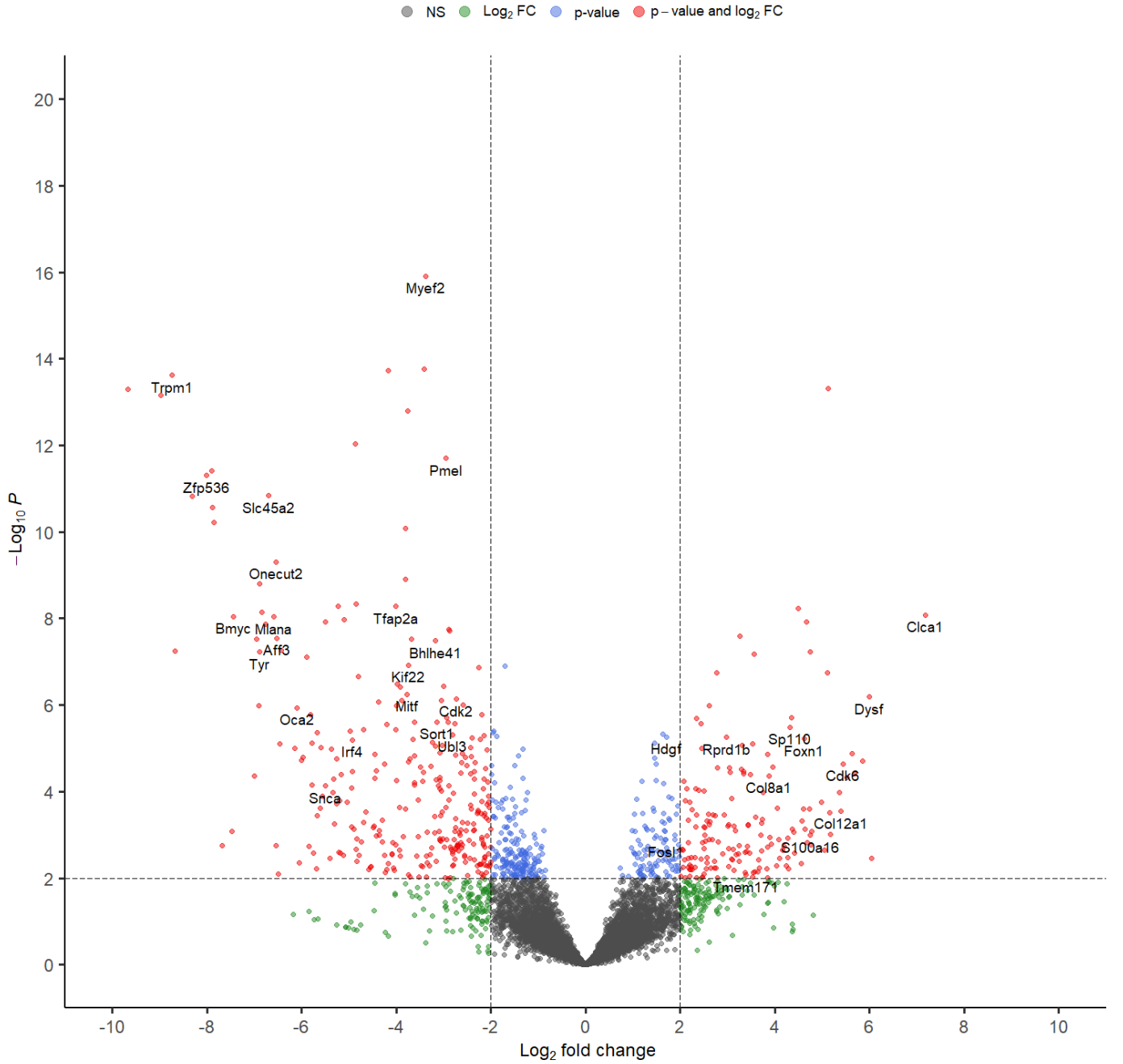
Figure 3.7 Unsupervised principal component analysis on expression profiles indicates two distinct groups of primary and resistant cell lines

Using the DESeq2 method I computed the regularized \log_2 transform of the normalized transcripts counts for all samples. PC1 and PC2 indicate the first and the second principal components along which the cell lines show the most variation in gene expression values. The more similar gene expression profiles are, the closer they appear on the PC1 axis.

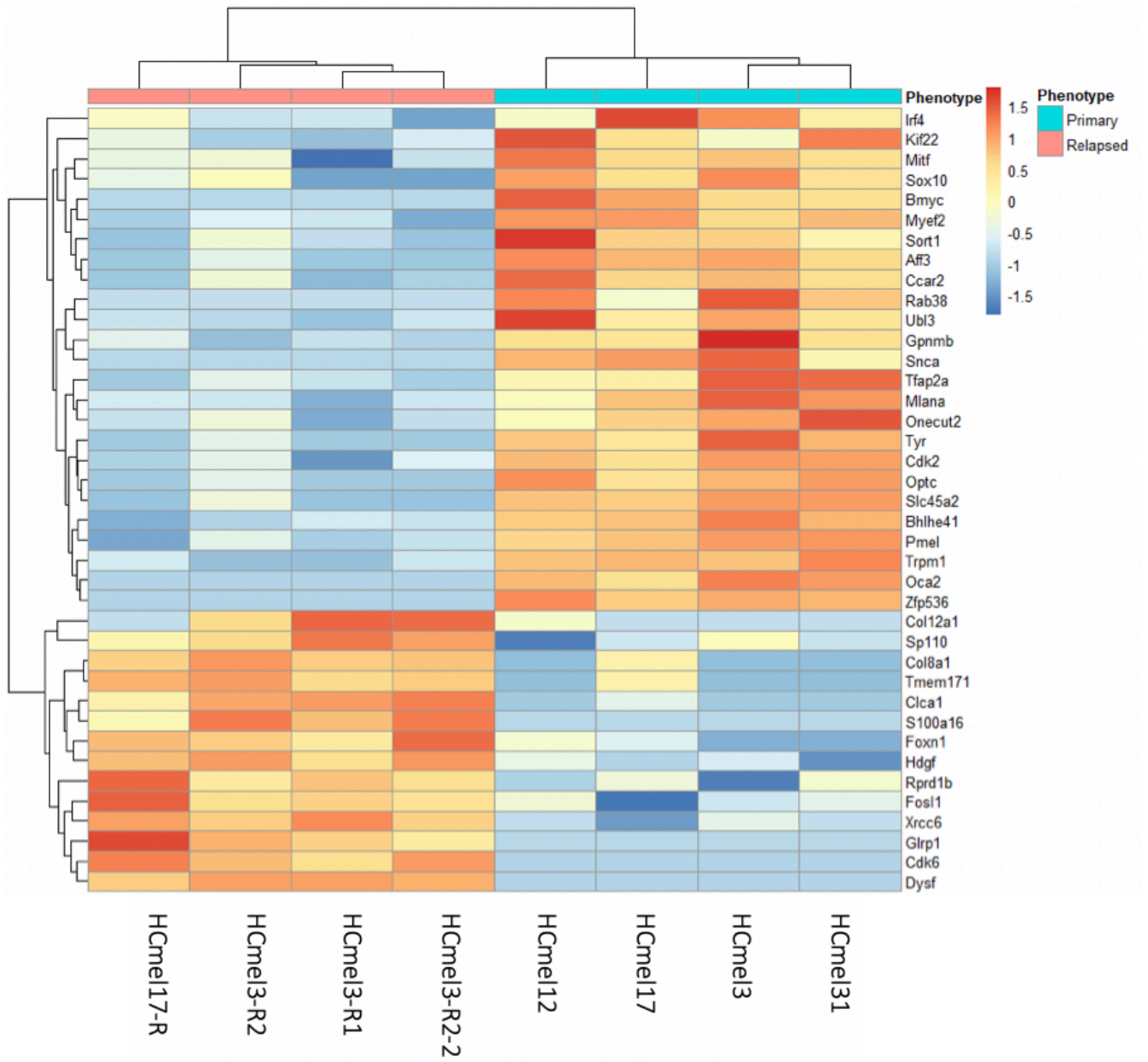
Figure 3.8 Differentially expressed genes in primary and ACT-resistant cell lines indicate downregulation of melanocytic differentiation and developmental genes in resistant phenotypes.

A) Volcano plot shows differentially expressed genes in resistant cell lines compared to primary cell lines. Red dots indicate the significant differential expression with values >2 for \log_2 fold change and Wald test adjusted p-value <0.01 which consist of 461 genes (only some of the most variable values are labeled with gene names to avoid visualization overlaps). **B)** Clustering heatmap (top) of the most variable differentially expressed genes between primary and ACT-resistant cell lines which appeared in the three top-ranked DAVID functional enrichment clusters(down). P-values are computed using a modified Fisher Exact test called EASE Score; the smaller, the more enriched. **C)** Bioprocesses enrichment bar plots for 461 differentially expressed genes in resistant cell lines show the frequency of up/downregulated genes in each bioprocess; Most of the downregulated genes contribute to melanocytic differentiation processes (top) while upregulated genes mainly enrich for proliferative cell processes (down). Hypergeometric distribution p-value cutoff =0.01, FDR=0.05 for multiple testing. **D)** Gene Ontology enrichment analysis for 461 differentially expressed genes reflects the contribution of immunogenic and proinflammatory bioprocesses with dedifferentiated ACT-resistant phenotype. **E)** Major Protein Networks of the most variable differentially expressed genes –identified by STRING (v 11.0)– recap target genes and broad biological interactions of MITF.

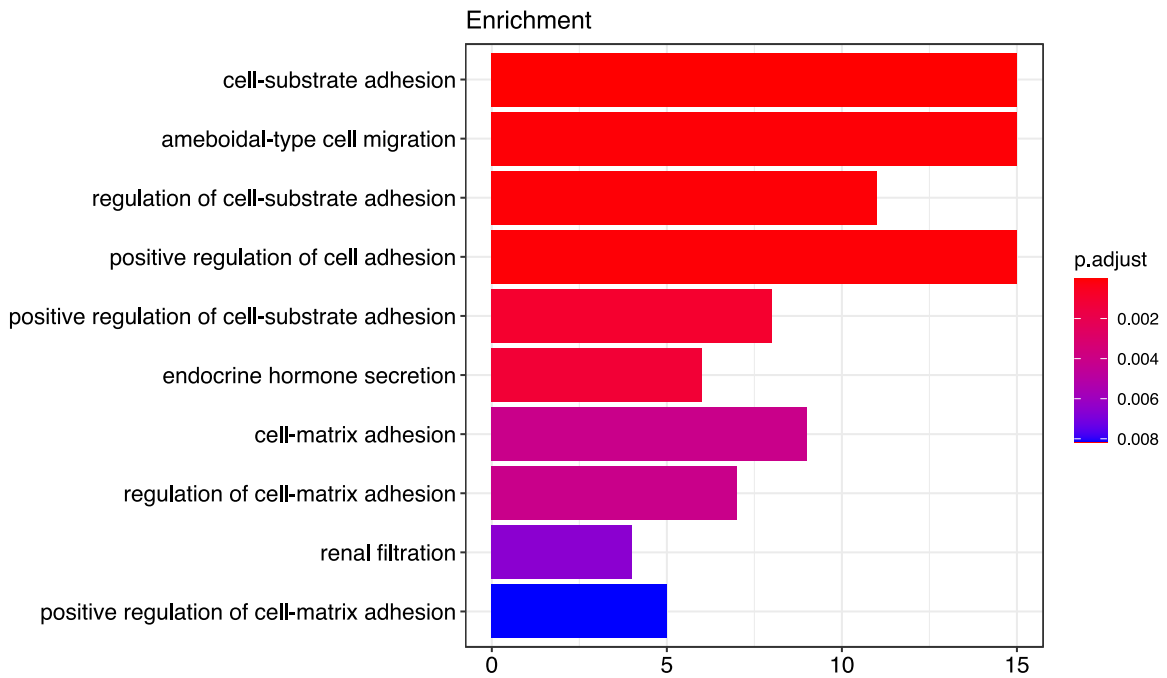
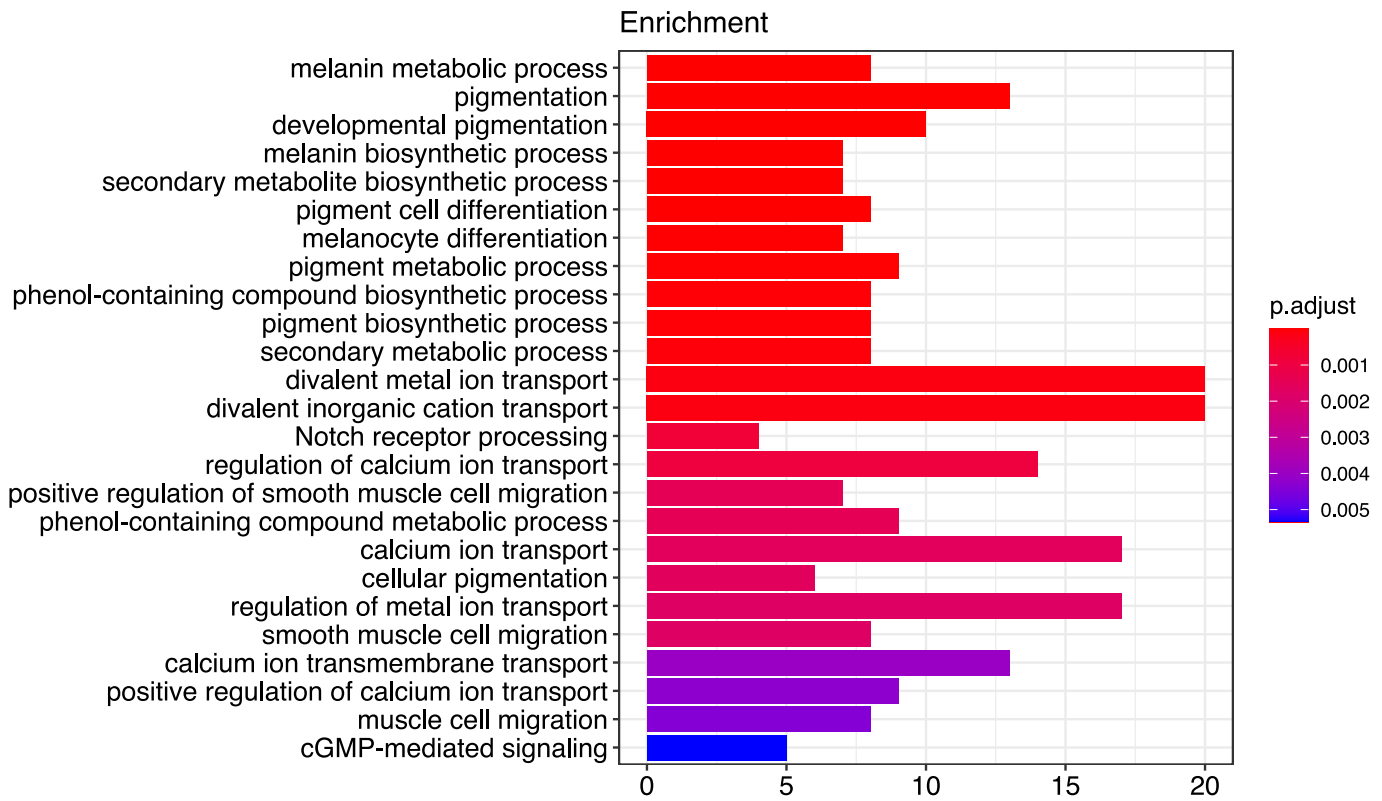
A



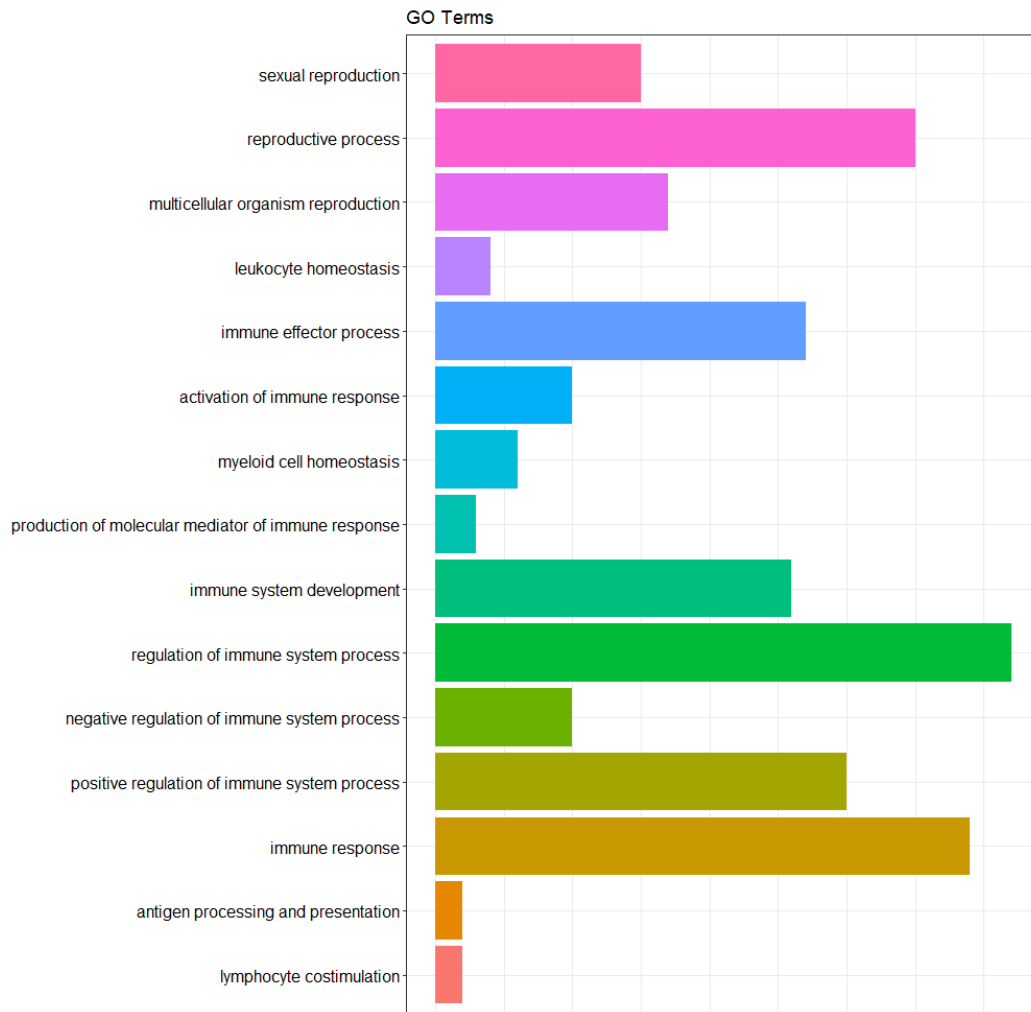
B



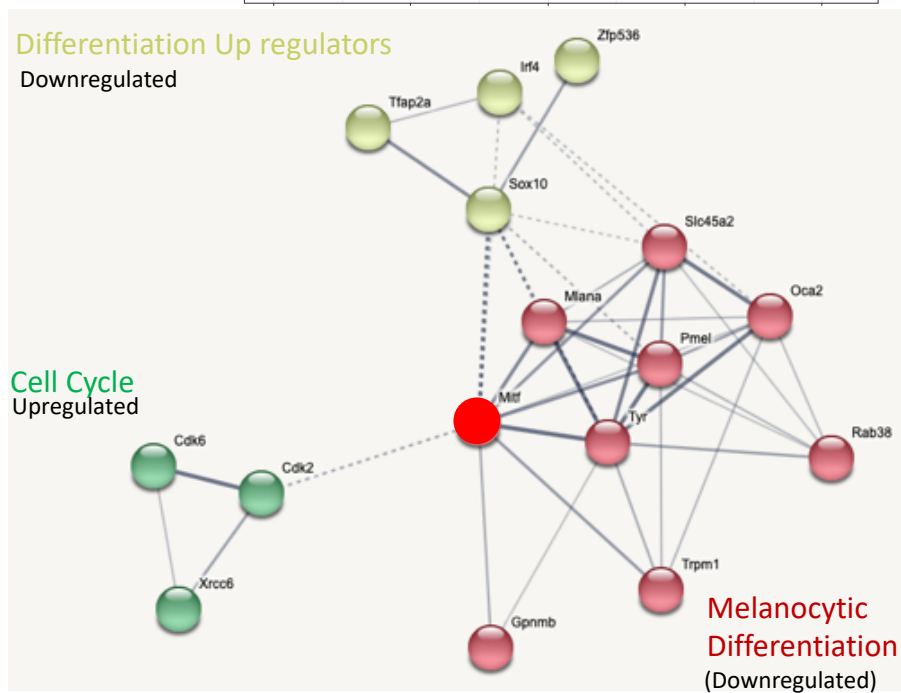
C



D



E



3.3 MeDIP-seq experiment and DNA-methylation profiling of the cell lines revealed the source of difference by DNA-methylation between primary and resistant cell lines

Landsberg et al. showed that melanomas resist T-cell therapy due to reversible dedifferentiation of the melanoma cells. The proinflammatory response was identified as a microenvironmental influencer in melanoma cell plasticity and dedifferentiation of ACT-resistant melanomas. Therefore, I hypothesized that the proinflammatory microenvironment drives therapy resistance via DNA-methylation alterations in melanoma cell differentiation genes.

To test this hypothesis, I conducted genome-wide DNA-methylation profiling –by Methylated DNA Immunoprecipitation followed by next-generation sequencing (MeDIP-seq)– for primary (HCmel) and resistant (HCmel-R) cell lines and analyzed the data to identify differentially methylated genomic regions. In this experiment methylation level is estimated as “Beta value” which is quantified using the ratio of CpG methylation intensities between methylated and unmethylated alleles.

3.3.1 MeDIP-seq data quality and post alignment coverage report

Pre-alignment quality control of MeDIP sequencing data showed the average Phred score per base position greater than 30 that yields greater than 99.9% accurate identification of nucleobases for all samples. Post alignment evaluation results showed 35-45% unique methylated DNA fragments mapped to mm10 mouse reference genome (Figure s3).

3.3.2 ACT-Resistant melanoma cells showed a distinct DNA-methylation landscape from primary melanoma cells

To explore the relationship between primary and resistant HCmel cell lines I conducted Principle Component Analysis (PCA) using beta values (transformed to absolute methylation and normalized counts). PCA results revealed distinct DNA methylation profiling between ACT-resistant samples from primary cell lines. Resistant profiles cluster close together on first and second principal components (PC1 and PC2) while primary melanoma cell lines appear heterogeneously separated.

3.3.3 CpG Islands indicate the source of difference by DNA-Methylation between primary and resistant cell lines

In this study, I questioned if expression-related genomic regions could indicate a significant difference between DNA methylation profiles of primary and ACT-resistant melanoma cells. Therefore, I performed differential methylation analysis using MeDIP sequencing profiles of HcMel-R samples compared to HcMel. The results showed major hypermethylation of CpG islands (CGIs) in HcMel-R and overall hypomethylation of all genomic regions. Transcriptional start sites (TSS) and CpG island shores revealed less difference by methylation data. (Figure 3.9)

3.3.4 Differentially methylated genes contribute to melanoma cell differentiation signature and reflect the proinflammatory microenvironment

To identify differentially methylated genes and corresponding biological functions in ACT-resistant melanoma cell lines I first defined a significant cutoff based on the difference of beta values for CGIs. Then I annotated gene ranges and gene names for differentially methylated regions (DMRs) and implemented the list of 659 differentially methylated known genes for Gene Ontology (GO) and bioprocess enrichment.

My results indicated key genes of melanoma cell differentiation and pigmentation namely *Mitf*, *Hps1*, *Kit*, *Rab27a*, *Slc45a2*, *Spns2*, *Sox11*, and *Ednrb* amongst the most variable differentially methylated genes.

125 differentially methylated genes were enriched for immune system processes among them *Gata2*, *Ifnar2*, *Irf1*, *Irf3*, *Il16*, *Il17rc*, *Il6ra*, *Il4ra*, *Il34* *Il7*, *Tnfsf11*, and *Thy1* are known for contributing to an inflammatory and pro-inflammatory response. (Figure 3.10)

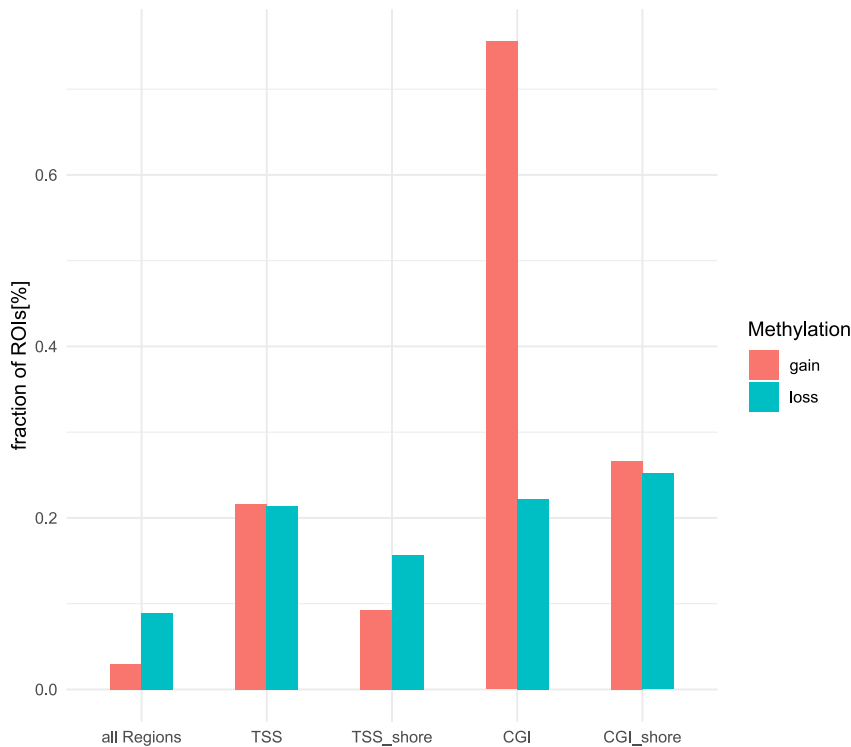
To integrate the results of differential analysis on DNA methylation and expression data, I took the intersection of differentially methylated genes separately with upregulated and downregulated genes. The integrated plot showed the genes with altered methylation and expression status in ACT-resistant versus primary melanoma cells. *MITF* gene/pathway stands among these genes (Figure 3.11).

I conducted Gene Ontology (GO) grouping and functional enrichment analysis for the gene in intersection area to see which biological functions could be regulated by methylation alterations (Figure 3.12). Significant enriched bioprocesses include developmental pigmentation (Mitf, Rab27a, Slc45a2), melanocyte differentiation and protein localization to cell surface (Mitf, Rab27a), extracellular matrix signaling (Fzd4), macrophage activation involved in immune response (Dysf), and response to interferon-alpha (Ifnar2).

3.3.5 Mutational load increased but could not fully explain the mechanism of reversible and de-differentiation mediated resistance

I conducted an integrative analysis to see whether the exclusively mutated genes in resistant cell lines could relate to differential expression in these cells. The intersection of genes with non-synonymous somatic mutation detected only in all resistant melanoma cells with the list of differentially expressed genes in these cells, include only one gene – Axl (Figure 3.13). So, I found only AXL gene as the exclusively mutated gene in all the resistant cell lines with evidence of upregulation of this gene by expression data. Upregulation of AXL is known in dedifferentiated and therapy resistant tumors but is not clearly known as driven by a genomic mutation, neither in reversible de-differentiation mediated resistance.

A



B

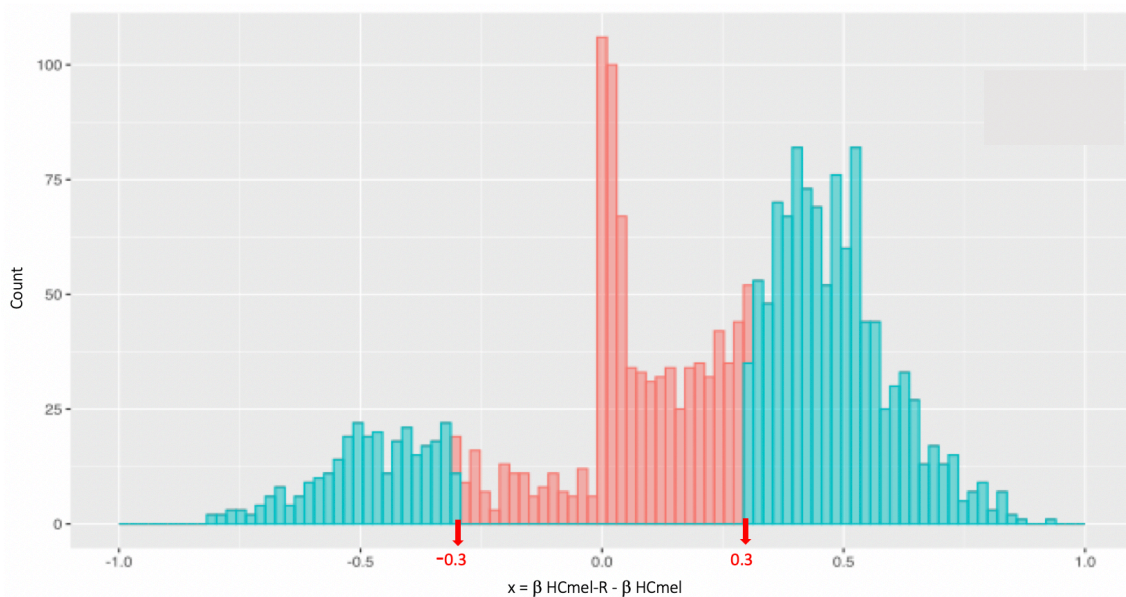
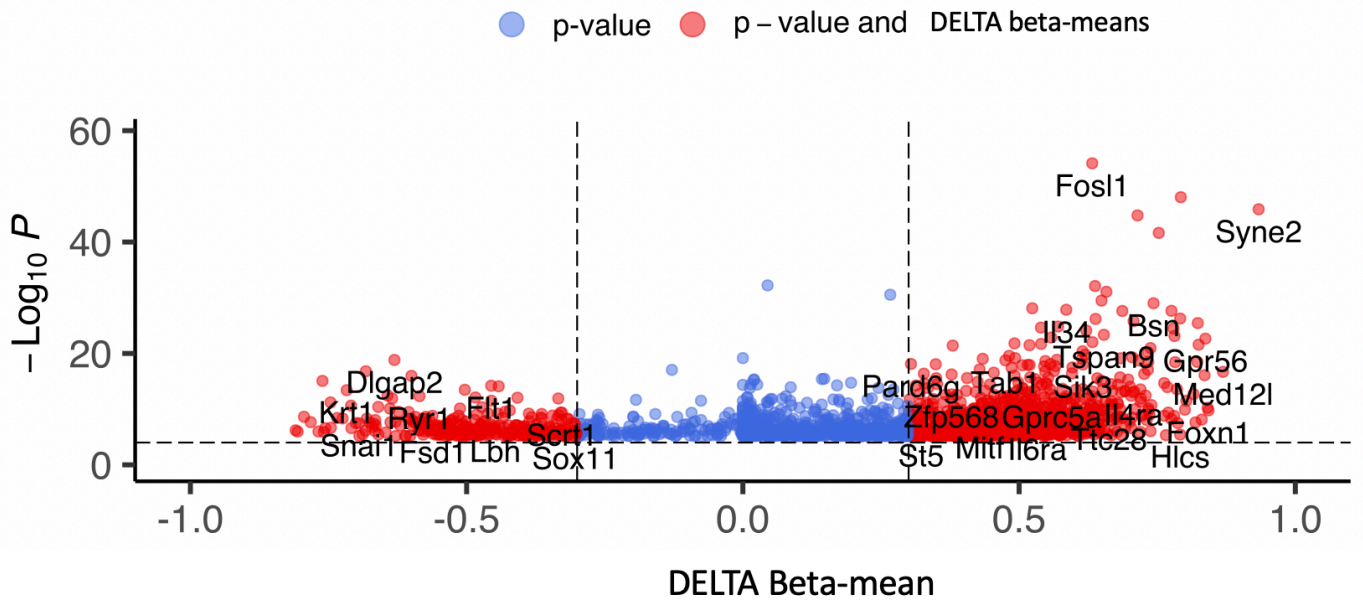


Figure 3.9 MeDIP-seq data analyses showed a genomic landscape of DNA methylation changes in HCmel and HCmel-R cell lines

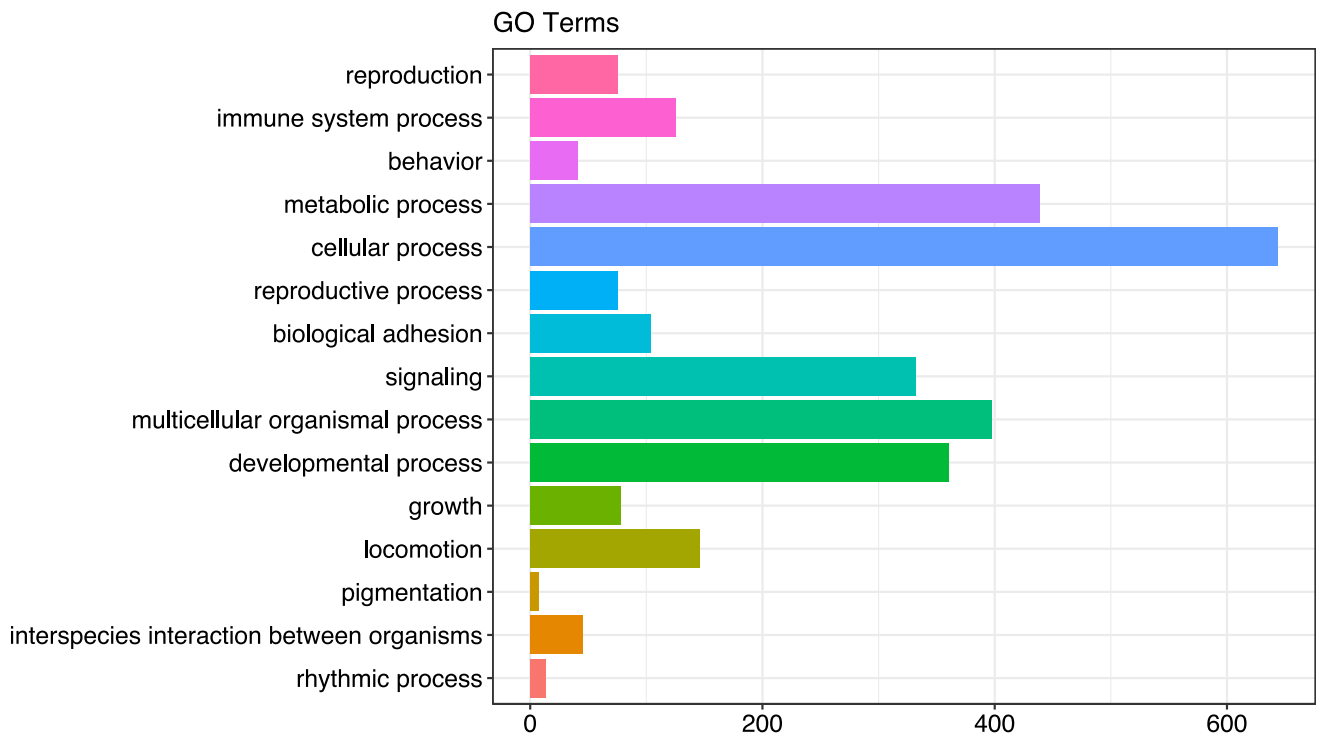
A) Bar plot shows DNA methylation changes per genomic region in HCmel-R cell lines compared to HCmel cell lines showed drastic hypermethylation in CpG Islands (CGIs) in contrast with overall hypomethylation in other targeted regions. ROI stands for region of interest.

B) Histogram is plotted to show distribution of differences of means of Beta values (β) in differentially methylated CGIs in HCmel-R compared to HCmel ($x = \beta_{\text{HCmel-R}} - \beta_{\text{HCmel}}$). I defined a cutoff of 0.3 for methylation changes for downstream analysis.

A



B



C

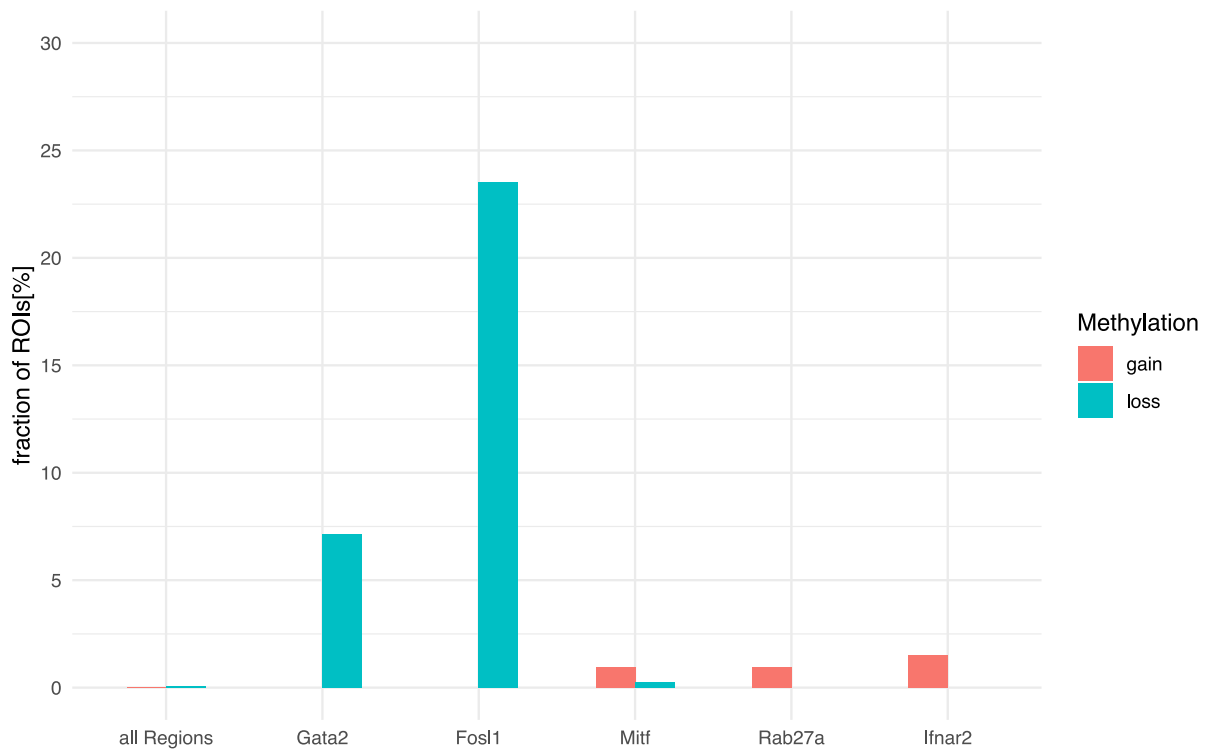


Figure 3.10 Differentially hypermethylated CGIs in HCmel-R cells mirrored downregulation of genes with known functions in melanoma cell differentiation while hypomethylated CGIs contribute to known genes in cell proliferation.

A) Volcano plot shows the most variable DNA-Methylation changes in annotated CGIs (Delta Beta values ≥ 0.3 and p values ≤ 0.01). Only some of most differentially methylated genes are labeled on corresponding spots for a better reading.

B) Bar plot shows Gene Ontology enrichment of differentially methylated genes per biological processes and counts of the involved genes in each process.

C) Bar plot features the enrichment of DNA methylation (gain or loss) per genomic region of interest (ROI) in HCmel-R cells compared to HCmel. I used QSEA statistical framework to assess the enrichment of differentially methylated genes; Mitf, Rab27a, Ifnar2, Gata2, and Fosl1 were selected for contribution to melanoma cell differentiation, proliferation, and immune response.

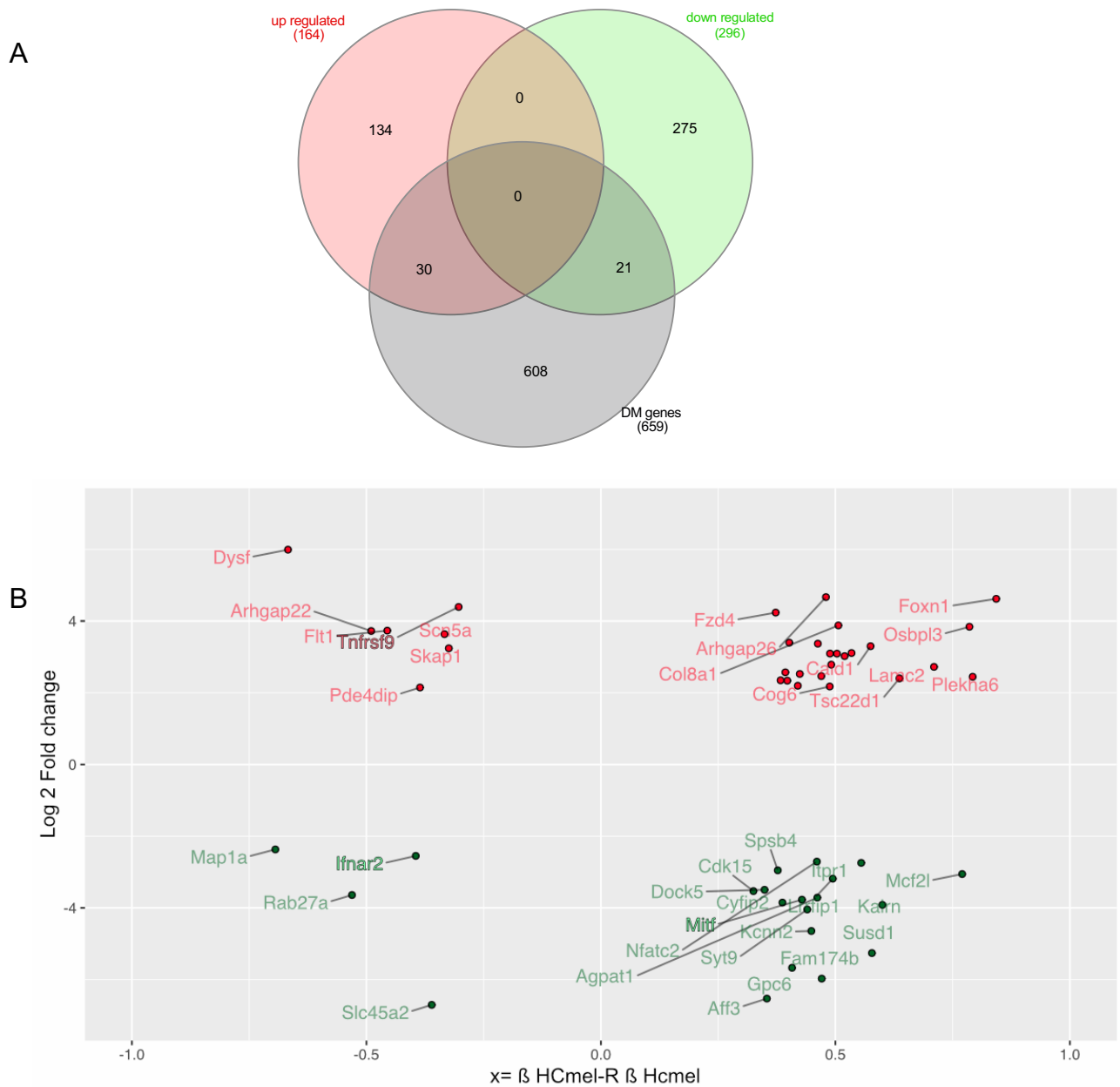


Figure 3.11 Intersection of differentially methylated and differentially expressed genes highlights the potential role of the MITF gene/pathway in ACT-resistant versus primary melanoma cells.

A) Venn diagram shows the intersection of upregulated (\log_2 FC > 2) and downregulated (\log_2 FC < -2) genes with differentially methylated (DM) genes ($\Delta\beta > 0.3$). Non-canonical gene names were filtered.

B) Scatter plot depicts the intersection of 51 differentially methylated and differentially expressed genes with expression values (\log_2 FC) and methylation differences ($\Delta\beta$ of resistant cells – primary cells).

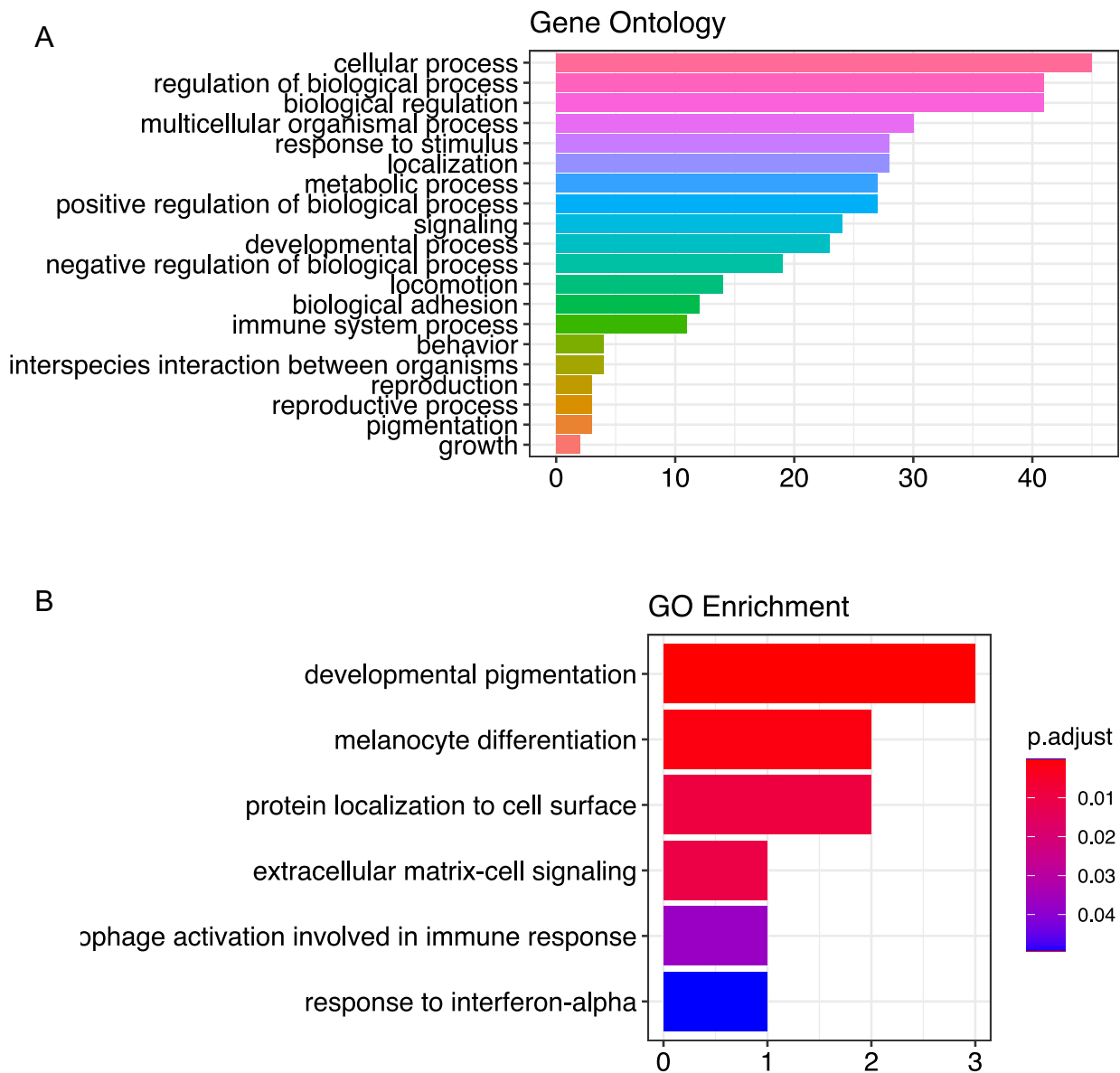


Figure 3.12 The interaction of immune response with melanoma cell development and differentiation is traced in integrative functional enrichment.

- A) Gene Ontology (GO) groups for the intersection of differentially methylated and differentially expressed genes (51 genes).
- B) Functional enrichment based on GO groups show the significant bioprocesses in these genes. (Hypergeometric distribution p -value cutoff =0.05)

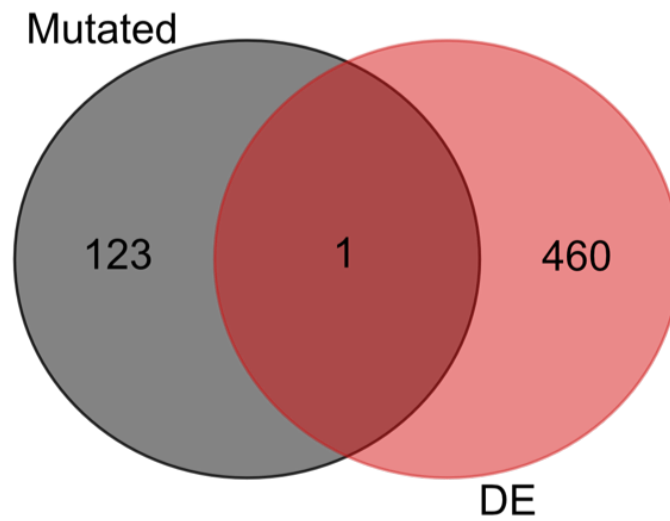


Figure 3.13 Integration of somatic mutations with differential expression (DE) analysis in resistant cell lines indicates one gene; AXL.

Venn diagram shows the intersection of 123 genes (which were known with gene ontologies out of 132 exclusively mutated genes in all resistant cell lines) with 461 differentially expressed genes. The intersection includes only one gene which is Axl.

4 Discussion

4.1 Key findings of this study

4.1.1 Hgf-Cdk4^{R24C} melanoma cell lines harbor additional driver mutations similar to the “Triple-WT” molecular subtype of human melanoma

Melanoma research and drug discoveries have been revolutionized by new tools and technologies for molecular profiling of melanomas because they could improve the efficacy of treatments by precise target selection and personalized medicine. I used the Hgf-Cdk4^{R24C} preclinical melanoma model under adoptive T cell transfer (ACT) immunotherapy to study the molecular mechanisms of immunotherapy resistance in melanoma. This model has been phenotypically well described for recapitulating clinical behavior of melanoma phenotype switching –from proliferative to invasive– and resistance to T cell-mediated immunotherapy (Landsberg et al., 2012). However, the model was not profiled for somatic mutations and genomic subtyping. Molecular subtypes of cutaneous human melanoma have been described in four major subtypes based on their mutational profiles; BRAF mutated, RAS mutated, NF1 mutated, and Triple-WT (wild-type). These subtypes have been shown to be predictive for immunotherapy outcomes. In addition, somatic mutational load and mutational signature have been demonstrated to be correlated with clinical responses to immunotherapies (Pérez-Guijarro et al., 2020)(Akbari et al., 2015).

I analyzed the mutational profile of Hgf-Cdk4^{R24C} melanoma cells. In this experimental mouse model, germline mutations of Hgf and Cdk4^{R24C} induce 5-15 spontaneous melanomas within the first year of life (Kohlmeyer et al., 2009). As not all melanocytes progressed to melanoma cells, I hypothesized that additional acquired mutations contribute to melanoma genesis in this model. Using exome sequencing data and mutational analysis I showed that Hgf-Cdk4^{R24C} melanoma cells harbor additional driver mutations in Trp53, Rac1, and Gna11 which recapitulate the genomic subtype of Triple-WT cutaneous human melanoma. Since HcMel melanoma cells were DMBA induced, it

was expected to find HRAS mutations in their mutation profiles but I could not find such mutations in my data. Comparative analysis of somatic mutation profiles between murine melanomas and cell lines would bring more information about specific mutational selection in vitro.

Counts of nonsynonymous somatic mutations indicated that in melanoma cells derived from the Hgf-Cdk4^{R24C} model (HCmel cell lines) mutational load is higher than other genetically engineered murine (GEM) preclinical models but lower than the popular spontaneous murine melanoma model B16 (Figure 3.3). Mutations counts in COSMIC melanoma cell lines show a much higher load of somatic mutations in human skin melanoma than available murine models.

In addition, I performed a comparative analysis between mutational profiles of ACT-resistant cell lines (HCmel-R) compared to primary melanoma cells (HCmel) all derived from of Hgf-Cdk4^{R24C} model. Mutational loads showed an increased count in ACT therapy-resistant cell lines (HCmel-R) compared to primary melanoma cells (HCmel) which means accumulation of somatic mutations. I identified the exclusively shared mutated genes in all ACT therapy-resistant cell lines which candidate for contribution to resistance mechanisms (Figure 3.5 and Table 3.1). Further functional experiments are required to delineate such contributions which were beyond the aims of this study.

4.1.2 Epigenetic alterations act beyond the somatic mutations in inflammation-induced reversible melanocytic dedifferentiation and ACT-therapy resistance

Genomic mutations could not explain the reversible resistant phenotype in the Hgf-Cdk4^{R24C} model (Figure 3.4) and melanocytic plasticity signature (MPS) which were observed experimentally and confirmed using expression data (Landsberg et al., 2012). Tsoi and colleagues elaborated on the melanocytic differentiation signature in melanoma subtyping and drug response. Their analysis using Landsberg's expression data again showed the loss of melanocytic differentiation in immunotherapy resistant melanoma cells compared to primary melanoma cells which indicated treatment-induced dedifferentiation in melanoma cells (Figure 4.1) (Tsoi et al., 2018). These findings are consistent with the results of my differential analysis using RNA-seq data which confirmed the loss of melanocytic differentiation signature with significant downregulation of MITF (Figure 3.8 A-B). Consequently, all of the main target genes of MITF were downregulated which

involve different pathways namely TYR, TYRP1, DCT, PMEL, MLANA as key genes of melanocytic differentiation, CDK2 in cell cycle control, BCL2 in cell survival and antiapoptotic response, and PPARGC1A in metabolism.

Comprehensive functional enrichment on differentially expressed genes showed that downregulated genes mostly contribute to developmental and differentiation proteins while upregulated genes contribute to cell proliferation, senescence, and invasion (Figure 3.8 C-D). These results confirmed our previous experimental findings and the hypothesis that melanoma cells escape T cell recognition through dedifferentiation and loss of melanocytic antigens.

I also observed upregulation of the AXL gene in our resistant cells which may indicate melanocytic dedifferentiation signature of $MITF^{low}$ AXL^{high} . But interestingly AXL was also amongst the exclusively mutated genes in resistant cell lines. I could not find any known function of this mutation that associates with upregulation of AXL, so with available data, I could not delineate if these findings suggest a novel intrinsic factor for melanocytic dedifferentiation signature of $MITF^{low}$ AXL^{high} or mirror a more complex tumor microenvironment with proinflammatory factors. According to cBioPortal (TCGA, Pan-Cancer Atlas) for Cancer Genomics, 13% of human skin melanomas harbor different coding mutations in the AXL gene which are not functionally characterized and are often associated with higher mRNA expression.

Integrative analysis of mutational profile, expression, and DNA methylation in patients-matched melanoma samples by Hugo and colleagues showed that accumulation of somatic mutations in melanoma patients could not predict patient's response to immunotherapy and targeted therapy, suggesting the regulatory contribution of non-genomic alterations in acquired resistance (Hugo et al., 2015) (Hugo et al., 2016).

MITF has been termed the "master transcriptional regulator" of melanocytic development and differentiation. It refers not only to a gene but also to a molecular pathway that coordinates a broad range of bioprocesses. Moreover, MITF appeared as a predominant interactor with tumor microenvironmental factors and immune response including inflammatory mechanisms in melanoma and other cancers (Ballotti et al., 2020).

Our protein interaction analysis demonstrated that MITF stands centrally in a network of differentially expressed genes which involves SOX10, IRF4, ZFP536, TFAP2A regulators of differentiation bioprocesses, CDK2, CDK6, XRCC6 in cell cycle control, and MLANA,

SLC45A2, OCA2, PMEL, TYR, RAB38, TRPM1, GPNMB in melanocytic differentiation which are known target genes of MITF (Figure 3.8 E). These experimental and computational data indicated the influential role of MITF expression and its altered mechanisms in MPS and ACT immunotherapy resistance in the Hgf-Cdk4^{R24C} model.

Based on our previous studies and experimental data I hypothesized that epigenetic factors regulate the proinflammatory-induced reversible melanocytic dedifferentiation and response to ACT immunotherapy. I considered DNA methylation alterations as the first line epigenetic mark to check for plastic melanocytic dedifferentiation in ACT-resistant melanoma. Our expression data confirmed the loss of melanocytic differentiation in ACT resistant melanoma cells which mirrored the melanocytic plasticity signature observed in corresponding Hgf-Cdk4^{R24C} melanoma. I implemented DNA methylation profiles of primary and ACT immunotherapy-resistant melanoma cells and analyzed them for differential methylation. My analyses results showed that ACT-resistant melanoma cells (HCmel-R) significantly differ from primary melanoma cells (HCmel) by DNA methylation landscape particularly in CpG islands (CGIs) (Figure 3.9). I observed global hypomethylation in all genomic regions of ACT-resistant methylation profiles compared to primary ones while CGIs appeared hypermethylated for a significant set of genes. Gene set enrichment analysis and bioprocesses enrichment on differentially methylated CGIs indicated a strong contribution of genes in melanoma cell differentiation and proliferation as well as immune response (Figure 3.10).

Integrative analysis of differential methylation and expressed genes indicated 51 genes with known functions in melanocytic differentiation, proliferation, and immune response including MITF (Figure 3.11). I found MITF amongst the most variable genes with corresponding hypermethylated GCI and downregulated expression in ACT-resistant melanoma cells of the Hgf-Cdk4^{R24C} model. These findings strongly suggest the regulatory role of epigenetic alterations specifically DNA methylation in proinflammatory-induced melanoma cell plasticity, loss of melanocytic antigens, and consequently T cell-mediated therapy resistance in our model.

4.2 Clinical relevance and applications

4.2.1 MITF pathway offers a potential target to improve immunotherapy using DNA-methylation targeted drugs

Lauss and colleagues previously showed that DNA methylation alterations correlate with MITF expression levels in melanoma patients. They showed that hypermethylation of the MITF gene promoter correlates with the downregulation of MITF and its target genes –the same as I showed in our preclinical model. In addition, they could restore MITF pathway activity using a hypomethylating agent (5-Aza) in human melanoma cells that confirmed the regulatory role of DNA methylation in MITF activity (Lauss et al., 2015).

Our findings contribute to the discovery of regulatory mechanisms of dedifferentiation-mediated immunotherapy resistance in melanoma specifically in MITF as master coordinator of melanocytic differentiation, proliferation, and immune response (Figure 4.2). These findings offer fundamental applications for reprogramming resistance mechanisms using methylation-targeted drugs against melanoma.

4.2.2 AXL is a potential target to overcome resistance to immunotherapy and targeted therapy in melanoma

I showed that an identical mutation with an increased level of gene expression in AXL receptor tyrosine kinase occurred in all ACT therapy-resistant melanoma samples of our preclinical model. Whether this mutation is functionally relevant to loss of melanoma cell differentiation and T cell recognition or it explains a separate mechanism of resistance requires further studies. AXL plays a key regulatory role in a variety of vital bioprocesses including proliferation, survival, motility, and immunogenic response (Gay et al., 2017). Although genomic mutations in AXL are not known as an oncogenic driver, overexpression of AXL has been detected in a variety of human malignancies including melanoma. Clinical and experimental studies indicated expression alterations in AXL correlated with patient's survival and therapy response and approached this gene as a therapeutic target or biomarker (Tirosh et al., 2016) (Boshuizen et al., 2018) (Gautron et

al., 2021). Soluble AXL (sAXL) has been shown to be correlated with shorter survival in invasive melanomas under immunotherapy and therefore is suggested as a biomarker for monitoring melanoma progression and therapy response (Flem-Karlsen et al., 2020). Our findings together with all these interesting pieces of evidence indicate the important but less delineated role of AXL in cancer therapy.

4.2.3 Targeting melanocytic dedifferentiation drivers as a mechanism of resistance to improve immunotherapy outcomes

Melanoma cell plasticity has appeared as an attractive candidate mechanism of resistance to targeted therapy and immunotherapy. Tumor cell plasticity and phenotype switching account for a variety of non-genetic resistance mechanisms that lead to therapy resistance, tumor cell survival, and proliferation. Our findings indicated that DNA methylation controls phenotype switching and immunotherapy resistance via dysregulation of MITF. Targeting the master regulator of dedifferentiation and phenotype plasticity contributes to reprogramming this mechanism of resistance and increasing the efficiency of therapeutic strategies and precision melanoma therapy.

4.3 Future perspectives and research suggestions

In this study, I focused on molecular experiments and computational analysis based on previous in-vitro and in-vivo experimental data and materials. My findings significantly pointed out the regulatory role of methylation alterations in proinflammatory induced melanoma cell dedifferentiation of the Hgf-Cdk4^{R24C} preclinical model. However, to translate these findings for clinical implications I suggest further computational and experimental validations:

4.3.1 Functional validation

Landsberg and colleagues showed that in murine and human melanoma cells, reversible dedifferentiation and loss of T cell-specific antigens under proinflammatory tumor microenvironment was reproducible by exposure to proinflammatory agent TNF α (Landsberg et al., 2012). Our molecular findings indicated epigenetic control underlying

this observation via DNA methylation alterations specifically the significant hypermethylation of the MITF gene/pathway. Therefore, I propose an experimental validation that tests the effect of a site-specific hypomethylating agent on MITF together with proinflammatory induction. I suggest using a CRISPER-Cas9-mediated epigenetic editing system to specifically modify the promoter methylation in order to restore the gene expression of the MITF pathway. Such experimental validation could be recruited using the same murine preclinical model as well as relevant clinical materials and human melanoma cells.

4.3.2 Bioinformatic validation; detection of immunogenic signatures which correlate with methylation alterations of MITF pathway in relevant clinical cohorts

Lauss and colleagues showed the correlation of DNA methylation alterations in MITF with its expression in clinical cohorts of melanoma (Lauss et al., 2015). I showed this correlation for the first time in a preclinical model with immunotherapy context (ACT therapy) and its association with tumor cell dedifferentiation-mediated resistance mechanisms in melanoma therapy. Based on these findings I suggest bioinformatic analysis to check for immune escape signatures including inflammatory-related bioprocesses with melanocytic plasticity signature (MPS) and altered DNA methylation marks in clinical cohorts of melanoma. Such exploratory analysis shed light on epigenetic mechanisms of MPS and their interconnection with tumor immunity and microenvironment. The same analytical approach could be conducted using matched melanoma samples on treatment to identify such interconnection in response to immunotherapy.

Very recently, Newell and colleagues published an integrative analysis using multi-omics data –Genome-wide mutations, methylation, and expression in addition to immune cell infiltrate profiling– in a cohort of skin melanoma patients to study molecular mechanisms of resistance and response to immune checkpoint inhibitors (Newell et al., 2021). Their results indicate that immunogenic tumor microenvironment and DNA methylation alterations are associated with response to immunotherapy while no specific genomic mutation correlated with therapy response. They specifically showed that high INF- γ

signature predicts response to immunotherapy. Although I did not have in-vivo data for my genome-wide study, I showed the trace of immune system bioprocesses using functional enrichment of differentially methylated genes in melanoma cells of the Hgf-Cdk4^{R24C} preclinical model. IFNAR2 –the encoding gene for essential subunits of interferons alpha and beta receptor– appeared amongst hypermethylated and downregulated genes in ACT therapy-resistant melanoma cells (Figure 3.10 and Figure 3.11). Downregulation of this gene has been shown in immunodeficiency. Targeting IF receptors has been recently shown to be effective for combating therapy resistance(Cao et al., 2021). These pieces of evidence arise more interest about epigenetic regulation of response and resistance mechanisms via Interferon Pathway/Signaling within the tumor microenvironment.

4.3.3 Histone modifications and methylation assays

Common epigenetic methylation alterations in tumor progression and response to therapy include DNA methylation marks as well as histone methylation. Methylation and acetylation are the most common regulatory modifications on histones that occur next to promoter and enhancer regions (Wang et al., 2009)(Miranda Furtado et al., 2019). Aberrant epigenetic histone modifications have been shown in cancer therapy outcomes. Comprehensive molecular analysis on other epigenetic alterations specifically histone methylation and DNA methylation using new technologies with higher resolution contribute to better demonstration of epigenetic regulatory mechanisms in melanoma therapy resistance.

(Tsoi et al., 2018)

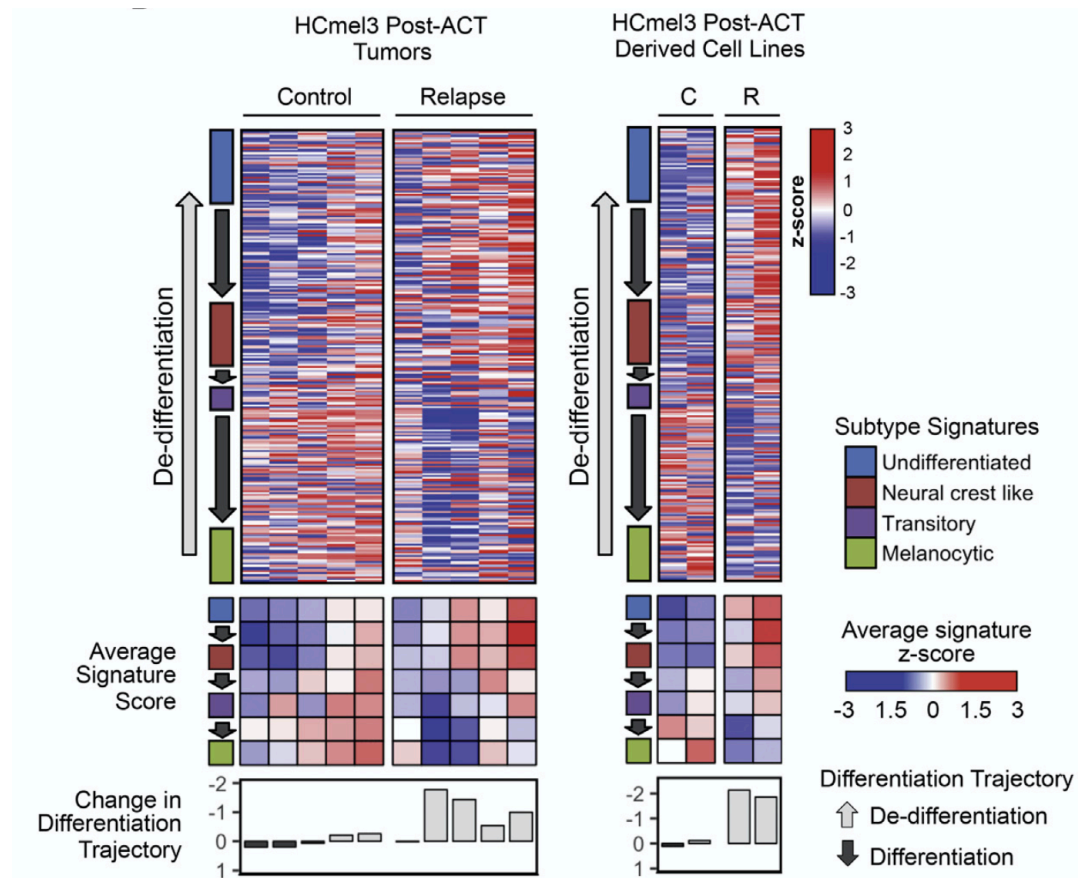


Figure 4.1 ACT immunotherapy-induced dedifferentiation in context of four-stage differentiation signature in melanoma

ACT immunotherapy resistant melanoma cells (HCmel3-R) show loss of melanocytic differentiation compared to primary melanoma cells (HCmel3). Tsoi et al. reproduced this signature using gene expression array data published by Landsberg et al. which showed Hgf-Cdk4^{R24C} melanomas resist to ACT immunotherapy through reversible and adaptive dedifferentiation.

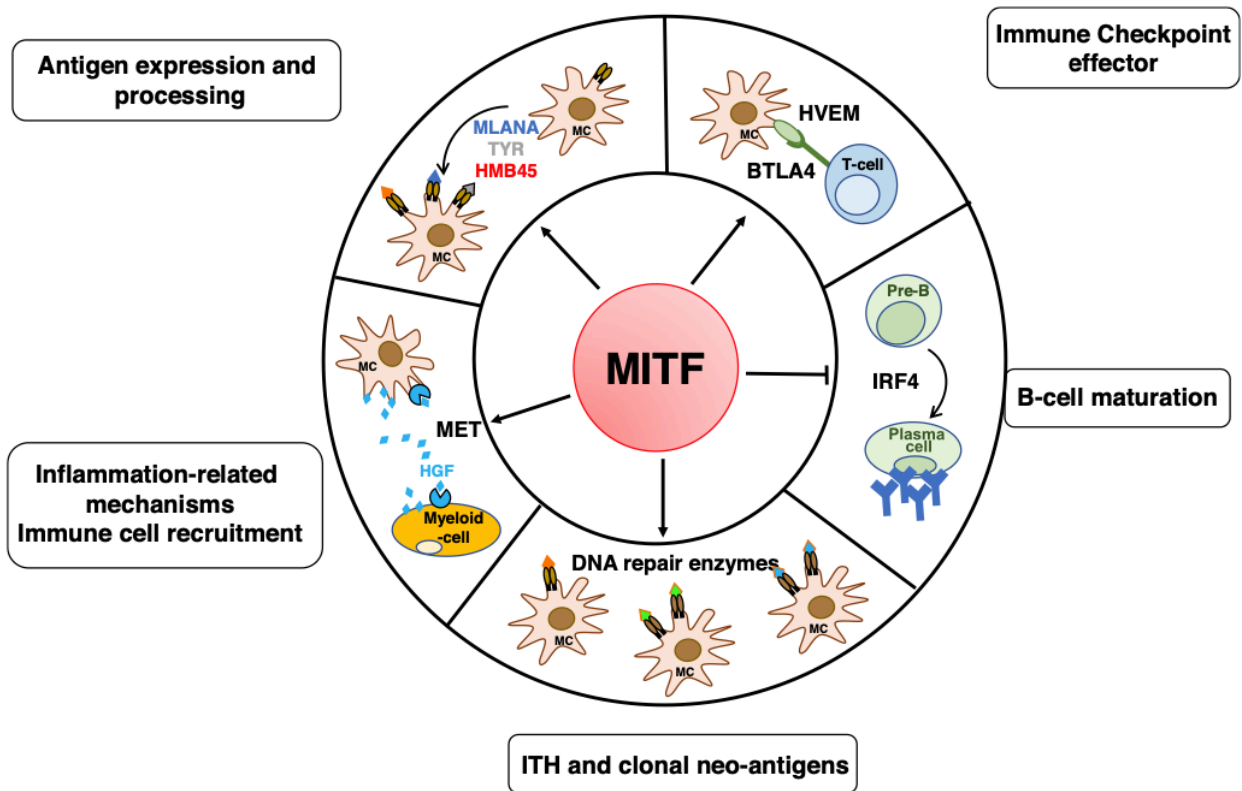


Figure 4.2 Broad biological functions and interactions of MITF gene/pathway in melanocytes, melanoma, and immune response (Ballotti et al., 2020).

5 Abstract

Molecular studies empowered novel therapeutic strategies against melanoma in recent years, however, therapy resistance lowers the efficacy of targeted therapies and immunotherapies and remained a complex obstacle. Dedifferentiation in melanoma indicates phenotypic plasticity and imposes resistance to immunotherapy and targeted therapy.

Murine preclinical models provide vital tools for comparative onco-genomics to study molecular mechanisms underlying tumor phenotypes and to improve therapeutic strategies in human patients. Hgf-Cdk4^{R24C} mouse preclinical model demonstrated invasive melanoma with proinflammatory induced dedifferentiation and resistance to T-cell mediated immunotherapy. Therefore, it serves as an informative and helpful model to study molecular mechanisms of adaptive therapy resistance in melanoma.

I performed the first integrative analysis of genome-wide mutations, methylation, and expression profiles of primary and relapsed melanoma cells of Hgf-Cdk4^{R24C} mouse preclinical model of human melanoma under adoptive T cell transfer (ACT) immunotherapy. I analyzed somatic mutations, differentially methylated genes, and differentially expressed genes and featured the corresponding biological pathways and functions.

My analyses revealed significant DNA methylation alterations in developmental and differentiation genes notably hypermethylation and downregulation of MITF in melanoma cells with dedifferentiated phenotype, loss of melanocyte-specific antigens, and resistance to ACT immunotherapy.

My findings consistent with my hypothesis indicated that reversible epigenetic alterations regulate melanocytic dedifferentiation and phenotype plasticity beyond genetic mutations. Using differential expression analysis and comparative exome data analysis I found an identical mutation in the AXL gene with upregulated expression in all ACT therapy-resistant melanoma cells. Delineation of the functional relevance of AXL mutation with melanoma cell plasticity and therapy resistance would bring more insights to therapeutic strategies.

I provided significant evidence indicating the importance of epigenetic regulation specifically DNA methylation in dedifferentiation-mediated therapy resistance in melanoma. Therefore, I suggest DNA methylation marks of the master regulator of melanocytic differentiation – MITF – as highly potential targets to restore melanoma cell differentiation and response to the therapy.

6 List of Figures

Figure 1.1 Adaptive phenotype plasticity in melanoma.....	14
Figure 1.2 Targeted genes and pathways in genetically engineered murine (GEM) models of cutaneous melanoma.	20
Figure 1.3 Mechanisms of resistance to cancer immunotherapy.....	25
Figure 1.4 A summary of commonly used methods for genome-wide DNA methylation profiling.....	29
Figure 1.5 Main steps of RNA sequencing experiment and analytical approaches	30
Figure 3.1 Exome data quality and sequencing coverage for HCmel and BCmel cell lines.	50
Figure 3.2 Evaluation of somatic variant calling in BCmel and HCmel exome profiles. .	51
Figure 3.3 Comparison of mutational landscapes between primary melanoma cell lines of different GEM models and spontaneous melanoma (B16)	52
Figure 3.4 Hgf-Cdk4R24C murine preclinical model of melanoma for studying resistance mechanism to adoptive T cell transfer (ACT) immunotherapy	53
Figure 3.5 Somatic nonsynonymous mutations were acquired in ACT therapy-resistant HCmel-R melanoma cell lines compared to primary HCmel cell lines.	54
Figure 3.6 RNA sequencing experiment, data quality, and coverage report for HCmel cell lines.	59
Figure 3.7 Unsupervised principal component analysis on expression profiles indicates two distinct groups of primary and resistant cell lines	60
Figure 3.8 Differentially expressed genes in primary and ACT-resistant cell lines indicate downregulation of melanocytic differentiation and developmental genes in resistant phenotypes.	61
Figure 3.9 MeDIP-seq data analyses showed a genomic landscape of DNA methylation changes in HCmel and HCmel-R cell lines	69
Figure 3.10 Differentially hypermethylated CGIs in HCmel-R cells mirrored downregulation of genes with known functions in melanoma cell differentiation while hypomethylated CGIs contribute to known genes in cell proliferation.....	71

Figure 3.11 Intersection of differentially methylated and differentially expressed genes highlights the potential role of the MITF gene/pathway in ACT-resistant versus primary melanoma cells.....	72
Figure 3.12 The interaction of immune response with melanoma cell development and differentiation is traced in integrative functional enrichment.	73
Figure 3.13 Integration of somatic mutations with differential expression (DE) analysis in resistant cell lines indicates one gene; AXL.....	74
Figure 4.1 ACT immunotherapy-induced dedifferentiation in context of four-stage differentiation signature in melanoma	83
Figure 4.2 Broad biological functions and interactions of MITF gene/pathway in melanocytes, melanoma, and immune response (Ballotti et al., 2020).....	84

7 List of Tables

Table 2.1 Origin and characteristics of the cell lines.....	33
Table 2.2 Medium components for cell culture	34
Table 3.1 Exclusively shared mutated genes between all ACT-resistant (HCmel-R) melanoma cell lines candidate for contribution to resistance mechanisms.....	55

8 References

Akbani, R., Akdemir, K.C., Aksoy, B.A., Albert, M., Ally, A., Amin, S.B., Arachchi, H., Arora, A., Auman, J.T., Ayala, B., Baboud, J., Balasundaram, M., Balu, S., Barnabas, N., Bartlett, J., Bartlett, P., Bastian, B.C., Baylin, S.B., Behera, M., Belyaev, D., Benz, C., Bernard, B., Beroukhim, R., Bir, N., Black, A.D., Bodenheimer, T., Boice, L., Boland, G.M., Bono, R., Bootwalla, M.S., Bosenberg, M., Bowen, J., Bowlby, R., Bristow, C.A., Brockway-Lunardi, L., Brooks, D., Brzezinski, J., Bshara, W., Buda, E., Burns, W.R., Butterfield, Y.S.N., Button, M., Calderone, T., Cappellini, G.A., Carter, C., Carter, S.L., Cherney, L., Cherniack, A.D., Chevalier, A., Chin, L., Cho, J., Cho, R.J., Choi, Y.-L., Chu, A., Chudamani, S., Cibulskis, K., Ciriello, G., Clarke, A., Coons, S., Cope, L., Crain, D., Curley, E., Danilova, L., D'Atri, S., Davidsen, T., Davies, M.A., Delman, K.A., Demchok, J.A., Deng, Q.A., Deribe, Y.L., Dhalla, N., Dhir, R., DiCara, D., Dinikin, M., Dubina, M., Ebrom, J.S., Egea, S., Eley, G., Engel, J., Eschbacher, J.M., Fedosenko, K.V., Felau, I., Fennell, T., Ferguson, M.L., Fisher, S., Flaherty, K.T., Frazer, S., Frick, J., Fulidou, V., Gabriel, S.B., Gao, J., Gardner, J., Garraway, L.A., Gastier-Foster, J.M., Gaudioso, C., Gehlenborg, N., Genovese, G., Gerken, M., Gershenwald, J.E., Getz, G., Gomez-Fernandez, C., Gribbin, T., Grimsby, J., Gross, B., Guin, R., Gutschner, T., Hadjipanayis, A., Halaban, R., Hanf, B., Haussler, D., Haydu, L.E., Hayes, D.N., Hayward, N.K., Heiman, D.I., Herbert, L., Herman, J.G., Hersey, P., Hoadley, K.A., Hodis, E., Holt, R.A., Hoon, D.SB., Hoppough, S., Hoyle, A.P., Huang, F.W., Huang, M., Huang, S., Hutter, C.M., Ibbes, M., Iype, L., Jacobsen, A., Jakrot, V., Janning, A., Jeck, W.R., Jefferys, S.R., Jensen, M.A., Jones, C.D., Jones, S.J.M., Ju, Z., Kakavand, H., Kang, H., Kefford, R.F., Khuri, F.R., Kim, J., Kirkwood, J.M., Klode, J., Korkut, A., Korski, K., Krauthammer, M., Kucherlapati, R., Kwong, L.N., Kycler, W., Ladanyi, M., Lai, P.H., Laird, P.W., Lander, E., Lawrence, M.S., Lazar, A.J., Łażniak, R., Lee, D., Lee, J.E., Lee, J., Lee, K., Lee, S., Lee, W., Leporowska, E., Leraas, K.M., Li, H.I., Lichtenberg, T.M., Lichtenstein, L., Lin, P., Ling, S., Liu, J., Liu, O., Liu, W., Long, G.V., Lu, Y., Ma, S., Ma, Y., Mackiewicz, A., Mahadeshwar, H.S., Malke, J.,

Mallery, D., Manikhas, G.M., Mann, G.J., Marra, M.A., Matejka, B., Mayo, M., Mehrabi, S., Meng, S., Meyerson, M., Mieczkowski, P.A., Miller, J.P., Miller, M.L., Mills, G.B., Moiseenko, F., Moore, R.A., Morris, S., Morrison, C., Morton, D., Moschos, S., Mose, L.E., Muller, F.L., Mungall, A.J., Murawa, D., Murawa, P., Murray, B.A., Nezi, L., Ng, S., Nicholson, D., Noble, M.S., Osunkoya, A., Owonikoko, T.K., Ozenberger, B.A., Pagani, E., Paklina, O.V., Pantazi, A., Parfenov, M., Parfitt, J., Park, P.J., Park, W.-Y., Parker, J.S., Passarelli, F., Penny, R., Perou, C.M., Pihl, T.D., Potapova, O., Prieto, V.G., Protopopov, A., Quinn, M.J., Radenbaugh, A., Rai, K., Ramalingam, S.S., Raman, A.T., Ramirez, N.C., Ramirez, R., Rao, U., Rathmell, W.K., Ren, X., Reynolds, S.M., Roach, J., Robertson, A.G., Ross, M.I., Roszik, J., Russo, G., Saksena, G., Saller, C., Samuels, Y., Sander, Chris, Sander, Cindy, Sandusky, G., Santoso, N., Saul, M., Saw, R.P.M., Schadendorf, D., Schein, J.E., Schultz, N., Schumacher, S.E., Schwallier, C., Scolyer, R.A., Seidman, J., Sekhar, P.C., Sekhon, H.S., Senbabaoglu, Y., Seth, S., Shannon, K.F., Sharpe, S., Sharpless, N.E., Shaw, K.R.M., Shelton, C., Shelton, T., Shen, R., Sheth, M., Shi, Y., Shiau, C.J., Shmulevich, I., Sica, G.L., Simons, J.V., Sinha, R., Sipahimalani, P., Sofia, H.J., Soloway, M.G., Song, X., Sougnez, C., Spillane, A.J., Szycała, A., Stretch, J.R., Stuart, J., Suchorska, W.M., Sucker, A., Sumer, S.O., Sun, Y., Synott, M., Tabak, B., Tabler, T.R., Tam, A., Tan, D., Tang, J., Tarnuzzer, R., Tarvin, K., Tatka, H., Taylor, B.S., Teresiak, M., Thiessen, N., Thompson, J.F., Thorne, L., Thorsson, V., Trent, J.M., Triche, T.J., Tsai, K.Y., Tsou, P., Van Den Berg, D.J., Van Allen, E.M., Veluvolu, U., Verhaak, R.G., Voet, D., Voronina, O., Walter, V., Walton, J.S., Wan, Y., Wang, Y., Wang, Z., Waring, S., Watson, I.R., Weinhold, N., Weinstein, J.N., Weisenberger, D.J., White, P., Wilkerson, M.D., Wilmott, J.S., Wise, L., Wiznerowicz, M., Woodman, S.E., Wu, C.-J., Wu, C.-C., Wu, J., Wu, Y., Xi, R., Xu, A.W., Yang, D., Yang, Liming, Yang, Lixing, Zack, T.I., Zenklusen, J.C., Zhang, H., Zhang, J., Zhang, W., Zhao, X., Zhu, J., Zhu, K., Zimmer, L., Zmuda, E., Zou, L., 2015. Genomic Classification of Cutaneous Melanoma. *Cell* 161, 1681–1696. <https://doi.org/10.1016/j.cell.2015.05.044>

Anders, S., Huber, W., 2010. Differential expression analysis for sequence count data. *Genome Biol.* 11, R106. <https://doi.org/10.1186/gb-2010-11-10-r106>

- Anders, S., Pyl, P.T., Huber, W., 2015. HTSeq--a Python framework to work with high-throughput sequencing data. *Bioinformatics* 31, 166–169. <https://doi.org/10.1093/bioinformatics/btu638>
- Arozarena, I., Wellbrock, C., 2019. Phenotype plasticity as enabler of melanoma progression and therapy resistance. *Nat. Rev. Cancer* 19, 377–391. <https://doi.org/10.1038/s41568-019-0154-4>
- Australian Pancreatic Cancer Genome Initiative, ICGC Breast Cancer Consortium, ICGC MML-Seq Consortium, ICGC PedBrain, Alexandrov, L.B., Nik-Zainal, S., Wedge, D.C., Aparicio, S.A.J.R., Behjati, S., Biankin, A.V., Bignell, G.R., Bolli, N., Borg, A., Børresen-Dale, A.-L., Boyault, S., Burkhardt, B., Butler, A.P., Caldas, C., Davies, H.R., Desmedt, C., Eils, R., Eyfjörd, J.E., Foekens, J.A., Greaves, M., Hosoda, F., Hutter, B., Illicic, T., Imbeaud, S., Imielinski, M., Jäger, N., Jones, D.T.W., Jones, D., Knappskog, S., Kool, M., Lakhani, S.R., López-Otín, C., Martin, S., Munshi, N.C., Nakamura, H., Northcott, P.A., Pajic, M., Papaemmanuil, E., Paradiso, A., Pearson, J.V., Puente, X.S., Raine, K., Ramakrishna, M., Richardson, A.L., Richter, J., Rosenstiel, P., Schlesner, M., Schumacher, T.N., Span, P.N., Teague, J.W., Totoki, Y., Tutt, A.N.J., Valdés-Mas, R., van Buuren, M.M., van 't Veer, L., Vincent-Salomon, A., Waddell, N., Yates, L.R., Zucman-Rossi, J., Andrew Futreal, P., McDermott, U., Lichter, P., Meyerson, M., Grimmond, S.M., Siebert, R., Campo, E., Shibata, T., Pfister, S.M., Campbell, P.J., Stratton, M.R., 2013. Signatures of mutational processes in human cancer. *Nature* 500, 415–421. <https://doi.org/10.1038/nature12477>
- Bald, T., Quast, T., Landsberg, J., Rogava, M., Glodde, N., Lopez-Ramos, D., Kohlmeyer, J., Riesenberger, S., van den Boorn-Konijnenberg, D., Hömig-Hölzel, C., Reuten, R., Schadow, B., Weighardt, H., Wenzel, D., Helfrich, I., Schadendorf, D., Bloch, W., Bianchi, M.E., Lugassy, C., Barnhill, R.L., Koch, M., Fleischmann, B.K., Förster, I., Kastenmüller, W., Kolanus, W., Hölzel, M., Gaffal, E., Tüting, T., 2014. Ultraviolet-radiation-induced inflammation promotes angiotropism and metastasis in melanoma. *Nature* 507, 109–113. <https://doi.org/10.1038/nature13111>
- Ballotti, R., Cheli, Y., Bertolotto, C., 2020. The complex relationship between MITF and the immune system: a Melanoma ImmunoTherapy (response) Factor? *Mol. Cancer* 19, 170. <https://doi.org/10.1186/s12943-020-01290-7>

- Bernstein, B.E., Meissner, A., Lander, E.S., 2007. The Mammalian Epigenome. *Cell* 128, 669–681. <https://doi.org/10.1016/j.cell.2007.01.033>
- Bock, C., Tomazou, E.M., Brinkman, A.B., Müller, F., Simmer, F., Gu, H., Jäger, N., Gnirke, A., Stunnenberg, H.G., Meissner, A., 2010. Quantitative comparison of genome-wide DNA methylation mapping technologies. *Nat. Biotechnol.* 28, 1106–1114. <https://doi.org/10.1038/nbt.1681>
- Boshuizen, J., Koopman, L.A., Krijgsman, O., Shahrabi, A., van den Heuvel, E.G., Ligtenberg, M.A., Vredevoogd, D.W., Kemper, K., Kuilman, T., Song, J.-Y., Pencheva, N., Mortensen, J.T., Foppen, M.G., Rozeman, E.A., Blank, C.U., Janmaat, M.L., Satijn, D., Breij, E.C.W., Peeper, D.S., Parren, P.W.H.I., 2018. Cooperative targeting of melanoma heterogeneity with an AXL antibody-drug conjugate and BRAF/MEK inhibitors. *Nat. Med.* 24, 203–212. <https://doi.org/10.1038/nm.4472>
- Cao, X., Liang, Y., Hu, Z., Li, H., Yang, J., Hsu, E.J., Zhu, J., Zhou, J., Fu, Y.-X., 2021. Next generation of tumor-activating type I IFN enhances anti-tumor immune responses to overcome therapy resistance. *Nat. Commun.* 12, 5866. <https://doi.org/10.1038/s41467-021-26112-2>
- Cheng, Y., He, C., Wang, M., Ma, X., Mo, F., Yang, S., Han, J., Wei, X., 2019. Targeting epigenetic regulators for cancer therapy: mechanisms and advances in clinical trials. *Signal Transduct. Target. Ther.* 4, 62. <https://doi.org/10.1038/s41392-019-0095-0>
- Cibulskis, K., Lawrence, M.S., Carter, S.L., Sivachenko, A., Jaffe, D., Sougnez, C., Gabriel, S., Meyerson, M., Lander, E.S., Getz, G., 2013. Sensitive detection of somatic point mutations in impure and heterogeneous cancer samples. *Nat. Biotechnol.* 31, 213–219. <https://doi.org/10.1038/nbt.2514>
- Conesa, A., Madrigal, P., Tarazona, S., Gomez-Cabrero, D., Cervera, A., McPherson, A., Szczeńniak, M.W., Gaffney, D.J., Elo, L.L., Zhang, X., Mortazavi, A., 2016. A survey of best practices for RNA-seq data analysis. *Genome Biol.* 17, 13. <https://doi.org/10.1186/s13059-016-0881-8>
- Corchete, L.A., Rojas, E.A., Alonso-López, D., De Las Rivas, J., Gutiérrez, N.C., Burguillo, F.J., 2020. Systematic comparison and assessment of RNA-seq procedures for

- gene expression quantitative analysis. *Sci. Rep.* 10, 19737. <https://doi.org/10.1038/s41598-020-76881-x>
- Dahl, C., Guldborg, P., 2007. The genome and epigenome of malignant melanoma. *APMIS* 115, 1161–1176. https://doi.org/10.1111/j.1600-0463.2007.apm_855.xml.x
- Danecek, P., Auton, A., Abecasis, G., Albers, C.A., Banks, E., DePristo, M.A., Handsaker, R.E., Lunter, G., Marth, G.T., Sherry, S.T., McVean, G., Durbin, R., n.d. The variant call format and VCFtools 3.
- Del Castillo Velasco-Herrera, M., van der Weyden, L., Nsengimana, J., Speak, A.O., Sjöberg, M.K., Bishop, D.T., Jönsson, G., Newton-Bishop, J., Adams, D.J., 2018. Comparative genomics reveals that loss of lunatic fringe (*LFNG*) promotes melanoma metastasis. *Mol. Oncol.* 12, 239–255. <https://doi.org/10.1002/1878-0261.12161>
- Dobin, A., Davis, C.A., Schlesinger, F., Drenkow, J., Zaleski, C., Jha, S., Batut, P., Chaisson, M., Gingeras, T.R., n.d. STAR: ultrafast universal RNA-seq aligner 7.
- Feinberg, A.P., Ohlsson, R., Henikoff, S., 2006. The epigenetic progenitor origin of human cancer. *Nat. Rev. Genet.* 7, 21–33. <https://doi.org/10.1038/nrg1748>
- Flem-Karlsen, K., Nyakas, M., Farstad, I.N., McFadden, E., Wernhoff, P., Jacobsen, K.D., Flørenes, V.A., Mælandsmo, G.M., 2020. Soluble AXL as a marker of disease progression and survival in melanoma. *PLOS ONE* 15, e0227187. <https://doi.org/10.1371/journal.pone.0227187>
- Frommer, M., McDonald, L.E., Millar, D.S., Collis, C.M., Watt, F., Grigg, G.W., Molloy, P.L., Paul, C.L., 1992. A genomic sequencing protocol that yields a positive display of 5-methylcytosine residues in individual DNA strands. *Proc. Natl. Acad. Sci.* 89, 1827–1831. <https://doi.org/10.1073/pnas.89.5.1827>
- Gaffal, E., Landsberg, J., Bald, T., Sporleder, A., Kohlmeyer, J., Tüting, T., 2011. Neonatal UVB exposure accelerates melanoma growth and enhances distant metastases in Hgf-Cdk4R24C C57BL/6 mice. *Int. J. Cancer* 129, 285–294. <https://doi.org/10.1002/ijc.25913>
- Gautron, A., Bachelot, L., Aubry, M., Leclerc, D., Quéméner, A.M., Corre, S., Rambow, F., Paris, A., Tardif, N., Leclair, H.M., Marin-Bejar, O., Coulouarn, C., Marine, J., Galibert, M., Gilot, D., 2021. CRISPR screens identify tumor-promoting genes

- conferring melanoma cell plasticity and resistance. *EMBO Mol. Med.* 13. <https://doi.org/10.15252/emmm.202013466>
- Gay, C.M., Balaji, K., Byers, L.A., 2017. Giving AXL the axe: targeting AXL in human malignancy. *Br. J. Cancer* 116, 415–423. <https://doi.org/10.1038/bjc.2016.428>
- Geraci, F., Saha, I., Bianchini, M., 2020. Editorial: RNA-Seq Analysis: Methods, Applications and Challenges. *Front. Genet.* 11, 220. <https://doi.org/10.3389/fgene.2020.00220>
- Glodde, N., Bald, T., van den Boorn-Konijnenberg, D., Nakamura, K., O'Donnell, J.S., Szczepanski, S., Brandes, M., Eickhoff, S., Das, I., Shridhar, N., Hinze, D., Rogava, M., van der Sluis, T.C., Ruotsalainen, J.J., Gaffal, E., Landsberg, J., Ludwig, K.U., Wilhelm, C., Riek-Burchardt, M., Müller, A.J., Gebhardt, C., Scolyer, R.A., Long, G.V., Janzen, V., Teng, M.W.L., Kastenmüller, W., Mazzone, M., Smyth, M.J., Tüting, T., Hölzel, M., 2017. Reactive Neutrophil Responses Dependent on the Receptor Tyrosine Kinase c-MET Limit Cancer Immunotherapy. *Immunity* 47, 789–802.e9. <https://doi.org/10.1016/j.immuni.2017.09.012>
- Grimm, C., Chavez, L., Vilardell, M., Farrall, A.L., Tierling, S., Böhm, J.W., Grote, P., Lienhard, M., Dietrich, J., Timmermann, B., Walter, J., Schweiger, M.R., Lehrach, H., Herwig, R., Herrmann, B.G., Morkel, M., 2013. DNA–Methylome Analysis of Mouse Intestinal Adenoma Identifies a Tumour-Specific Signature That Is Partly Conserved in Human Colon Cancer. *PLoS Genet.* 9, e1003250. <https://doi.org/10.1371/journal.pgen.1003250>
- Hayward, N.K., Wilmott, J.S., Waddell, Nicola, Johansson, P.A., Field, M.A., Nones, K., Patch, A.-M., Kakavand, H., Alexandrov, L.B., Burke, H., Jakrot, V., Kazakoff, S., Holmes, O., Leonard, C., Sabarinathan, R., Mularoni, L., Wood, S., Xu, Q., Waddell, Nick, Tembe, V., Pupo, G.M., De Paoli-Iseppi, R., Vilain, R.E., Shang, P., Lau, L.M.S., Dagg, R.A., Schramm, S.-J., Pritchard, A., Dutton-Regester, K., Newell, F., Fitzgerald, A., Shang, C.A., Grimmond, S.M., Pickett, H.A., Yang, J.Y., Stretch, J.R., Behren, A., Kefford, R.F., Hersey, P., Long, G.V., Cebon, J., Shackleton, M., Spillane, A.J., Saw, R.P.M., López-Bigas, N., Pearson, J.V., Thompson, J.F., Scolyer, R.A., Mann, G.J., 2017. Whole-genome landscapes of major melanoma subtypes. *Nature* 545, 175–180. <https://doi.org/10.1038/nature22071>

- Hemesath, T.J., Steingrimsson, E., McGill, G., Hansen, M.J., Vaught, J., Hodgkinson, C.A., Arnheiter, H., Copeland, N.G., Jenkins, N.A., Fisher, D.E., 1994. microphthalmia, a critical factor in melanocyte development, defines a discrete transcription factor family. *Genes Dev.* 8, 2770–2780. <https://doi.org/10.1101/gad.8.22.2770>
- Ho, M., Riesenberger, S., Becker, A., n.d. A Preclinical Model of Malignant Peripheral Nerve Sheath Tumor-like Melanoma Is Characterized by Infiltrating Mast Cells. *Cancer Res.* 14.
- Hodis, E., Watson, I.R., Kryukov, G.V., Arola, S.T., Imielinski, M., Theurillat, J.-P., Nickerson, E., Auclair, D., Li, L., Place, C., DiCara, D., Ramos, A.H., Lawrence, M.S., Cibulskis, K., Sivachenko, A., Voet, D., Saksena, G., Stransky, N., Onofrio, R.C., Winckler, W., Ardlie, K., Wagle, N., Wargo, J., Chong, K., Morton, D.L., Stemke-Hale, K., Chen, G., Noble, M., Meyerson, M., Ladbury, J.E., Davies, M.A., Gershenwald, J.E., Wagner, S.N., Hoon, D.S.B., Schadendorf, D., Lander, E.S., Gabriel, S.B., Getz, G., Garraway, L.A., Chin, L., 2012. A Landscape of Driver Mutations in Melanoma. *Cell* 150, 251–263. <https://doi.org/10.1016/j.cell.2012.06.024>
- Hoek, K.S., Eichhoff, O.M., Schlegel, N.C., Döbbeling, U., Kobert, N., Schaerer, L., Hemmi, S., Dummer, R., 2008. *In vivo* Switching of Human Melanoma Cells between Proliferative and Invasive States. *Cancer Res.* 68, 650–656. <https://doi.org/10.1158/0008-5472.CAN-07-2491>
- Hoek, K.S., Schlegel, N.C., Brafford, P., Sucker, A., Ugurel, S., Kumar, R., Weber, B.L., Nathanson, K.L., Phillips, D.J., Herlyn, M., Schadendorf, D., Dummer, R., 2006. Metastatic potential of melanomas defined by specific gene expression profiles with no BRAF signature. *Pigment Cell Res.* 19, 290–302. <https://doi.org/10.1111/j.1600-0749.2006.00322.x>
- Hölzel, M., Bovier, A., Tüting, T., 2013. Plasticity of tumour and immune cells: a source of heterogeneity and a cause for therapy resistance? *Nat. Rev. Cancer* 13, 365–376. <https://doi.org/10.1038/nrc3498>
- Huang, D., Sherman, B.T., Tan, Q., Collins, J.R., Alvord, W.G., Roayaei, J., Stephens, R., Baseler, M.W., Lane, H.C., Lempicki, R.A., 2007. The DAVID Gene Functional Classification Tool: a novel biological module-centric algorithm to functionally

- analyze large gene lists. *Genome Biol.* 8, R183. <https://doi.org/10.1186/gb-2007-8-9-r183>
- Huergo-Zapico, L., Parodi, M., Cantoni, C., Lavarello, C., Fernández-Martínez, J.L., Petretto, A., DeAndrés-Galiana, E.J., Balsamo, M., López-Soto, A., Pietra, G., Bugatti, M., Munari, E., Marconi, M., Mingari, M.C., Vermi, W., Moretta, L., González, S., Vitale, M., 2018. NK-cell Editing Mediates Epithelial-to-Mesenchymal Transition via Phenotypic and Proteomic Changes in Melanoma Cell Lines. *Cancer Res.* 78, 3913–3925. <https://doi.org/10.1158/0008-5472.CAN-17-1891>
- Hugo, W., Shi, H., Sun, L., Piva, M., Song, C., Kong, X., Moriceau, G., Hong, A., Dahlman, K.B., Johnson, D.B., Sosman, J.A., Ribas, A., Lo, R.S., 2015. Non-genomic and Immune Evolution of Melanoma Acquiring MAPKi Resistance. *Cell* 162, 1271–1285. <https://doi.org/10.1016/j.cell.2015.07.061>
- Hugo, W., Zaretsky, J.M., Sun, L., Song, C., Moreno, B.H., Hu-Lieskovan, S., Berent-Maoz, B., Pang, J., Chmielowski, B., Cherry, G., Seja, E., Lomeli, S., Kong, X., Kelley, M.C., Sosman, J.A., Johnson, D.B., Ribas, A., Lo, R.S., 2016. Genomic and Transcriptomic Features of Response to Anti-PD-1 Therapy in Metastatic Melanoma. *Cell* 165, 35–44. <https://doi.org/10.1016/j.cell.2016.02.065>
- Kawakami, A., Fisher, D.E., 2017. The master role of microphthalmia-associated transcription factor in melanocyte and melanoma biology. *Lab. Invest.* 97, 649–656. <https://doi.org/10.1038/labinvest.2017.9>
- Keane, T.M., Goodstadt, L., Danecek, P., White, M.A., Wong, K., Yalcin, B., Heger, A., Agam, A., Slater, G., Goodson, M., Furlotte, N.A., Eskin, E., Nellåker, C., Whitley, H., Cleak, J., Janowitz, D., Hernandez-Pliego, P., Edwards, A., Belgard, T.G., Oliver, P.L., McIntyre, R.E., Bhomra, A., Nicod, J., Gan, X., Yuan, W., van der Weyden, L., Steward, C.A., Bala, S., Stalker, J., Mott, R., Durbin, R., Jackson, I.J., Czechanski, A., Guerra-Assunção, J.A., Donahue, L.R., Reinholdt, L.G., Payseur, B.A., Ponting, C.P., Birney, E., Flint, J., Adams, D.J., 2011. Mouse genomic variation and its effect on phenotypes and gene regulation. *Nature* 477, 289–294. <https://doi.org/10.1038/nature10413>
- Khong, H.T., Restifo, N.P., 2002. Natural selection of tumor variants in the generation of “tumor escape” phenotypes. *Nat. Immunol.* 3, 7.

- Kim, M., Costello, J., 2017. DNA methylation: an epigenetic mark of cellular memory. *Exp. Mol. Med.* 49, e322–e322. <https://doi.org/10.1038/emm.2017.10>
- Kohlmeyer, J., Cron, M., Landsberg, J., Bald, T., Renn, M., Mikus, S., Bondong, S., Wikasari, D., Gaffal, E., Hartmann, G., Tuting, T., 2009. Complete Regression of Advanced Primary and Metastatic Mouse Melanomas following Combination Chemoimmunotherapy. *Cancer Res.* 69, 6265–6274. <https://doi.org/10.1158/0008-5472.CAN-09-0579>
- Konieczkowski, D.J., Johannessen, C.M., Abudayyeh, O., Kim, J.W., Cooper, Z.A., Piris, A., Frederick, D.T., Barzily-Rokni, M., Straussman, R., Haq, R., Fisher, D.E., Mesirov, J.P., Hahn, W.C., Flaherty, K.T., Wargo, J.A., Tamayo, P., Garraway, L.A., 2014. A Melanoma Cell State Distinction Influences Sensitivity to MAPK Pathway Inhibitors. *Cancer Discov.* 4, 816–827. <https://doi.org/10.1158/2159-8290.CD-13-0424>
- Landsberg, J., Kohlmeyer, J., Renn, M., Bald, T., Rogava, M., Cron, M., Fatho, M., Lennerz, V., Wölfel, T., Hölzel, M., Tuting, T., 2012. Melanomas resist T-cell therapy through inflammation-induced reversible dedifferentiation. *Nature* 490, 412–416. <https://doi.org/10.1038/nature11538>
- Langmead, B., Salzberg, S.L., 2012. Fast gapped-read alignment with Bowtie 2. *Nat. Methods* 9, 357–359. <https://doi.org/10.1038/nmeth.1923>
- Lauss, M., Haq, R., Cirenajwis, H., Phung, B., Harbst, K., Staaf, J., Rosengren, F., Holm, K., Aine, M., Jirström, K., Borg, Å., Busch, C., Geisler, J., Lønning, P.E., Ringnér, M., Howlin, J., Fisher, D.E., Jönsson, G., 2015. Genome-Wide DNA Methylation Analysis in Melanoma Reveals the Importance of CpG Methylation in MITF Regulation. *J. Invest. Dermatol.* 135, 1820–1828. <https://doi.org/10.1038/jid.2015.61>
- Lee, J.H., Shklovskaya, E., Lim, S.Y., Carlino, M.S., Menzies, A.M., Stewart, A., Pedersen, B., Irvine, M., Alavi, S., Yang, J.Y.H., Strbenac, D., Saw, R.P.M., Thompson, J.F., Wilmott, J.S., Scolyer, R.A., Long, G.V., Kefford, R.F., Rizos, H., 2020. Transcriptional downregulation of MHC class I and melanoma dedifferentiation in resistance to PD-1 inhibition. *Nat. Commun.* 11, 1897. <https://doi.org/10.1038/s41467-020-15726-7>

- Lex, A., Gehlenborg, N., 2014. Sets and intersections. *Nat. Methods* 11, 779–779. <https://doi.org/10.1038/nmeth.3033>
- Li, H., 2013. Aligning sequence reads, clone sequences and assembly contigs with BWA-MEM. *ArXiv13033997 Q-Bio*.
- Li, P., Piao, Y., Shon, H.S., Ryu, K.H., 2015. Comparing the normalization methods for the differential analysis of Illumina high-throughput RNA-Seq data. *BMC Bioinformatics* 16, 347. <https://doi.org/10.1186/s12859-015-0778-7>
- Lienhard, M., Grasse, S., Rolff, J., Frese, S., Schirmer, U., Becker, M., Börno, S., Timmermann, B., Chavez, L., Sülthmann, H., Leschber, G., Fichtner, I., Schweiger, M.R., Herwig, R., 2017. QSEA—modelling of genome-wide DNA methylation from sequencing enrichment experiments. *Nucleic Acids Res.* 45, e44–e44. <https://doi.org/10.1093/nar/gkw1193>
- Love, M.I., Huber, W., Anders, S., 2014. Moderated estimation of fold change and dispersion for RNA-seq data with DESeq2. *Genome Biol.* 15, 550. <https://doi.org/10.1186/s13059-014-0550-8>
- Matsushita, H., Vesely, M.D., Koboldt, D.C., Rickert, C.G., Uppaluri, R., Magrini, V.J., Arthur, C.D., White, J.M., Chen, Y.-S., Shea, L.K., Hundal, J., Wendl, M.C., Demeter, R., Wylie, T., Allison, J.P., Smyth, M.J., Old, L.J., Mardis, E.R., Schreiber, R.D., 2012. Cancer exome analysis reveals a T-cell-dependent mechanism of cancer immunoediting. *Nature* 482, 400–404. <https://doi.org/10.1038/nature10755>
- McLaren, W., Gil, L., Hunt, S.E., Riat, H.S., Ritchie, G.R.S., Thormann, A., Flicek, P., Cunningham, F., 2016. The Ensembl Variant Effect Predictor. *Genome Biol.* 17, 122. <https://doi.org/10.1186/s13059-016-0974-4>
- Mehta, A., Kim, Y.J., Robert, L., Tsoi, J., Comin-Anduix, B., Berent-Maoz, B., Cochran, A.J., Economou, J.S., Tumei, P.C., Puig-Saus, C., Ribas, A., 2018. Immunotherapy Resistance by Inflammation-Induced Dedifferentiation. *Cancer Discov.* 8, 935–943. <https://doi.org/10.1158/2159-8290.CD-17-1178>
- Meissner, A., 2005. Reduced representation bisulfite sequencing for comparative high-resolution DNA methylation analysis. *Nucleic Acids Res.* 33, 5868–5877. <https://doi.org/10.1093/nar/gki901>
- Merlino, G., Herlyn, M., Fisher, D.E., Bastian, B.C., Flaherty, K.T., Davies, M.A., Wargo, J.A., Curiel-Lewandrowski, C., Weber, M.J., Leachman, S.A., Soengas, M.S.,

- McMahon, M., Harbour, J.W., Swetter, S.M., Aplin, A.E., Atkins, M.B., Bosenberg, M.W., Dummer, R., Gershenwald, J.E., Halpern, A.C., Herlyn, D., Karakousis, G.C., Kirkwood, J.M., Krauthammer, M., Lo, R.S., Long, G.V., McArthur, G., Ribas, A., Schuchter, L., Sosman, J.A., Smalley, K.S., Steeg, P., Thomas, N.E., Tsao, H., Tuetting, T., Weeraratna, A., Xu, G., Lomax, R., Martin, A., Silverstein, S., Turnham, T., Ronai, Z.A., 2016. The state of melanoma: challenges and opportunities. *Pigment Cell Melanoma Res.* 29, 404–416. <https://doi.org/10.1111/pcmr.12475>
- Mica, Y., Lee, G., Chambers, S.M., Tomishima, M.J., Studer, L., 2013. Modeling Neural Crest Induction, Melanocyte Specification, and Disease-Related Pigmentation Defects in hESCs and Patient-Specific iPSCs. *Cell Rep.* 3, 1140–1152. <https://doi.org/10.1016/j.celrep.2013.03.025>
- Miranda Furtado, C.L., Dos Santos Luciano, M.C., Silva Santos, R.D., Furtado, G.P., Moraes, M.O., Pessoa, C., 2019. Epidrugs: targeting epigenetic marks in cancer treatment. *Epigenetics* 14, 1164–1176. <https://doi.org/10.1080/15592294.2019.1640546>
- Mortazavi, A., Williams, B.A., McCue, K., Schaeffer, L., Wold, B., 2008. Mapping and quantifying mammalian transcriptomes by RNA-Seq. *Nat. Methods* 5, 621–628. <https://doi.org/10.1038/nmeth.1226>
- Müller, J., Krijgsman, O., Tsoi, J., Robert, L., Hugo, W., Song, C., Kong, X., Possik, P.A., Cornelissen-Steijger, P.D.M., Foppen, M.H.G., Kemper, K., Goding, C.R., McDermott, U., Blank, C., Haanen, J., Graeber, T.G., Ribas, A., Lo, R.S., Peeper, D.S., 2014. Low MITF/AXL ratio predicts early resistance to multiple targeted drugs in melanoma. *Nat. Commun.* 5, 5712. <https://doi.org/10.1038/ncomms6712>
- Newell, F., Pires da Silva, I., Johansson, P.A., Menzies, A.M., Wilmott, J.S., Addala, V., Carlino, M.S., Rizos, H., Nones, K., Edwards, J.J., Lakis, V., Kazakoff, S.H., Mukhopadhyay, P., Ferguson, P.M., Leonard, C., Koufariotis, L.T., Wood, S., Blank, C.U., Thompson, J.F., Spillane, A.J., Saw, R.P.M., Shannon, K.F., Pearson, J.V., Mann, G.J., Hayward, N.K., Scolyer, R.A., Waddell, N., Long, G.V., 2021. Multiomic profiling of checkpoint inhibitor-treated melanoma: Identifying predictors of response and resistance, and markers of biological discordance. *Cancer Cell* S1535610821006127. <https://doi.org/10.1016/j.ccell.2021.11.012>

- PCAWG Mutational Signatures Working Group, PCAWG Consortium, Alexandrov, L.B., Kim, J., Haradhvala, N.J., Huang, M.N., Tian Ng, A.W., Wu, Y., Boot, A., Covington, K.R., Gordenin, D.A., Bergstrom, E.N., Islam, S.M.A., Lopez-Bigas, N., Klimczak, L.J., McPherson, J.R., Morganella, S., Sabarinathan, R., Wheeler, D.A., Mustonen, V., Getz, G., Rozen, S.G., Stratton, M.R., 2020. The repertoire of mutational signatures in human cancer. *Nature* 578, 94–101. <https://doi.org/10.1038/s41586-020-1943-3>
- Peng, W., Chen, J.Q., Liu, C., Malu, S., Creasy, C., Tetzlaff, M.T., Xu, C., McKenzie, J.A., Zhang, C., Liang, X., Williams, L.J., Deng, W., Chen, G., Mbofung, R., Lazar, A.J., Torres-Cabala, C.A., Cooper, Z.A., Chen, P.-L., Tieu, T.N., Spranger, S., Yu, X., Bernatchez, C., Forget, M.-A., Haymaker, C., Amaria, R., McQuade, J.L., Glitza, I.C., Cascone, T., Li, H.S., Kwong, L.N., Heffernan, T.P., Hu, J., Bassett, R.L., Bosenberg, M.W., Woodman, S.E., Overwijk, W.W., Lizée, G., Roszik, J., Gajewski, T.F., Wargo, J.A., Gershenwald, J.E., Radvanyi, L., Davies, M.A., Hwu, P., 2016. Loss of PTEN Promotes Resistance to T Cell–Mediated Immunotherapy. *Cancer Discov.* 6, 202–216. <https://doi.org/10.1158/2159-8290.CD-15-0283>
- Pérez-Guijarro, E., Day, C.-P., Merlino, G., Zaidi, M.R., 2017. Genetically engineered mouse models of melanoma: Mouse Models of Melanoma. *Cancer* 123, 2089–2103. <https://doi.org/10.1002/cncr.30684>
- Pérez-Guijarro, E., Yang, H.H., Araya, R.E., El Meskini, R., Michael, H.T., Vodnala, S.K., Marie, K.L., Smith, C., Chin, S., Lam, K.C., Thorkelsson, A., Iacovelli, A.J., Kulaga, A., Fon, A., Michalowski, A.M., Hugo, W., Lo, R.S., Restifo, N.P., Sharan, S.K., Van Dyke, T., Goldszmid, R.S., Weaver Ohler, Z., Lee, M.P., Day, C.-P., Merlino, G., 2020. Multimodel preclinical platform predicts clinical response of melanoma to immunotherapy. *Nat. Med.* 26, 781–791. <https://doi.org/10.1038/s41591-020-0818-3>
- Rambow, F., Marine, J.-C., Goding, C.R., 2019. Melanoma plasticity and phenotypic diversity: therapeutic barriers and opportunities. *Genes Dev.* 33, 1295–1318. <https://doi.org/10.1101/gad.329771.119>
- Riesenberg, S., Groetchen, A., Siddaway, R., Bald, T., Reinhardt, J., Smorra, D., Kohlmeyer, J., Renn, M., Phung, B., Aymans, P., Schmidt, T., Hornung, V., Davidson, I., Goding, C.R., Jönsson, G., Landsberg, J., Tüting, T., Hölzel, M., 2015.

- MITF and c-Jun antagonism interconnects melanoma dedifferentiation with pro-inflammatory cytokine responsiveness and myeloid cell recruitment. *Nat. Commun.* 6, 8755. <https://doi.org/10.1038/ncomms9755>
- Robinson, M.D., Oshlack, A., 2010. A scaling normalization method for differential expression analysis of RNA-seq data. *Genome Biol.* 11, R25. <https://doi.org/10.1186/gb-2010-11-3-r25>
- Rosenthal, R., McGranahan, N., Herrero, J., Taylor, B.S., Swanton, C., 2016. deconstructSigs: delineating mutational processes in single tumors distinguishes DNA repair deficiencies and patterns of carcinoma evolution. *Genome Biol.* 17, 31. <https://doi.org/10.1186/s13059-016-0893-4>
- Saleh, J., 2018. Murine models of melanoma. *Pathol. - Res. Pract.* 214, 1235–1238. <https://doi.org/10.1016/j.prp.2018.07.008>
- Sarkar, D., Leung, E.Y., Baguley, B.C., Finlay, G.J., Askarian-Amiri, M.E., 2015. Epigenetic regulation in human melanoma: past and future. *Epigenetics* 10, 103–121. <https://doi.org/10.1080/15592294.2014.1003746>
- Schellenberg, A., Lin, Q., Schüler, H., Koch, C.M., Jousseen, S., Denecke, B., Walenda, G., Pallua, N., Suschek, C.V., Zenke, M., Wagner, W., 2011. Replicative senescence of mesenchymal stem cells causes DNA-methylation changes which correlate with repressive histone marks. *Aging* 3, 873–888. <https://doi.org/10.18632/aging.100391>
- Shaffer, S.M., Dunagin, M.C., Torborg, S.R., Torre, E.A., Emert, B., Krepler, C., Beqiri, M., Sproesser, K., Brafford, P.A., Xiao, M., Eggan, E., Anastopoulos, I.N., Vargas-Garcia, C.A., Singh, A., Nathanson, K.L., Herlyn, M., Raj, A., 2017. Rare cell variability and drug-induced reprogramming as a mode of cancer drug resistance. *Nature* 546, 431–435. <https://doi.org/10.1038/nature22794>
- Shipony, Z., Mukamel, Z., Cohen, N.M., Landan, G., Chomsky, E., Zeligler, S.R., Fried, Y.C., Ainbinder, E., Friedman, N., Tanay, A., 2014. Dynamic and static maintenance of epigenetic memory in pluripotent and somatic cells. *Nature* 513, 115–119. <https://doi.org/10.1038/nature13458>
- Spranger, S., Spaapen, R.M., Zha, Y., Williams, J., Meng, Y., Ha, T.T., Gajewski, T.F., 2013. Up-Regulation of PD-L1, IDO, and Tregs in the Melanoma Tumor

- Microenvironment Is Driven by CD8⁺ T Cells. *Sci. Transl. Med.* 5, 200ra116-200ra116. <https://doi.org/10.1126/scitranslmed.3006504>
- Supek, F., Bosnjak, M., 2011. REVIGO Summarizes and Visualizes Long Lists of Gene Ontology Terms. *PLoS ONE* 6, 9.
- Tate, J.G., Bamford, S., Jubb, H.C., Sondka, Z., Beare, D.M., Bindal, N., Boutselakis, H., Cole, C.G., Creatore, C., Dawson, E., Fish, P., Harsha, B., Hathaway, C., Jupe, S.C., Kok, C.Y., Noble, K., Ponting, L., Ramshaw, C.C., Rye, C.E., Speedy, H.E., Stefancsik, R., Thompson, S.L., Wang, S., Ward, S., Campbell, P.J., Forbes, S.A., 2019. COSMIC: the Catalogue Of Somatic Mutations In Cancer. *Nucleic Acids Res.* 47, D941–D947. <https://doi.org/10.1093/nar/gky1015>
- Thorvaldsdottir, H., Robinson, J.T., Mesirov, J.P., 2013. Integrative Genomics Viewer (IGV): high-performance genomics data visualization and exploration. *Brief. Bioinform.* 14, 178–192. <https://doi.org/10.1093/bib/bbs017>
- Tirosh, I., Izar, B., Prakadan, S.M., Wadsworth, M.H., Treacy, D., Trombetta, J.J., Rotem, A., Rodman, C., Lian, C., Murphy, G., Fallahi-Sichani, M., Dutton-Regester, K., Lin, J.-R., Cohen, O., Shah, P., Lu, D., Genshaft, A.S., Hughes, T.K., Ziegler, C.G.K., Kazer, S.W., Gaillard, A., Kolb, K.E., Villani, A.-C., Johannessen, C.M., Andreev, A.Y., Van Allen, E.M., Bertagnolli, M., Sorger, P.K., Sullivan, R.J., Flaherty, K.T., Frederick, D.T., Jané-Valbuena, J., Yoon, C.H., Rozenblatt-Rosen, O., Shalek, A.K., Regev, A., Garraway, L.A., 2016. Dissecting the multicellular ecosystem of metastatic melanoma by single-cell RNA-seq. *Science* 352, 189–196. <https://doi.org/10.1126/science.aad0501>
- Tormo, D., Ferrer, A., Bosch, P., Gaffal, E., Basner-Tschakarjan, E., Wenzel, J., Tüting, T., 2006. Therapeutic Efficacy of Antigen-Specific Vaccination and Toll-Like Receptor Stimulation against Established Transplanted and Autochthonous Melanoma in Mice. *Cancer Res.* 66, 5427–5435. <https://doi.org/10.1158/0008-5472.CAN-06-0399>
- Tsoi, J., Robert, L., Paraiso, K., Galvan, C., Sheu, K.M., Lay, J., Wong, D.J.L., Atefi, M., Shirazi, R., Wang, X., Braas, D., Grasso, C.S., Palaskas, N., Ribas, A., Graeber, T.G., 2018. Multi-stage Differentiation Defines Melanoma Subtypes with Differential Vulnerability to Drug-Induced Iron-Dependent Oxidative Stress. *Cancer Cell* 33, 890-904.e5. <https://doi.org/10.1016/j.ccell.2018.03.017>

- Tumeh, P.C., Harview, C.L., Yearley, J.H., Shintaku, I.P., Taylor, E.J.M., Robert, L., Chmielowski, B., Spasic, M., Henry, G., Ciobanu, V., West, A.N., Carmona, M., Kivork, C., Seja, E., Cherry, G., Gutierrez, A.J., Grogan, T.R., Mateus, C., Tomasic, G., Glaspy, J.A., Emerson, R.O., Robins, H., Pierce, R.H., Elashoff, D.A., Robert, C., Ribas, A., 2014. PD-1 blockade induces responses by inhibiting adaptive immune resistance. *Nature* 515, 568–571. <https://doi.org/10.1038/nature13954>
- van der Weyden, L., Patton, E.E., Wood, G.A., Foote, A.K., Brenn, T., Arends, M.J., Adams, D.J., 2016. Cross-species models of human melanoma: Cross-species models of human melanoma. *J. Pathol.* 238, 152–165. <https://doi.org/10.1002/path.4632>
- Verfaillie, A., Imrichova, H., Atak, Z.K., Dewaele, M., Rambow, F., Hulselmans, G., Christiaens, V., Svetlichnyy, D., Luciani, F., Van den Mooter, L., Claerhout, S., Fiers, M., Journe, F., Ghanem, G.-E., Herrmann, C., Halder, G., Marine, J.-C., Aerts, S., 2015. Decoding the regulatory landscape of melanoma reveals TEADS as regulators of the invasive cell state. *Nat. Commun.* 6, 6683. <https://doi.org/10.1038/ncomms7683>
- Wang, K., Li, M., Hakonarson, H., 2010. ANNOVAR: functional annotation of genetic variants from high-throughput sequencing data. *Nucleic Acids Res.* 38, e164–e164. <https://doi.org/10.1093/nar/gkq603>
- Wang, Z., Schones, D.E., Zhao, K., 2009. Characterization of human epigenomes. *Curr. Opin. Genet. Dev.* 19, 127–134. <https://doi.org/10.1016/j.gde.2009.02.001>
- Winder, M., Virós, A., 2018. Mechanisms of Drug Resistance in Melanoma, in: Mandalà, M., Romano, E. (Eds.), *Mechanisms of Drug Resistance in Cancer Therapy*. Springer International Publishing, Cham, pp. 91–108. https://doi.org/10.1007/164_2017_17
- Yong, W.-S., Hsu, F.-M., Chen, P.-Y., 2016. Profiling genome-wide DNA methylation. *Epigenetics Chromatin* 9, 26. <https://doi.org/10.1186/s13072-016-0075-3>
- Yu, G., 2018. clusterProfiler: An universal enrichment tool for functional and comparative study (preprint). *Bioinformatics*. <https://doi.org/10.1101/256784>
- Zaidi, M.R., Day, C.-P., Merlino, G., 2008. From UVs to Metastases: Modeling Melanoma Initiation and Progression in the Mouse. *J. Invest. Dermatol.* 128, 2381–2391. <https://doi.org/10.1038/jid.2008.177>

9 Acknowledgment

First, I would like to thank my advisors Prof. Dr. med. Jennifer Landsberg and Prof. Dr. Benedikt Brors for giving me this great opportunity to work with their teams and resources to conduct my doctoral thesis.

In addition, I would like to thank Prof. Dr. med. Peter Krawitz and Prof. Dr. med. Michael Hölzel for their support and being part of my Ph.D. committee.

My special thanks to Dr. Charles Imbusch for mentoring my computational work –the most challenging part of my research– and the new skills I developed with his help and support.

I would like to thank Amir Hossein Kayvanjoo my best friend and Ph.D. fellow at the University of Bonn and ImmunoSensation Cluster of Excellence, for his indispensable support and all the fun we had together during our Ph.D. life.

I am grateful to all of the lab members and external colleagues who contributed to this study and helped me with their professional or moral support especially Susanna Ramirez Valladolid, Pia Kuster, and Dr. Sadaf Mughal.

In addition, I highly appreciate the academic, social and financial support from the Bonn international graduate school (ImmunoSensation) and the German Academic Exchange Service (DAAD) during different phases of my doctoral research training until graduation.

I would like to express my appreciation with deep sorrow to Jonas Hausen my friend and a post-doctoral researcher at the core unit of bioinformatics (CUBA) of the university hospital of Bonn, who helped me with the first lessons in Bioinformatics. Jonas passed away in a tragic accident but I promised to keep his memories alive.

Last but not least, I would like to warmly thank my partner Albert and my daughter Darya who without them I was not motivated and empowered enough to survive the enormous physical and mental load at work and home. Besides, my warmest appreciations go to my dearest ones in Iran, Farnoush, Narjes, and Fatemeh, without their continuous help and emotional support I was not able to accomplish this very long and demanding journey from Iran to Germany.

10 Curriculum Vitae

Personal Information

Full name: Atie Kashef



Academic Education

- Sep. 2017 – present: Doctor of Philosophy, University of Bonn, Bonn, Germany
Ph.D. program in Experimental Medicine with a focus on Epi/Genomics
- Oct. 2009 – Jan. 2012: Master of Science, University of Social Welfare and Rehabilitation Sciences (USWR), Tehran, Iran
Master training and thesis in Molecular Human Genetics
- Nov. 2004 – Aug. 2008: Bachelor of Science, Shiraz University of Medical Sciences
Medical Laboratory Sciences, Shiraz, Iran

Scientific Networks

- Bonn Cluster of Excellence (ImmunoSensation): International training for Immunoscience
- Bonn International Graduate School (BIGS): doctoral training and research facilities
- Lise Meitner Gesellschaft e.V (LMG): Board member

Doctoral Research Collaborations and Internships

- Feb. 2020: Division of Applied Bioinformatics, DKFZ, Heidelberg: Collaboration with the lab of Computational Onco-Immunology for analyzing exome data and somatic mutations

- Feb. – Apr. 2017: NGS Core Facility, Max-Planck Institute for Molecular Genetics, Berlin: MeDIP-seq and RNA-seq experiments and NGS data processing

Doctoral Research Grants and Fellowships

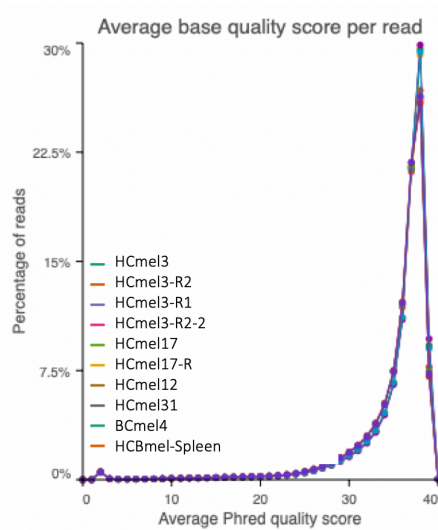
- Jun. – Dec. 2021: Graduation Scholarship from DAAD (Deutsche Akademische Austauschdienst)
- Apr. 2018: Travel Grant: from Bonn International Graduate School to attend the annual conference of the American Society of Human Genetics (ASHG), San Diego, USA (this grant was withdrawn after the USA banned Iranian citizens to travel and enter to the United States of America).
- Sep. 2017: Technical Exchange fellowship: from ImmunoSensation Bonn Cluster of Excellence for ECSEQ Bioinformatics Summer School in NGS Data Analysis, Berlin, Germany

Contribution to Scientific Meetings

- May 2017: Poster presentation at the European Cancer Epigenetics Conference, Heidelberg, Germany
- Jun 2017: Poster presentation at the DGfI (Deutsche Gesellschaft für Immunology) autumn school “Current Concepts in Immunology”, Merseburg, Germany
- Sep 2018: Selected talk at the summer school “Immunology meets Technology” by Bonn Cluster of Excellence, “Abtei Frauenwörth im Chiemsee”, Germany
- Nov 2018: Poster presentation and co-chair of scientific panels at the Cluster Science Days, Bonn, Germany
- Jun 2019: Poster presentation at the European Human Genetics Conference, Gothenburg, Sweden
- Nov 2019: Poster presentation at the EMBL (European Molecular Biology Laboratory) Conference of Cancer Genomics, Heidelberg, Germany
- Jun 2020: Participation at the European Human Genetics Conference, Online
- Nov 2021: Poster presentation at the Custer Science Days, Bonn, Germany

Supplement

A



B

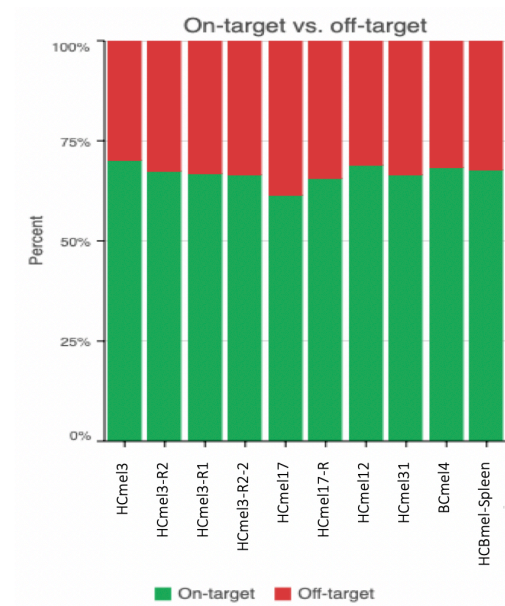
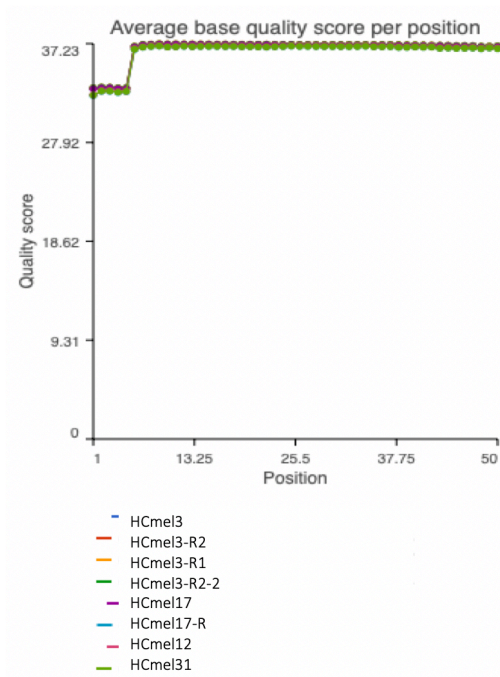


Figure s1. Supplementary data to exome data quality and sequencing coverage for HCmel and BCmel cell lines. A) Average base quality scores show greater than 30 Phred score quality for all the samples which means greater than 99.9% accuracy of the base calling by sequencing experiment. B) Post alignment coverage reports show efficient target enrichment with 60-70% on-target coverage. I reevaluated and plotted data using Partek Flow alignment and quality control toolkits.

A



B

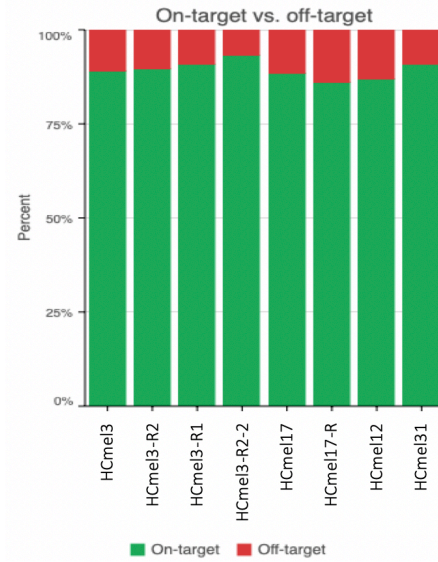
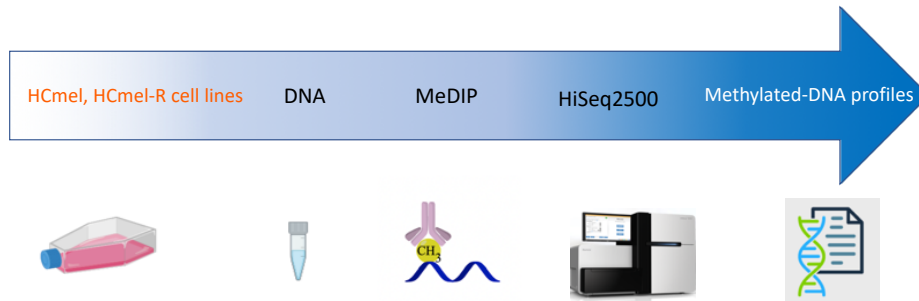


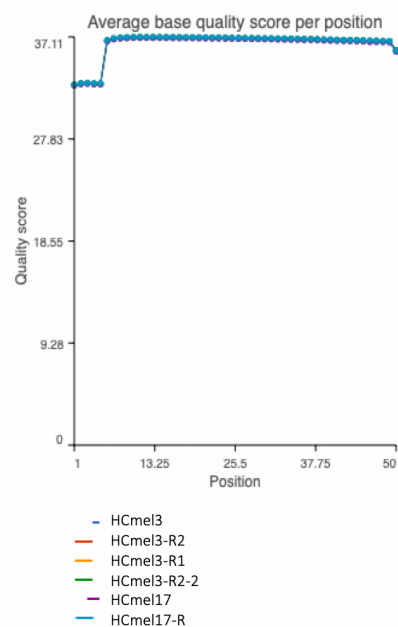
Figure s2. RNA sequencing quality and coverage report for HCmel and HCmel-R cell lines.

A) Base calling quality shows the average of 35 Phred score per base position. B) Target enrichment coverage plot shows at least 80% successful on-target enrichment for all samples. I used Partek Flow bioinformatic toolkit for alignment and post alignment quality control.

A



B



C

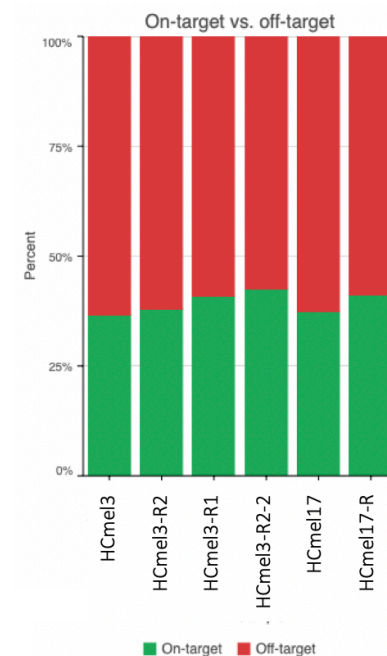


Figure s3. MeDIP-seq data quality and post alignment coverage report high quality of base calling and efficient capture of Methylated DNA.

A) Grafical summary of MeDIP-seq experiment for genome-wide methylated-DNA enrichment using immunoprecipitation followed by next generation sequencing.

B) Sequencing data quality shows average base quality of 35 Phred score per base position for each cell line. C) Post alignment quality report for methylated-DNA reads aligned with BWA-mem against mouse genome reference mm10. Plots are generated using Partek Flow bioinformatic toolkit.

A

Enrichment Score: 3.92		Count	P_Value	Benjamini
Albinism		4	8.5E-6	1.4E-3
melanosome membrane		4	1.4E-5	2.4E-3
melanin biosynthetic process		4	1.9E-5	9.6E-3
Melanin biosynthesis		3	2.9E-4	2.2E-2
Disease mutation		5	3.8E-4	2.2E-2
sequence variant		7	1.1E-2	1.0E0
Enrichment Score: 2.01		Count	P_Value	Benjamini
RNA polymerase II core promoter proximal region sequence-specific DNA binding		9	1.5E-4	3.1E-2
transcriptional repressor activity, RNA polymerase II core promoter proximal region sequence-specific binding		5	2.3E-3	2.4E-1
negative regulation of transcription from RNA polymerase II promoter		7	8.2E-2	1.0E0
Repressor		4	3.3E-1	1.0E0
Enrichment Score: 1.31		Count	P_Value	Benjamini
RNA polymerase II core promoter proximal region sequence-specific DNA binding		9	1.5E-4	3.1E-2
DNA-binding		15	2.7E-3	9.2E-2
Transcription		15	9.9E-3	2.8E-1
Transcription regulation		14	1.8E-2	3.7E-1
transcription, DNA-templated		15	2.2E-2	1.0E0
nucleoplasm		15	2.6E-2	6.7E-1
Nucleus		26	2.8E-2	3.7E-1
Activator		7	3.1E-2	3.8E-1
DNA binding		14	5.0E-2	1.0E0
regulation of transcription, DNA-templated		15	8.4E-2	1.0E0
transcription factor activity, sequence-specific DNA binding		8	8.5E-2	1.0E0
positive regulation of transcription, DNA-templated		6	9.1E-2	1.0E0

B

Enrichment Score: 7.2		Count	P_Value	Benjamini
Developmental protein		80	4.1E-12	6.7E-10
multicellular organism development		81	1.5E-9	5.2E-6
cell differentiation		55	2.4E-5	5.9E-3
Differentiation		43	1.1E-4	2.3E-3
Enrichment Score: 6.72		Count	P_Value	Benjamini
proteinaceous extracellular matrix		36	1.0E-8	1.3E-6
extracellular matrix		33	6.6E-8	5.5E-6
Extracellular matrix		24	1.0E-5	3.0E-4
Enrichment Score: 4.67		Count	P_Value	Benjamini
Glycoprotein		208	2.0E-11	1.6E-9
glycosylation site:N-linked (GlcNAc...)		196	2.2E-6	5.0E-3
extracellular region		103	4.2E-6	2.1E-4
Disulfide bond		154	9.4E-6	3.0E-4
Secreted		92	2.6E-5	7.1E-4
signal peptide		167	8.7E-5	6.5E-2
Signal		200	3.3E-4	5.0E-3
extracellular space		75	9.1E-3	9.7E-2
disulfide bond		116	8.4E-2	1.0E0

Figure s4. Melanoma cell differentiation genes and developmental proteins were strongly enriched in biological functions of differentially expressed and differentially methylated genes. Biological functions enrichment and classification results using Database for Annotation, Visualization, and Integrated Discovery (DAVID v6.8) for differentially expressed genes (A) and differentially methylated genes (B).

	ID	Description	Count	geneID
GO:0000003	GO:0000003	reproduction	3	Fzd4/Kalrn/Mfge8
GO:0002376	GO:0002376	immune system process	11	Fit1/Foxn1/Ifnar2/Mitf/Nfatc2/Rab11fip5/Rab27a/Rbfox2/Sdc4/Skap1/Dysf
GO:0007610	GO:0007610	behavior	4	Fzd4/Kalrn/Map1a/Rin1
GO:0008152	GO:0008152	metabolic process	27	Aff3/Agpat1/Cdk15/Cog6/Col5a1/Cyfp2/Fit1/Foxn1/Fzd4/Hecw2/Ifnar2/Kalrn/Lrrfp1/Map1a/Mcf2l/Mitf/Nfatc2/Rab27a/Rbfox2/Sdc4/Skap1/Spsb4/Tsc22d1/Usp24/Dysf/Tnfrsf9/Slc45a2
GO:0009987	GO:0009987	cellular process	45	Aff3/Agpat1/Cdk15/Cog6/Col5a1/Col8a1/Cyfp2/Dock5/Fam174b/Fit1/Foxn1/Frmd5/Fzd4/Hecw2/Ifnar2/Itpr1/Kalrn/Kcnn2/Lamc2/Lrrfp1/Map1a/Mcf2l/Mfge8/Mitf/Nfatc2/Pde4dip/Ptgir/Rab11fip5/Rab27a/Rbfox2/Rin1/Scn5a/Sdc4/Skap1/Spsb4/Syt9/Tsc22d1/Usp24/Dysf/Arhgap22/Tnfrsf9/Cald1/Arhgap26/Slc45a2/Gpc6
GO:0022414	GO:0022414	reproductive process	3	Fzd4/Kalrn/Mfge8
GO:0022610	GO:0022610	biological adhesion	12	Col5a1/Col8a1/Cyfp2/Dock5/Frmd5/Fzd4/Lamc2/Mfge8/Sdc4/Skap1/Dysf/Gpc6
GO:0023052	GO:0023052	signaling	24	Cyfp2/Dock5/Fit1/Fzd4/Ifnar2/Itpr1/Kalrn/Kcnn2/Map1a/Mcf2l/Mitf/Nfatc2/Ptgir/Rab11fip5/Rbfox2/Rin1/Scn5a/Skap1/Spsb4/Syt9/Dysf/Arhgap22/Arhgap26/Gpc6
GO:0032501	GO:0032501	multicellular organismal process	30	Aff3/Agpat1/Col5a1/Col8a1/Cyfp2/Dock5/Fit1/Foxn1/Fzd4/Hecw2/Itpr1/Kalrn/Kcnn2/Lamc2/Map1a/Mfge8/Mitf/Nfatc2/Rab11fip5/Rab27a/Rbfox2/Rin1/Scn5a/Sdc4/Dysf/Arhgap22/Tnfrsf9/Cald1/Slc45a2/Gpc6
GO:0032502	GO:0032502	developmental process	23	Aff3/Col5a1/Col8a1/Cyfp2/Dock5/Fit1/Foxn1/Fzd4/Hecw2/Itpr1/Kalrn/Lamc2/Map1a/Mfge8/Mitf/Nfatc2/Rab27a/Rbfox2/Scn5a/Sdc4/Dysf/Arhgap22/Gpc6
GO:0040007	GO:0040007	growth	2	Cyfp2/Dysf
GO:0040011	GO:0040011	locomotion	14	Col5a1/Dock5/Fit1/Foxn1/Frmd5/Fzd4/Kalrn/Lamc2/Mitf/Nfatc2/Rbfox2/Sdc4/Dysf/Gpc6
GO:0043473	GO:0043473	pigmentation	3	Mitf/Rab27a/Slc45a2
GO:0044419	GO:0044419	interspecies interaction between organisms	5	Ifnar2/Ptgir/Rab11fip5/Rab27a/Kalrn
GO:0048518	GO:0048518	positive regulation of biological process	27	Agpat1/Col8a1/Cyfp2/Dock5/Fit1/Foxn1/Frmd5/Fzd4/Hecw2/Itpr1/Kalrn/Lamc2/Lrrfp1/Map1a/Mcf2l/Mfge8/Mitf/Nfatc2/Pde4dip/Rab27a/Scn5a/Sdc4/Skap1/Spsb4/Syt9/Tsc22d1/Dysf
GO:0048519	GO:0048519	negative regulation of biological process	19	Col5a1/Dock5/Fit1/Frmd5/Fzd4/Hecw2/Itpr1/Kalrn/Lrrfp1/Map1a/Mitf/Nfatc2/Ptgir/Rab11fip5/Rbfox2/Sdc4/Tsc22d1/Dysf/Tnfrsf9
GO:0050789	GO:0050789	regulation of biological process	41	Aff3/Agpat1/Cdk15/Col5a1/Col8a1/Cyfp2/Dock5/Fit1/Foxn1/Frmd5/Fzd4/Hecw2/Ifnar2/Itpr1/Kalrn/Kcnn2/Lamc2/Lrrfp1/Map1a/Mcf2l/Mfge8/Mitf/Nfatc2/Pde4dip/Ptgir/Rab11fip5/Rab27a/Rbfox2/Rin1/Scn5a/Sdc4/Skap1/Spsb4/Syt9/Tsc22d1/Dysf/Arhgap22/Tnfrsf9/Cald1/Arhgap26/Gpc6
GO:0050896	GO:0050896	response to stimulus	28	Aff3/Col5a1/Cyfp2/Dock5/Fit1/Fzd4/Ifnar2/Itpr1/Kalrn/Lamc2/Mcf2l/Mitf/Nfatc2/Ptgir/Rab11fip5/Rab27a/Rbfox2/Rin1/Scn5a/Sdc4/Skap1/Spsb4/Syt9/Dysf/Arhgap22/Arhgap26/Slc45a2/Gpc6
GO:0051179	GO:0051179	localization	28	Cog6/Col5a1/Dock5/Fit1/Foxn1/Frmd5/Fzd4/Hecw2/Itpr1/Kalrn/Kcnn2/Lamc2/Map1a/Mfge8/Mitf/Nfatc2/Osblp3/Rab11fip5/Rab27a/Rbfox2/Rin1/Scn5a/Sdc4/Skap1/Syt9/Dysf/Slc45a2/Gpc6
GO:0051704	GO:0051704	multi-organism process	2	Kalrn/Mfge8

GO:0065007	GO:0065007	biological regulation	41	Aff3/Agpat1/Cdk15/Col5a1/Col8a1/Cyfp2/Dock5/Flt1/Foxn1/Frmd5/Fzd4/Hecw2/Ifnar2/Itpr1/Kalrn/Kcnn2/Lamc2/Lrrfp1/Map1a/Mcf2l/Mfge8/Mitf/Nfatc2/Pde4dip/Ptgir/Rab11fip5/Rab27a/Rbfox2/Rin1/Scn5a/Sdc4/Skap1/Spsb4/Syt9/Tsc22d1/Dysf/Arhgap22/Tnfrsf9/Cald1/Arhgap26/Gpc6
-------------------	------------	-----------------------	----	--

Table s1. List of gene IDs in intersection of differential methylation with differential expression analysis which were grouped by gene ontology. (Supplement to figure 3.12)